MAY - AUG. 1998
Volume IV Number II

THE ASEAN JOURNAL OF RADIOLOGY

Published by The Radiological Society and
The Royal College of Radiologists of Thailand,
Bangkok, Thailand

Supported through an educational grant from

MAY - AUG. 1998
Volume IV Number II

ISSN 0859 144X

THE ASEAN JOURNAL OF RADIOLOGY

Published by The Radiological Society and
The Royal College of Radiologists of Thailand,
Bangkok, Thailand

Supported through an educational grant from

THE ASEAN JOURNAL OF RADIOLOGY

Volume IV Number II MAY. - AUG. 1998

CONTENTS

THE ASEAN JOURNAL OF RADIOLOGY

Volume IV Number II MAY. - AUG. 1998

CONTENTS

PRIMARY OSTEOSARCOMA OF THE CALVARIA

Patchrin PEKANAN, Suphaneewan JAOVISIDTHA, Pimjai SIRIWONGPAIRAT, Sirintara PONGPECH, Pakorn JIARAKONGMUN

ABSTRACT

Two cases of calvarial osteosarcoma was presented using images of plain films and CT scan. The first case was a 22-year-old female patient who had bony density mass of osteoblastic osteosarcoma at left frontal bone. The involved bone showed a mixed osteolytic and permeative lesions . The second case was a 4-year-old boy who had bony density mass of chondroblastic osteosarcoma at right temporal region. The involved bone also showed a mixed osteolytic and permeative lesions.

INTRODUCTION

Primary osteogenic sarcoma of the skull is rare. A review of the records of more than 1,200 osteogenic sarcoma patients over a 60-year period discovered 19 cases(1.6%) arising in the skull.[1] Ten cases were primary de novo tumors, while six cases were superimposed on Paget disease, two occurred as a complication of previous irradiation, and one arose in association with fibrous dysplasia. The mean patient age was 26 years in the group with the primary neoplasms. Thirteen neoplasms involved the calvarium, while the other six occurred in the skull base. The spectrum of the images by radiologic examinations include purely osteolytic lesions, sclerotic lesions and permeative destructive lesions.

The primary calvarial osteogenic sarcoma in our institution is also unusual and two cases of this condition are presented.

CASE REPORTS

Case 1

A 22-years-old female patient from Srisakes province (north-eastern part of Thailand) presented to the plastic and maxillofacial division due to the palpable left frontal mass for 3 months. The mass was a hard , enlarging and non-tender one. No other symptoms were complained and the physical examination otherwise was normal.

Plain film of the skull in PA and lateral views (Fig. 1) showed a round shape osteoblastic area of left frontal bone. In lateral skull projection (Fig.1), and bone window of the CT scan (Fig.2) revealed that the destruction of the all table- layers of the frontal bone was obvious. The destruction was composed of osteolytic and permeative areas (Fig.2,3). Mild expansion of the medulla of the frontal bone was observed (Fig.3). Bony density occupied most area of the tumor was noted (Fig.4). Dense tumor matrix and tumor bone was probably responsible for this density (Fig. 5). The subgaleal tumor extension contains no tumor matrix (Fig. 6).

At operation, the 4.5 cm- diameter soft tissue mass at the outer cortex of left frontal bone was found and was biopsied. The pathological diagnosis was osteoblastic osteosarcoma, moderately differentiated. The patient received chemotherapy and was in the process of follow–up.

Department of Radiology, Ramathibodi Hospital , Rama 6 Street, Bangkok 10400, Thailand

Case 2

A 4-year -old boy, from Pathumthani province (central part of Thailand) , had a lump at right temporal area for 3 years. The lump enlarged rapidly for 5 months. He had pain around the lump and had ear pain for 3 weeks. He noted limitation of the temporomandibular joint movement. On physical examination, a firm and fixed 12 cm - diameter mass was noted at right temporal fossa , displacing right ear laterally .The mass protruded into the external auditory canal. Limitation of the mouth opening and deviation of the jaw to the left was observed.

PA and lateral plain films of the skull revealed an ill defined border dense area in the right temporal bone with irregular outline of the tables (Fig.7). CT scan showed a mass at and around the right temporal bone. The subgaleal part of the mass had only minimal calcification (Fig.8). The intracranial part of the mass contained much of the bony density area(Fig.9) which was due to tumor bone and matrix. Bone window revealed a mixed permeative lesion and an expanding osteolytic areas with sclerotic rim at the right temporal bone (Fig. 10).

At operation the tumor involving posterior part of right temporal bone, auditory canal, infratemporal fossa, lateral orbital wall, zygomatic arch, ramus of the mandible and the temporal lobe was found. Accidental tear of the intracranial lateral sinus and massive bleeding(4000 cc) was encountered. Cardiac arrest occurred in the operative room and finally the patient passed away .At pathology, the tumor was found to be high grade, chondroblastic osteosarcoma .

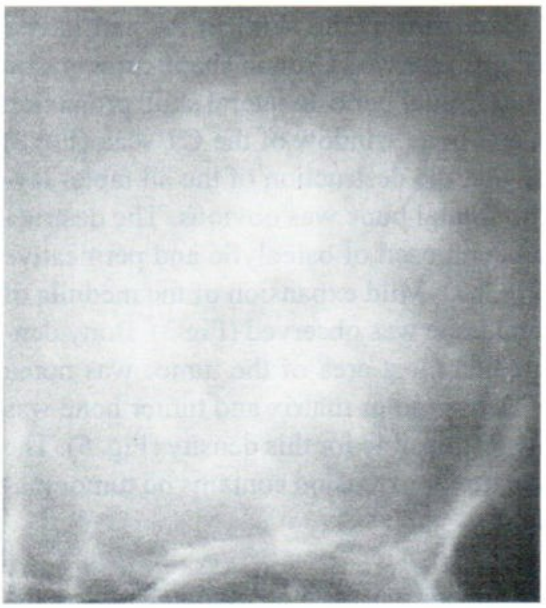

Fig. 1. Case 1. Plain film of the skull in PA and lateral views showed a round shape osteoblastic area of left frontal bone. All layers bony destruction was shown in lateral projection.

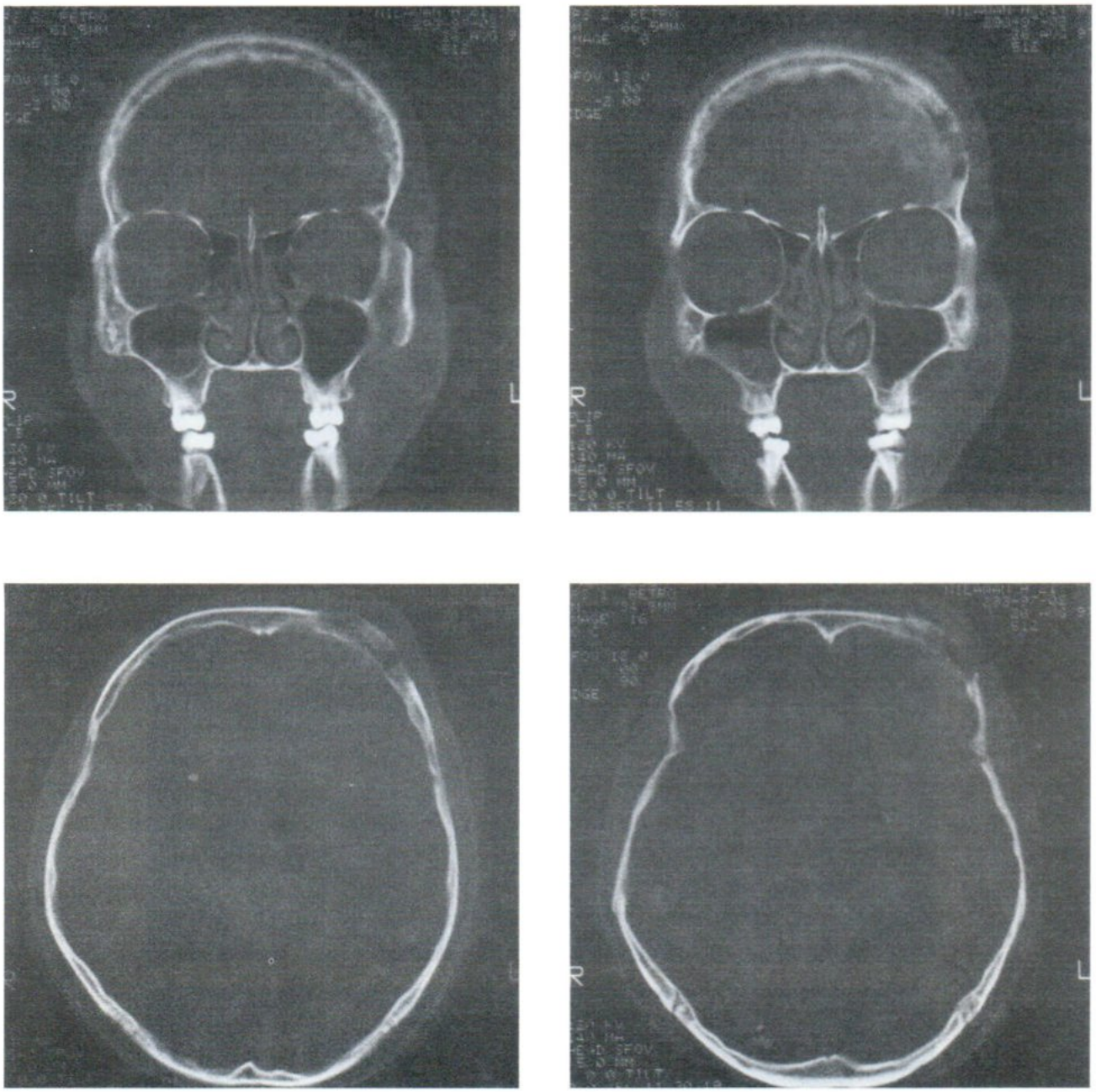

Fig. 2. Case 1. Bone window of the CT scan revealed that the destruction of the all table-layers of the frontal bone was obvious. The destruction was composed of osteolytic and permeative areas.

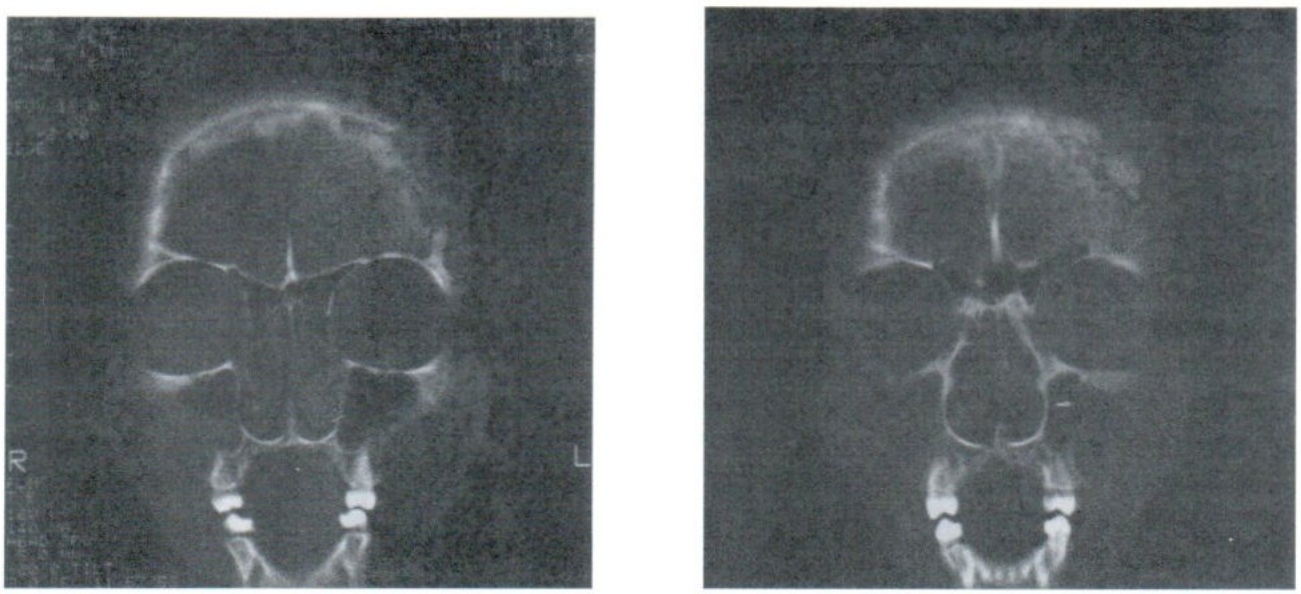

Fig. 3. Case 1. Bone window of the CT scan , mild expansion of the medulla of the frontal bone was observed.

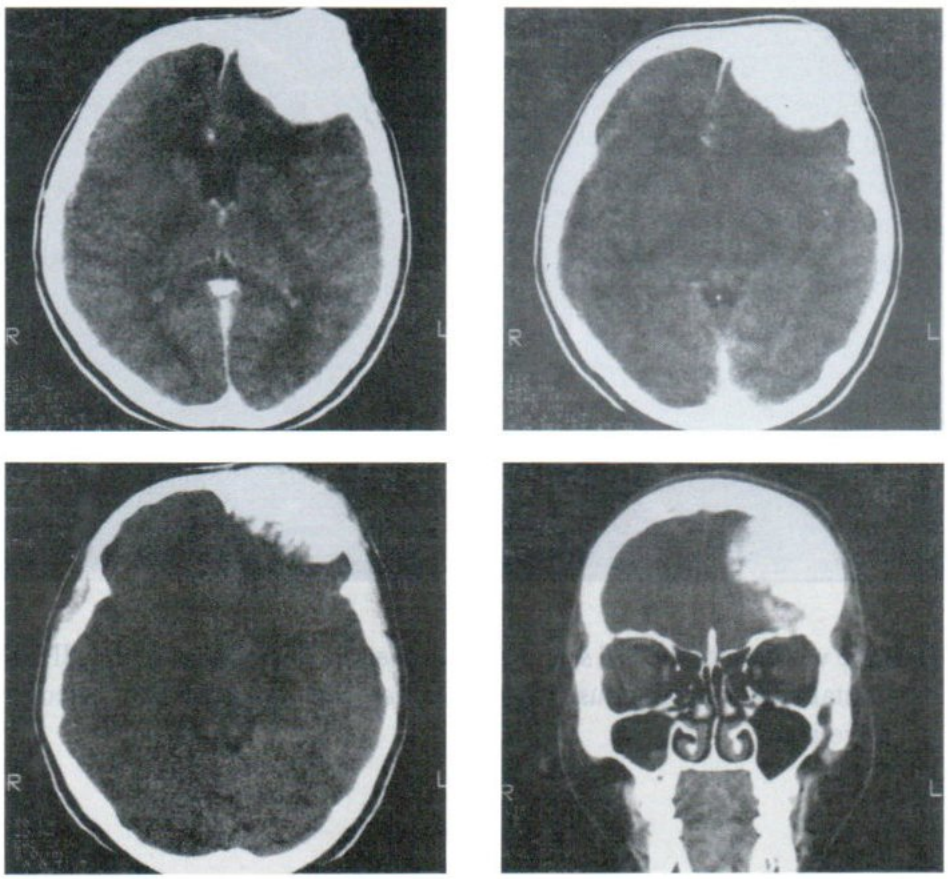

Fig. 4. Case 1. Soft tissue window of the CT scan of the lesion showed that the nearly entire part of the mass was bony dense.

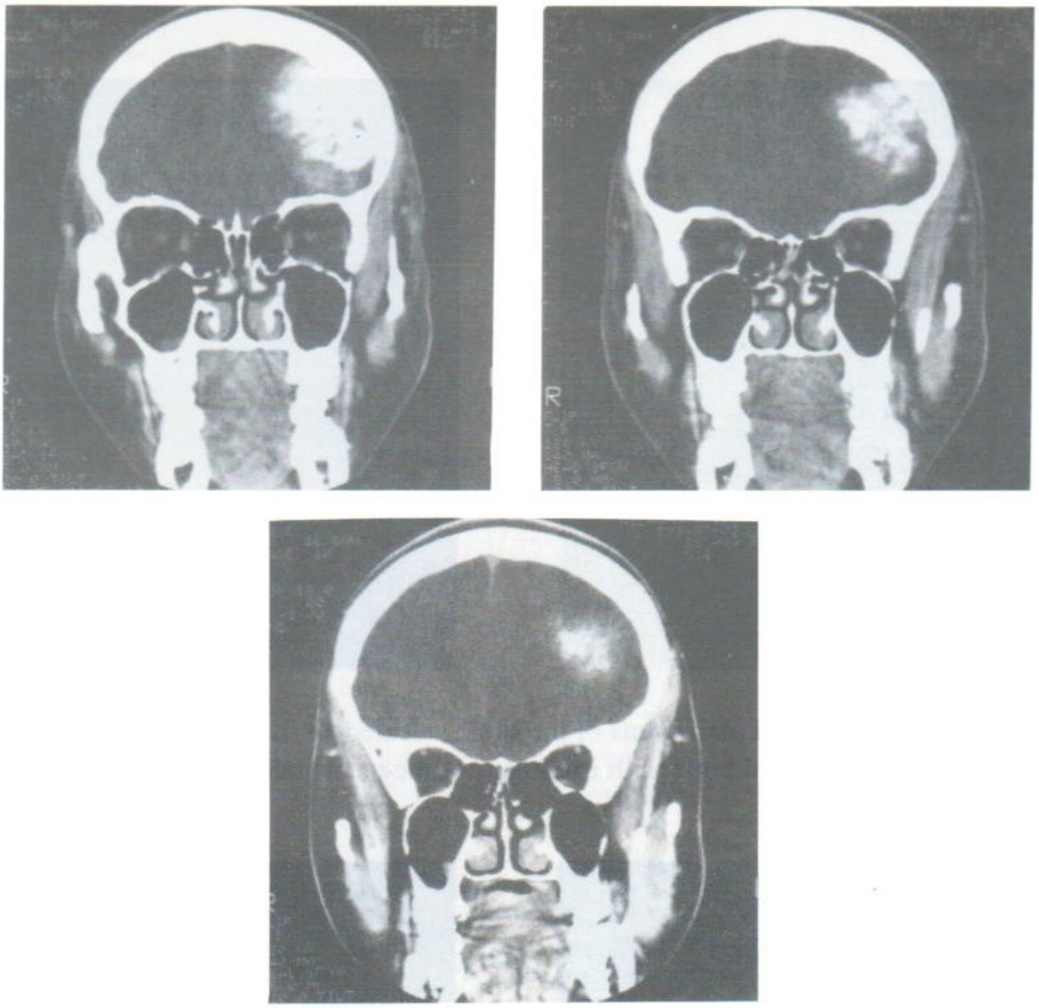

Fig. 5. Case 1. CT scan of the lesion showed that the lesion contained heavy calcification.

Fig. 6. Case 1. CT scan of the lesion showed that the extracranial subgaleal part of the lesion contained no calcification.

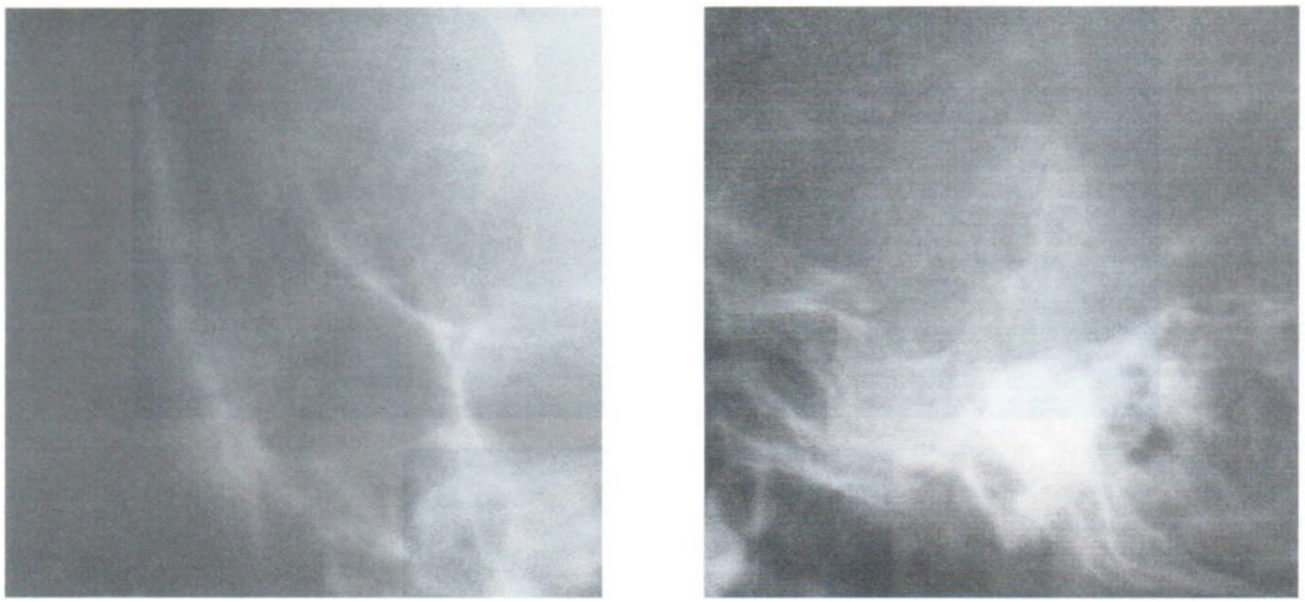

Fig. 7. Case 2. PA and lateral plain films of the skull revealed an ill defined border dense area in the right temporal bone with irregular outline of the tables.

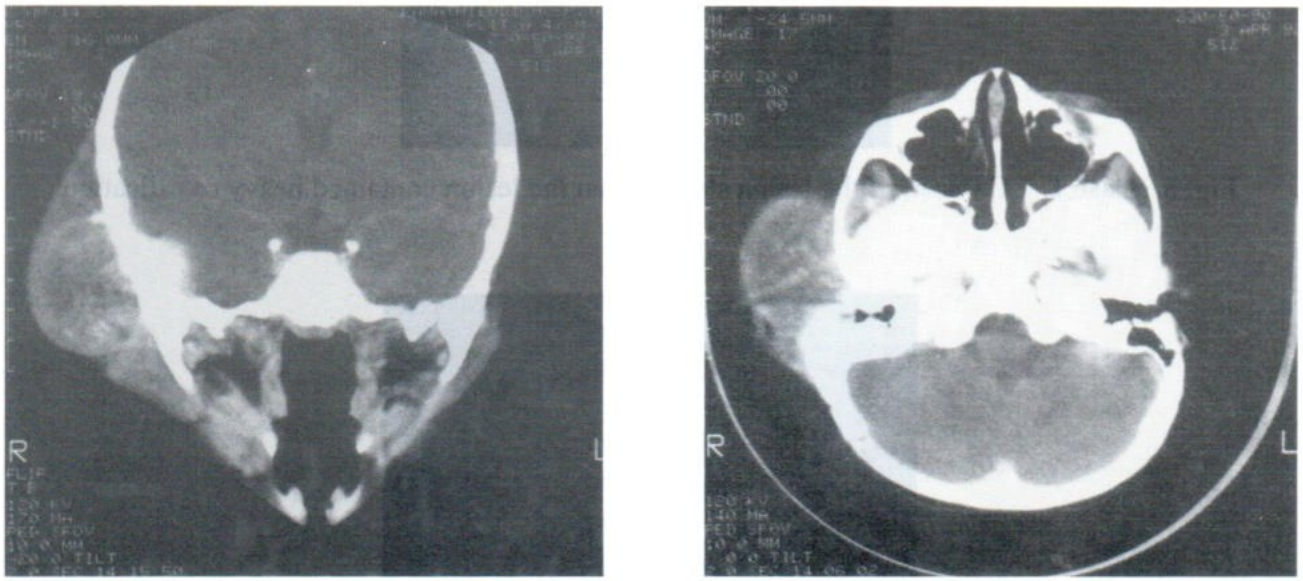

Fig. 8. Case 2. The extracranial part of the mass showed minimal calcification by CT scan.

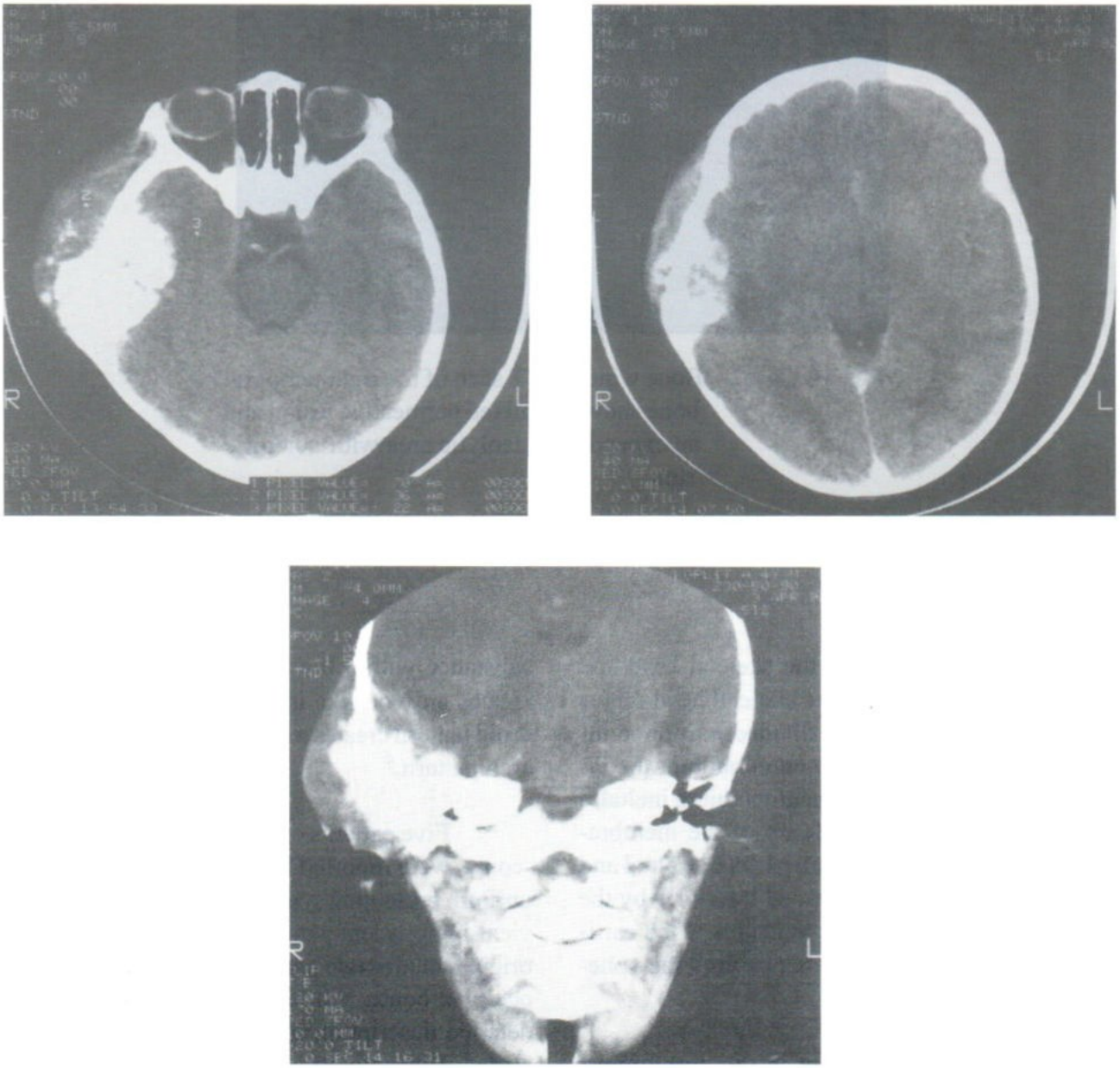

Fig. 9. Case 2. Most of the intracranial part of the mass showed dense calcification by CT scan.

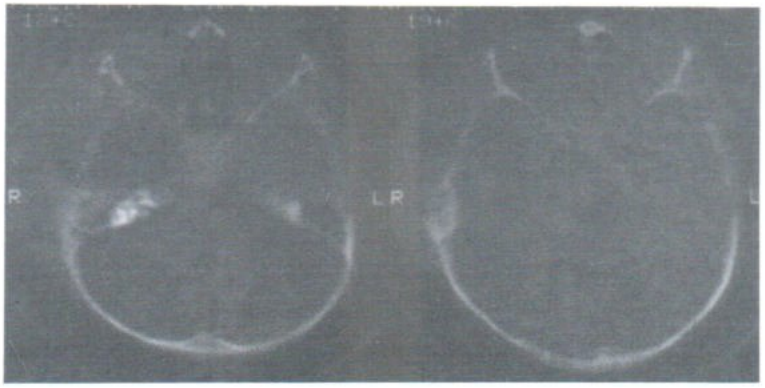

Fig. 10 Case2. Bone window CT scan of the right temporal bone showed a mixed permeative lesion and an expanding osteolytic area with sclerotic rim.

DISCUSSION

The skull includes the skeletal head and mandible: the cranium is the skeletal head minus the mandible. The skull is divided into three interconnected portions: the neurocranium, the facial area, and the base. The neurocranium includes the calvaria, which is made up of the membranous portions of the occipital, parietal, frontal and temporal bones, and is bounded inferiorly by the base of the skull , which is made up of the cartilaginous portions of these bones plus the sphenoid and ethmoid bones.[2]

Osteogenic sarcoma is the commonest bone neoplasm of the long bones, with the greatest predilection for the metaphyses, most frequently the distal femur and proximal tibia.[3] It primarily affects older children and young adults.[4] Very few osteosarcomas occur before age 5 or over age 30.[5] Radiographically, most long bone osteosarcoma (46%) demonstrate a mixed pattern, with osteoblastic and osteolytic type accounting for 32% and 22% respectively. Periosteal reaction is associated with 80% of long bone lesions. The majority of osteosarcomas have matrix mineralization, calcification of the osteoid or osteoid-like substance within the tumor; the osteoid pattern creates an ivorylike increased density, the chondroid pattern creates a stippled,flocculent, or ringarch pattern.[6]

Five patients of primary calvarial osteosar -coma were reported by Lee et al.[3] There was no uniform presenting symptom and there was no cervical lymphadenopathy. The bony site of tumor origin included two parietal, two temporal and one occipital bones. All lesions were osteolytic. The detailed description of each cases were not presented. Two patients of osteogenic sarcoma of the calvarium was described in children (12-year-old girl and 11- year-old boy) by Kornreich et al.[7] The described CT scan in one case showed a destructive lesion in all layers of the right parietal bone with irregular and expanding margins and an associated small non-calcified soft tissue mass without dural invasion. The skull (right parietal bone) of another case was involved as a part of multifocal osteosarcoma (another site was at distal femur). The CT scan of the latter case showed a remarkable extracranial soft tissue mass with hyperdense borders without bone destruction: but the inner

table was irregular with formation of internal body spicules. The tumor invaded the epidural space.

Shramek et al,[8] reported a case of osteogenic sarcoma at left occipitoparietal bone in an 8-year-old boy. The CT of this case showed a heavily calcified left occipitoparietal mass with extra-and intracranial components. The calvaria was thin at the region of the mass. MRI showed much of the soft tissue component of the lesion which was isointense to the brain on both T1-and T2-weighted images with signal of acute hemorrhage at the peripheral of the mass.

In conclusion, two cases of calvarial osteosarcoma have following characteristics:

1. Both patients were young, 4-year-old boy and 22- year-old woman.
2. Both masses had heavy calcifications or bony density in the portions that surrounded the originated pathological bones.
3. Associated extracranial masses were lumpy and contained small areas of calcification.
4. The involved calvaria (frontal, and temporal bones), showed mixed permeative and osteolytic areas.
5. The cases of the reviewed literatures also showed no osteoblastic lesions of the involved calvaria.

REFERENCES

1. Huvos AG, Sundaresan N, Bretsky SS, Butler A. Cancer 1985;56:1214-1221
2. Silverman FN, Kuhn JP. Caffey's pediatric x-ray diagnosis: an integrated imaging approach. 9 ed. St.Louis: Mosby ,1993:4
3. Lee YY, Tassel PV, Nauert C, Raymond AK, Edeiken J. Craniofacial osteosarcoma: plain film, CT, and MR findings in 46 cases. AJNR 1988;9:379-384
4. Edeiken J. Roentgen diagnosis of disease of bone, 3rd ed. Baltimore: Williams & Wilkins, 1981:181-223
5. Wilner D. Radiology of bone tumors and allied disorder.ed. Philadelphia: W.B. Saunders, 1982:1897-2169
6. Sweet DE, Madewell JE, Ragsdale BD. Radiologic and pathologic analysis of solitary bone lesions. Part II: periosteal reactions. Radiol Clin North Am 1981;19(4): 785-814
7. Kornreich L, Grunebaum M, Ziv N, Cohen Y. Osteogenic sarcoma of the calvarium in children: CT manifestations. Neuroradiology 1988;30:439-441
8. Shramek JK, Kassner G, White SS. MR appearance of osteogenic sarcoma of the calvaria. AJR 1992;158:661-662

บริษัท คงศักดิ์เอ็กซเรย์การแพทย์อุตสาหกรรม จำกัด
KONGSAK X-RAY MEDICAL INDUSTRY COMPANY LIMITED
212/1 PHAHONYOTHIN SOI 55 BANGKHEN BANGKOK 10220
TEL. 5213214, 5511794 CABLE: KELEX FAX: 5523744

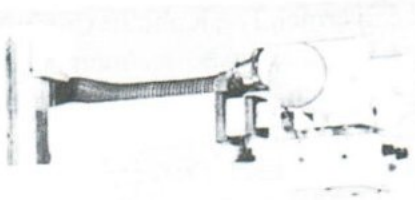

KELEX
50 mA 100 KV MOBILE TYPE DIAGNOSTIC X-RAY UNIT MODEL MD 50-99

- # เหมาะสำหรับคลีนิคเอกชนและโรงพยาบาลทั่วไป
- # มีช่างผู้ชำนาญให้การบริการ ตลอดอายุการใช้งาน
- # พร้อมทั้งจำหน่ายอุปกรณ์เอ็กซเรย์

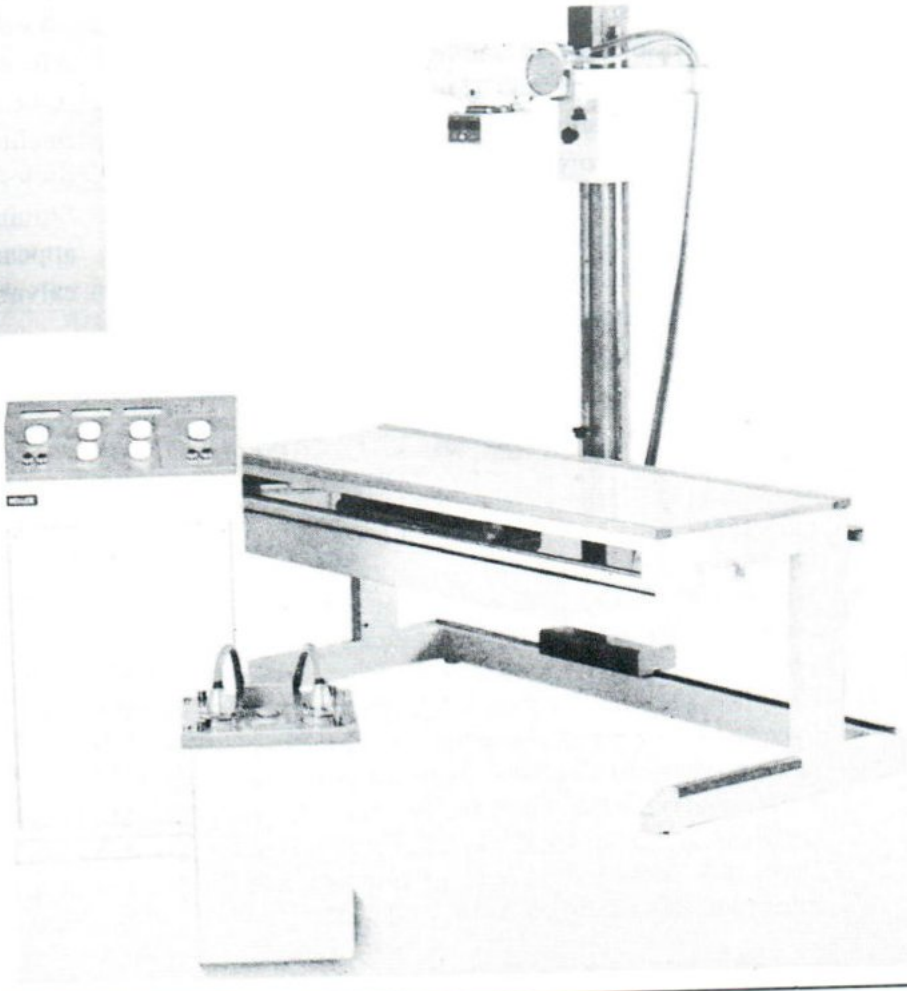

KELEX
MD 100-99 X-RAY SYSTEM
FULL WAVE 100 MA 100 KV

ULTRASONOGRAPHY OF INTRA-ABDOMINAL LYMPHADENOPATHY IN A CHILD WITH PENICILLIOSIS MARNEFFEI

Pannee VISRUTARATNA[1], MD., Virat SIRISANTHANA[2], MD.

ABSTRACT

We report a case of 6-year-old boy with disseminated penicilliosis marneffei. He had hemophilia A and acquired human immunodeficiency virus (HIV) infection from blood transfusion. Ultrasonography showed multiple enlarged mesenteric and retroperitoneal lymph nodes, hepatosplenomegaly without focal lesions, and a small amount of ascites.

INTRODUCTION

Patients with human immunodeficiency virus (HIV) infection are susceptible to a great variety of opportunistic infections, which vary according to geography. In Southeast Asia, *Penicillium marneffei* has been reported as an important pathogen in HIV-associated opportunistic infections[1,2]. Recently, *P. marneffei* infection was reported in Thai children infected with HIV[3]. We describe abdominal ultrasonograms of a boy with disseminated penicilliosis marneffei.

CASE REPORT

A 6-year-old boy had had prolonged fever for 2 weeks. He had been diagnosed as having hemophilia A when he was 4 months old, and had been given cryoprecipitate many times. He was found to be HIV-infected at the age of 3 years and 4 months. His father and his mother were HIV antibody negative. He had had abdominal pain for one day when he came to our hospital. Physical examination revealed hepatosplenomegaly and mild tenderness of the abdomen. His body temperature was 38.6°C. His chest film was normal. Abdominal ultrasonography showed multiple enlarged mesenteric lymph nodes and multiple enlarged retroperitoneal lymph nodes (Figs. 1 and 2). Hepatosplenomegaly without focal mass lesions and a small amount of ascites were also seen. His hemoculture grew *P. marneffei*. His Wright's-stained bone marrow aspiration revealed yeast cells with clear central septation consistent with *P. marneffei*. His fever subsided 4 days after initiation of amphotericin B and repeated hemoculture was negative. During this hospitalization he developed severe gastrointestinal bleeding and went into hypovolemic shock. He expired after his parents did not allow him to undergo further treatment.

[1] Department of Radiology, Faculty of Medicine, Chiang Mai University, Chiang Mai 50200, THAILAND.
[2] Department of Pediatrics, Faculty of Medicine, Chiang Mai University, Chiang Mai 50200, THAILAND.

Fig 1. Transverse sonogram of left side abdomen shows multiple enlarged mesenteric lymph nodes.

Fig 2. Longitudinal sonogram of mid upper abdomen shows enlarged liver and multiple enlarged mesenteric and retroperitoneal lymph nodes.

DISCUSSION

P. marneffei is a fungus that can cause systemic mycosis in both healthy and immuno-compromised patients. It is endemic in Southeast Asia and the southern part of China.[4] The first person infected naturally by this fungus was a Caucasian minister with Hodgkin's disease in 1973 who had been touring Southeast Asia.[5] After that, cases were reported from Southeast Asia and the southern part of China. In 1988, Peto et al.[6] reported the first case of an HIV-infected patient who had traveled in Southeast Asia and subsequently developed penicilliosis marneffei. Recently, penicilliosis marneffei has been reported in HIV-infected patients who have been living in or traveling through the endemic area.

There have been at least 27 reported cases of P. marneffei in children, 22 of whom were HIV-positive.[2,3,7-9] One 11-year-old boy from Hong Kong had lung, liver, spleen, and kidney involvement.[2] The other 21 cases were from northern Thailand.[3] 90% of these Thai patients had generalized lymphadenopathy, 90% had hepatomegaly, 81% had fever, 67% had papular skin lesions with central umbilication, and 67% had splenomegaly.

P. marneffei tends to involve the reticuloendothelial system. Our experience confirms this. We have seen several HIV-infected children and adults with *P. marneffei* infection who had acute abdominal pain and on laparotomy, they were found to have mesenteric and retroperitoneal lymphadenopathy. To our knowledge there have been no reports of abdominal ultrasonograms of children with penicilliosis marneffei.

If an HIV-infected patient has multiple mesenteric and multiple retroperitoneal lymphadenopathy, one should suspect *M. tuberculosis*, *M. avium-intracellulare*, *H. capsulatum*, or lymphoma. However, if a patient lives in Southeast Asia, one should add *P. marneffei* to the list of pathogens.

REFERENCES

1. Supparatpinyo K, Khamwan C, Baosoung V, Nelson KE, Sirisanthana T. Disseminated *Penicillium marneffei* infection in Southeast Asia. Lancet 1994;344:110-113.
2. Li PCK, Tsui MS, Ma KF. *Penicillium marneffei*: indicator disease for AIDS in South East Asia. AIDS 1992;6:240-241.
3. Sirisanthana V, Sirisanthana T. Disseminated *Penicillium marneffei* infection in human immunodeficiency virus-infected children. Pediatr Infect Dis J, 1995;14:935-940.
4. Deng Z, Ribas JL, Gibson DW, Connor DH. Infections caused by *Penicillium marneffei* in China and Southeast Asia: review of eighteen published cases and report of four more Chinese cases. Rev Infect Dis 1988;10:640-652.
5. DiSalvo AF, Fickling AM, Ajello L. Infection caused by *Penicillium marneffei* - description of first natural infection in man. Am J Clin Pathol 1973;60:259-263.
6. Peto TEA, Bull R, Millard PR. Mackenzie DWR, Campbell CK, Haines ME, Mitchell RG. Systemic mycosis due to *Penicillium marneffei* in a patient with antibody to human immunodeficiency virus. J Infect 1988;16:285-290.
7. Deng Z, Connor DH. Progressive disseminated penicilliosis caused by *Penicillium marneffei*: report of eight cases and differentiation of the causative organism from *Histoplasma capsulatum*. Am J Clin Pathol 1985;84:323-327.
8. Yuen WC, Chan YF, Loke SL, Seto WH, Poon GP, Wong KK. Chronic lymphadenopathy caused by *Penicillium marneffei*: a condition mimicking tuberculous lymphadenopathy. Br J Surg 1986;73:1007-1008.
9. Jayanetra P, Nitiyanant P, Ajello L, et al. Penicilliosis marneffei in Thailand: report of five human cases. Am J Trop Med Hyg 1984;33:637-644.

Process beautiful images without a drop of liquid in sight.

DryView Imager

It's no mirage. Our Imation™ DryView™ laser imager, with its revolutionary new dry processing technology, really does eliminate the hassles and costs of messy, toxic chemicals. It also travels well, because it doesn't depend on plumbing. And it costs a lot less than the competition. All this and the DryView imager produces images sharp as a cactus needle. No wonder we're a world leader in medical laser imaging. And it's only from Imation, formerly a part of 3M. Contact us at info@imation.com or see us at www.imation.com. **We're thinking what you're thinking.**

IMATION
Borne of 3M Innovation

Imation (Thailand) Limited, 99/349, 9th Floor Na-Nakorn Building, Chengwatana Road, Donmuang, Bangkok 10210. Ph: (662) 576 0067-9 Fax: (662) 576 0065.

South Asia

Singapore	Malaysia	Philippines	Pakistan	Mumbai, India	Bangalore, India	Delhi, India
(65) 383 7676	(03) 703 7576	(632) 812 6981	(9221) 584 0176	(9122) 837 7053	(9180) 552 0407	(9111) 622 0234

SONOGRAPHIC MEASUREMENT OF THE NORMAL LIVER MARGINAL ANGLES

Wanna TRIVITAYARATANA, B.Sc.(RT), M.D., M.Sc.(Biostatistics),[1]
Pichit TRIVITAYARATANA, B.Sc.(RT), M.Sc.(Anatomy),[1]
Wanchat LAOPRASERT, M.D.,[2] Chaiyut SOPANNARAT, B.Sc.(RT),[3]
Pratharn WONGTALA, B.Sc.(RT)[4]

ABSTRACT

The liver marginal angles have been measured in 937 normal health check-up subjects by ultrasound. They were 57.7 % men and 42.3 % women. The aims of this study were to evaluate correlation between liver marginal angles and physical data, age, sex. The results show that the mean of weight, height, BMI and LIMA in male were larger than female. The average of LLMA, LIMA and RIMA were 41.6 ± 4.4, 39.3 ± 4.3 and 45.9 ± 8.6 degrees, respectively. There were negative correlation between age and sex, age and weight, age and height, while correlation between sex and weight, sex and height, sex and AP diameter were positive. Sex can predict the LIMA from the equation: LIMA = 38.17 + 2.09 (sex).....equation I. Physical data that were used to predict the RIMA were BMI and height from the equation: RIMA = 56.89 + 1.05 (BMI) - 20.27 (Ht). From the classification of obesity, mean BMI was 21.42 kg/m^2(body surface area) for men, 20.89 kg/m^2 for women. Among the normal health check-up subjects, the overweight group constitutes 7.3 % of the total cases.

LLMA = Left lateral marginal angle, transverse cut
LIMA = Left inferior marginal angle, sagittal cut
RIMA = Right inferior marginal angle, sagittal cut
BMI = Body mass index
(sex) in equation I means: male = 1, female = 0

INTRODUCTION

Measurements of liver in case of mild hepatomegaly based on percussion and palpation are inaccurate and unreliable in some obese patients,[1] while radiography or radionuclide studies expose the patient to gamma radiation.[2,3] Ultrasound has been found to be both accurate, reliable, without contraindication,[4] more sensitive than computed tomography[5] and without radiation hazard.[6] A measurement of liver marginal angles, called the angle sign is the one of sonographic criteria of hepatomegaly. The liver is enlarged when LLMA, LIMA and RIMA measure more than 45, 45 and 75 degrees,[7,8] respectively. However, despite the widespread of clinical uses, we still have no general accepted standards of liver marginal angles in normal Thai people. We therefore con-

[1] Dept. of Radiological Technology, Faculty of Medical Technology, Mahidol University.
[2] Taksin Hospital
[3] Wachira-Phuket Hospital
[4] Mukdaharn Hospital

ducted a prospective study of a large group of healthy subjects to evaluate the physical data, to correlate liver marginal angles with sex, age, weight, height, BMI and AP diameter at xiphoid level.

MATERIALS AND METHODS

Subjects: One thousand consecutive health check-up volunteers were examined by ultrasound between september 1996 and october 1997. Sixty-three subjects were excluded because of (a) a history of hepatic, biliary, pancreatic disease, subjective abnormal ultrasound, clinical (n=38) or laboratory finding (n=17), (b) increase alcohol intake, defined as daily consumption, for at least three years, of more than 20 ml. of ethanol for women and more than 60 ml. of ethanol for men[9,10] (n=2), (c) abnormal chest radiographs(n=6). There were 541 men and 396 women, age between 17-75 years . Sex, age(years), weight(kg.), height(m.), AP diameter(cm.) at xiphoid level, medical history and results of the physical examination were recorded, along with hematocrit, white cell count, platelet, SGOT, SGPT, HBs-Ag and anti-HBs. BMI was calculated from the equation: $BMI = Wt/(Ht^2)$, for the classification of the obesity.[11] All subjects had normal radiographs.

Ultrasound examination: We employed a high resolution real time scanner with a 3.75 MHz transducer (Toshiba imager). Subjects were examined (a) supine to demonstrated LLMA and LIMA (b) with the right side elevated 10-15 degrees to show the RIMA. Transverse scans of the liver were obtained in the midline, 2-3 cm. below xiphoid process, the portal vein in left lobe is the reference landmark for measuring LLMA as shown in figure 1. LIMA were measured by sagittal scans in the midline, 2-3 cm. below xiphoid process, the abdominal aorta is the reference landmark as shown in figure 2. For the right side elevated 10-15 degrees, sagittal scans were obtained by placing the upper edge of transducer at the lower edge of right costal margin, RIMA were measured at the mid point of right kidney as shown in figure 3. All angles were measured during deep inspiration in order to minimize masking by the lung and eliminate morphological variation due to respiration.

(n = number of subjects who were excluded)

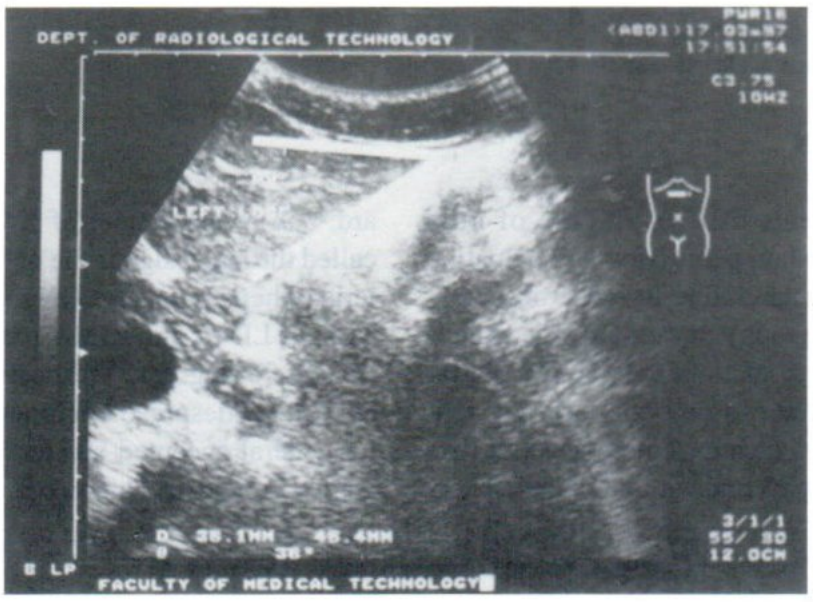

Fig. 1 Left lateral marginal angle, transverse cut

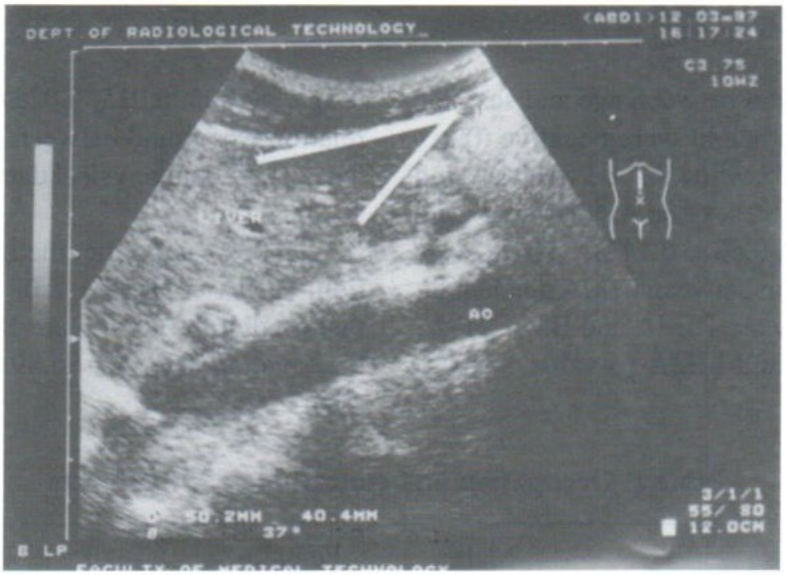

Fig. 2 Left inferior marginal angle, sagittal cut

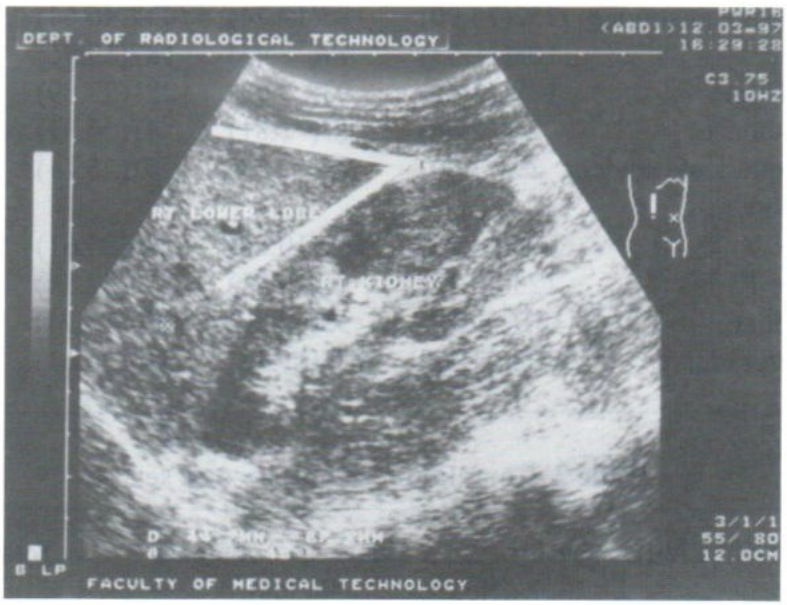

Fig. 3 Right inferior marginal angle, sagittal cut

Statistics: The data were analyzed by using a SPSS-PC program. Descriptive statistics and correlation for physical data, sex, age, BMI, LLMA, LIMA and RIMA were evaluated. Independent t-test was used to compare the mean of all parameters with sex. Multiple regression analysis was carried out for age, sex, physical data, BMI and all angles by stepwise regression method.

RESULTS

The occupation and education of 937 subjects are shown in table 1. Table 2 show the correlation of sex and the classification of obesity. Women was less obese than men (p-value = 0.042). Mean values, standard deviation and range are shown in table 3. The mean of physical data, age and all angles were compared with sex as shown in table 4. In male, mean of weight, height, BMI and LIMA were larger than female (p-value = <0.005,<0.005, 0.042 and 0.005). No significant difference was found between AP diameter, LLMA, RIMA and sex (p-value = 0.060, 0.772 and 0.110)

The correlation between age and sex, age and weight, age and height were negative ($r = -0.171, -0.168, -0.323$), while that between sex and weight, sex and height, sex and AP diameter were positive ($r = 0.472, 0.638, 0.142$). There were significant correlation between RIMA and height, RIMA and AP diameter, RIMA and BMI, RIMA and LLMA, RIMA and LIMA (p-value = 0.012, 0.013, <0.005, 0.015, 0.025). No significant correlation was found between LLMA and physical data, LIMA and physical data as shown in table 5.

Sex can predict the LIMA from the equation: LIMA = 38.17 + 2.09 (sex). Physical data that predict the RIMA are BMI and height from the equation: RIMA = 56.89 + 1.05 (BMI) - 20.27 (Ht).

Table 1 Occupation and education of 937 subjects

	Male No.(%)	Female No.(%)	Total No.(%)
Occupation			
Government service	252(26.90)	185(19.74)	437(46.64)
Farmer	108(11.53)	79(8.43)	187(19.96)
Employee	128(13.66)	93(9.93)	221(23.59)
Wife-house	24(2.56)	17(1.81)	41(4.37)
undergraduate student	29(3.09)	22(2.35)	51(5.44)
Education			
Grade 6	138(14.73)	102(10.88)	240(25.61)
Grade 12	123(13.13)	91(9.71)	214(22.84)
Diploma	81(8.64)	59(6.30)	140(14.94)
Undergraduate	198(21.13)	145(15.48)	343(36.61)

Table 2 Correlation of obesity and sex

BMI	Classification of obesity	Male No.(%)	Female No.(%)	Total
< 20	Underweight	158(29.1)	191(48.3)	349(37.2)
20-25	Normal	349(64.6)	171(43.1)	520(55.5)
25-30	Overweight	34(6.3)	34(8.6)	68(7.3)
Total		541(57.7)	396(42.3)	937(100.0)

χ^2 - test = 6.314 P-value = 0.042*

* significant at $\alpha = 0.05$

Table 3 Mean, standard deviation, range of clinical features and liver marginal angles

	Mean	SD	Range
Age (years)	34.77	13.39	17 - 75
Weight (kg.)	56.26	7.65	36 - 81
Height (m.)	1.63	0.08	1.39 - 1.80
AP diameter (cm.)	19.68	3.60	15.0 - 24.5
BMI (kg./m.^{2})	21.09	2.01	14.7 - 28.5
LLMA (degrees)	41.64	4.47	31 - 59
LIMA (degrees)	39.38	4.33	28 - 54
RIMA (degrees)	45.99	8.68	27 - 77

Table 4 Comparison of mean ± SD of clinical features and liver marginal angles in sex

	Male	Female	P-value
Age (years)	32.81±13.23	37.44±13.24	0.045*
Weight (kg.)	59.76± 7.82	51.51± 7.42	<0.005**
Height (m.)	1.68± 0.06	1.57± 0.07	<0.005**
AP diameter (cm.)	20.36± 7.05	18.75± 2.29	0.060
BMI (kg./m.^{2})	21.42± 1.68	20.89± 1.43	0.042*
LLMA (degrees)	41.73± 3.96	41.50± 5.11	0.772
LIMA (degrees)	40.27± 4.14	38.17± 4.32	0.005**
RIMA (degrees)	44.96± 8.31	47.30± 9.04	0.110

* significant at $\alpha = 0.05$

** significant at $\alpha = 0.01$

Table 5 Correlation between clinical features and liver marginal angles

		Age	Sex	Weight	Height	AP diameter	BMI	LLMA	LIMA	RIMA
Age	r	1.000	-0.171	-0.168	-0.323	0.016	0.071	-0.060	-0.129	0.014
	p	@	0.045*	0.049*	<0.005**	0.852	0.404	0.480	0.132	0.870
Sex	r	-0.171	1.000	0.472	0.638	0.142	0.059	0.026	0.239	-0.139
	p	0.045*	@	<0.005**	<0.005**	0.096	0.487	0.763	0.005**	0.105
Weight	r	-0.168	0.472	1.000	0.610	0.223	0.743	0.065	0.127	0.119
	p	0.049*	<0.005**	@	<0.005**	0.009**	<0.005**	0.448	0.138	0.164
Height	r	-0.323	0.638	0.610	1.000	0.009	-0.068	-0.027	0.146	-0.213
	p	<0.005**	<0.005**	<0.005**	@	0.914	0.428	0.752	0.088	0.012*
AP	r	0.016	0.142	0.223	0.009	1.000	0.270	0.049	0.108	0.211
diameter	p	0.852	0.096	0.009**	0.914	@	0.001**	0.569	0.208	0.013*
BMI	r	0.071	0.059	0.743	-0.068	0.270	1.000	0.090	0.040	0.329
	p	0.404	0.487	<0.005**	0.428	0.001**	@	0.295	0.636	<0.005**
LLMA	r	-0.060	0.026	0.065	-0.027	0.049	0.090	1.000	0.157	0.207
	p	0.480	0.763	0.448	0.752	0.569	0.295	@	0.067	0.015*
LIMA	r	-0.129	0.239	0.127	0.146	0.108	0.040	0.157	1.000	0.191
	p	0.132	0.005**	0.138	0.088	0.208	0.636	0.067	@	0.025*
RIMA	r	0.014	-0.139	0.119	-0.213	0.211	0.329	0.207	0.191	1.000
	p	0.870	0.105	0.164	0.012*	0.013*	<0.005**	0.015*	0.025*	@

@ coefficient cannot be computed
* significant at $\alpha = 0.05$
** significant at $\alpha = 0.01$

DISCUSSION

In the previous studies, liver size was measured in many diameters by clinical methods, autopsy, ultrasound, radiography and radionuclide studies.[1,2,6,12-19] Some of these authors noted positive correlation between liver size and height, liver size and sex,[1,18] while liver size has negative correlation with age.[20] In the last decade, ultrasonography has been routinely used for the study of abdominal structures.[21] It gives a quantitative and reproducible estimate of total liver span, which reflects the hepatic dullness at physical examination and of liver span below the rib margin.[22] The bedside examination of the liver does not provide any accurate information regarding the actual volume of the liver[15] and its angles. Unfortunately, a few authors studied the normal liver marginal angles and showed the upper limit of angles, no information about the correlation between the angles and physical data.

We attempted to measure the normal liver marginal angles by ultrasound and employed the physical data to predict the angles. It was found that the average of LLMA, LIMA and RIMA are 41.6 ± 4.4, 39.3 ± 4.3 and 45.9 ± 8.6 degrees. LIMA increases in male. RIMA increases with AP diameter and BMI but decreases with height. We can use the physical data to predict RIMA . Both left marginal angles correlated poorly with the physical data. We feel that it is not necessary to

routinely record the physical data for sonographic measurements.

From the physical data, age and sex, show that weight and height decreases with age, male is more obese than female. Mean BMI is 21.42 kg./m.^{2} for men, 20.89 kg./m.^{2} for women. From classification of obesity, 37.2 %, 55.5 % and 7.3 % of subjects is underweight, normal and overweight. It was indicated that the overweight subjects of the normal health check-up subjects increases the risk for medical complication such as hypertension, insulin resistance, hyperuricemia and dyslipoproteinemia.[11,23] The physical data is still worth for health check-up program.

ACKNOWLEDGEMENTS

This work was supported by the faculty of Medical Technology, Mahidol university,1997.

REFERENCES

1. Niederau C, Sonnenberg A, Muller JE, Erckenbrecht JF, et al. Sonographic Measurement of the Normal Liver, Spleen, Pancreas and Portal Vein. Radiology 1983; 149: 537-540.
2. Sullivan S, Krasner N, Williams R. The Clinical Estimation of Liver Size : a Comparison of Techniques and an Analysis of the Source of Error. Br med J 1976; 2: 1042-1043.
3. Peternal WW, Schaefer JW, Schiff L. Clinical Evaluation of Liver Size and Hepatic Scintiscan. Am J Dig Dis 1966; 11:346-350.
4. Wright R, Millward-Sadler GH, Albertti KGMM, Karran S. Liver and Biliary disease. 2nd ed. London: W.B. Saunders, 1985.
5. Leevy CM, Sherlock G, Tygstrup N. Disease of the Liver and Biliary Tract. 1st ed. New York: Rava Press, 1994.
6. Carr D, Duncan JG, Railton R, Smith CB. Liver volumn Determination by Ultasound : a Feasible Study. Br J. Radiol 1976; 49: 776-778.
7. Weill FS. Ultrasonography of Digestive Diseases. St Louis: The C.V. Mosby, 1978.
8. Swobodnik W, Herrmann M, Altwein JE, Basting RF. Atlas of Ultrasound Anatomy. 1st ed. New York: Thieme Medical Publishing, 1991.
9. Pequignot G, Chabert C, Eydoux H, Courcoul MA. Increase in the Risk of Cirrhosis as a Function of Alcohol Intake. J Stud Alcohol 1975; 35: 1059.
10. Niederau C, Sonnenberg A. Liver Size Evaluated by Ultrasound : ROC curves for Hepatitis and Alcoholism. Radiology 1984; 153: 503-505.
11. Smith LH, Plum F, Carpenter CCJ, Andreoli TE. Cecil Essentials of Medicine. 2nd ed. Philadelphia : W.B. Saunders, 1990.
12. Sapira JD, Williamson DL. How big is the Normal liver? Arch Intern Med 1979;139: 971-973.
13. Naftalis J, Leevy CM. Clinical Estimation of Liver Size. Am J Dig Dis 1963;8:236-243.
14. Pietri H, Boscaini M, Berthezene P, Durbec J P, et al. Hepatic Morphotypes: Their Statistical Individualization Using Ultrasonography. J ultrasound Med 1988;7: 189-196.
15. Zoli M, Magalotti D, Grimaldi M, Gueli C, et al. Physical Examination of the Liver: Is it still worth it ? Am J Gastroenterol 1995;9:1428-1432.
16. Chen CM, Wang JJ. Clinical and Sonographic Assessment of Liver Size in Normal Clinese Neonated. Acta Paediatrica 1993 ;82:345-347.

17. Holder LE, Strife J, Padikal TN, Perkins PJ, et al. Liver Size Determination in Pediatrics Using Sonographic and Scintigraphic Techniques. Radiology 1975;117: 349-353.
18. Deland FH, North WA. Relationship between Liver Size and Body Size. Radiology 1968; 91: 1195-1198.
19. Meidl EJ, Ende J. Evaluation of Liver Size by Physical Examination. J Gen Intern Med 1993;8:635-637.
20. DeLand FH. Normal Spleen Size. Radiology 1970;97:589-592.
21. Okuda K. Advances in Hepatobiliary Ultrasonography. Hepatology 1981;1:662-672.
22. Gosink BB, Leymaster CE. Ultrasonic Determination of Hepatomegaly. J Clin Ultrasound 1981;9:37-41.
23. Wyngaarden JB, Smith LH, Bennett JC. Cevil Textbook of Medicine. 19th ed. Philadelphia: W.B. Saunders, 1992.

PLAIN FILMS EVALUATION IN PATIENTS WITH JEJUNAL INJURY BY BLUNT ABDOMINAL TRAUMA

Patchrin PEKANAN,[1] Rachanee SINSAWATJAROEN,[1,2] Auichai KARNJANAPITAK[3]

ABSTRACT

Roentgen findings in 10 cases of jejunal injury by blunt abdominal trauma were retrospectively reviewed. Free fluid, free air, small bowel rigidity, dilatation of the duodenal loop, dilatation of the stomach and the normal gas pattern was seen. Free fluid was present in 60% of cases, free air in 30% of cases and normal gas pattern in 40% of cases. Small bowel rigidity and dilated duodenal loop occurred in association with the injury to the small bowel and the duodenal loop respectively. But the gastric dilatation did not indicate gastric injury. Without solid organ injury, the presence of free fluid should arouse the suspicion of the bowel injury. Lack of positive findings on plain films of the abdomen did not exclude bowel injury. Jejunal perforation occurred in the sites far from the fixed region in 50% of cases.

INTRODUCTION

Blunt abdominal injury is associated with small bowel rupture in 5% to 10% of cases.[1,2] The mortality rate remains in the region of 30%.[3] Significant factors affecting mortality are multiple injuries and therapeutic delay of 24 hours or more. The usual association of blunt small bowel injury with a focal blow to the abdominal wall, which may be caused by a slight blow. [4] a seatbelt or bicycle handlebar has been emphasized by Dickinson. [1] All reports in the literature agreed that the segments of the small intestine most commonly involved are duodenum near the ligament of Treitz, jejunum just beyond the ligament, and the ileum just proximal to the ileocecal valve. [5] Plain films of the abdomen are usually included in the evaluation of the blunt abdominal trauma, we conducted a retrospective study of the plain films in the patients with jejunal injury.

PATIENTS AND METHODS

Between 1991-1995, 72 patients with blunt abdominal trauma admitted to the hospital. Ten cases had jejunal injury. Plain films of the abdomen of the cases of jejunal injury were reviewed and compared with the operative findings.The detailed information was summarized in the table 1.

RESULTS

All patients were male. The age range was 18 to 62 years old ; two cases were 18-20 years old, 5 cases were between 21-30 years old, 2 cases were between 31-40 years old and a case of 62 years old. Car accident occurred in 6 cases, fall injury was seen in 3 cases and an assault was noted in one case.

1= Department of Radiology, Ramathibodi Hospital , Rama 6 Street , Bangkok 10400, Thailand
2= Department of Radiology, Haatyai Hospital , Haatyai , Songkla, Thailand
3= Department of Surgery, Ramathibodi Hospital

Plain film findings were: free fluid in 6 cases, limitation in fluid evaluation in 2 cases; free air in 3 cases; rigidity of small bowel loops in one case; dilatation of the duodenal loop in 2 cases; gastric dilatation in 2 cases; downward displacement of the splenic flexure in one case and normal gas pattern in 4 cases.

Jejunal injury was noted at the following sites: 2 inches from the ligament of Treitz (LOT) in 1 case, 1 foot from LOT in 2 cases, 2-2.5 feet from LOT in 4 cases, at mid jejunum in 1 case , at distal jejunum in 1 case and no information concerning the site of jejunal injury in 1 case.

Dilated duodenal loop was associated with loop injury in one case and without duodenal injury in another case.

Rigidity of small bowel loop was seen in associated tear of the ileal serosa.

There was no gastric injury in the cases that had gastric dilatation.

No splenic injury or surrounding hematoma in the case that had downward displacement of the splenic flexure .

Normal gas pattern was seen in both single and multiple organs/ loops injury.

No.	Age	Cause	Radiographic findings	Operative findings
1	25	assault	Free fluid Free air Rigidity of small bowel	-Rupture of distal jejunum, 3 mm diameter -Tear rectus muscle and hematoma -Tear serosa of ileum -Subserosal hemorrhage at the trans verse colon
2	27	Fall	Free fluid Normal gas pattern	-Hemoperitoneum, 2000 cc -Tear mesentery of jejunum, 2.5 feet from ligament of Treitz -Tear splenic capsule with active bleeding -Contusion of cecum and ascending colon
3	30	Car accident	-Free fluid, free air -Dilated 2 nd part duodenum	-Ruptured jejunum, 2.5 feet from ligament of Treitz -contusion of the 1st and 2nd part of the duodenum -Hematoma at tail of pancreas

4	34	Car accident	-Normal bowel gas pattern -Poor technique for free fluid evaluation	-Ruptured jejunum, 2 cm in diameter -Small amount of hemoperitoneum
5	62	Fall	-Free fluid -Gastric dilatation	-Hemoperitoneum, 500-600 cc -Two perforated sites of jejunum, 2 feet from the ligament of Treitz -Hematoma at mesentery of ileum
6	29	Car accident	-Free air -Downward displacement of splenic flexure	-Tear jejunum, 2 inches from ligament of Treitz -Hematoma at mesentery of cecum -Fluid in cul de sac , 100 cc
7	35	Fall	-Normal bowel gas pattern -Poor technique for free fluid evaluation	-Rupture and contusion proximal jejunum, 1 foot from ligament of Treitz
8	21	Car accident	-Free fluid -Normal gas pattern	Hemoperitoneum, 300 cc -Perforation of mid-jejunum -Hematoma at medial wall of ascending colon, lesser omentum, superior border of pancreas
9	19	Car accident	-Free fluid -Fixed dilated 2nd and 3rd part of the duodenum	-Perforation of jejunum, 2 feet from ligament of Treitz -Serosal tear of cecum, contusion of ascending and descending colon
10	18	Car accident	-Gastric dilatation	-Rupture jejunum,1 foot from ligament of Treitz -Left retroperitoneum hematoma

DISCUSSION

The vast majority of intestinal injuries result from automobile accidents, and impact against the steering wheel is the most frequent cause of the damage to the small bowel in adults.[6] The portion of the bowel which is most often injured is that which happens to occupy a midline position at the moment of impact. Other less common sites of damage are the first portion of the jejunum and the terminal ileum, where the intestine is fixed.

Because the small intestine and its mesentery are mobile and easily compressible, it generally escapes injury from compression forces that seriously damage solid viscera. The most common mechanism of nonpenetrating intestinal trauma involves crushing of the bowel against the spine.[7] The anatomical proximity of the abdominal wall to the anterior lordotic curvature of the lumbosacral spine accounts for a high incidence of injury to the portion of the bowel that overlies that segment of the vertebral column.

A second mechanism of small intestinal injury in blunt abdominal trauma involves tearing or shearing of the bowel and its mesentery at points of fixation. The proximal jejunum is relatively fixed at the duodenal-jejunal junction by a short mesentery and the ligament of Treitz. Similarly, the terminal ileum is fixed at its junction with the large bowel by fixation of the cecum, and by a short terminal mesentery and several peritoneal folds. Shearing forces applied to these two sites may result in tears and perforations of the bowel. Pathological fixation of the bowel also predisposes to injury. The relationship of intestinal injury to intra-abdominal adhesions has been well documented [8] and knowledge of a previous operation should increase the suspicion of possible intestinal damage in victims of blunt trauma. Similarly, fixation of the small intestine within an inguinal hernia has led to perforation. When the fixation of the intestine is in relation to the spine the possibility of injury increases.

Bursting of a distended or kinked loop of intestine is a rare mode of jejunal or ileal injury, if it occurs at all. Rupture of the duodenum is known to result from a sudden elevation of intraluminal pressure in the face of a closed pylorus and kinking at the duodenal –jejunal angle. Compressive forces applied beyond the ligament of Treitz are readily dissipated by the free movement of intestinal contents, so that bursting injuries of the small bowel are unusual.[9]

When the bowel ruptures, the serosa splits first followed by the mucosa. The submucosa is the last layer to give way.[10] Rupture of the small bowel occurs most frequently on the antimesenteric border.

The diagnosis of small bowel injury is based on the usual findings associated with damage to the abdominal viscera. These include abdominal pain, signs of peritoneal irritation on physical examination, a positive abdominal tap, an elevated leukocyte count. A negative abdominal tap and normal roentgenograms do not by any means rule out small bowel damage, particularly during the first 24 hours after injury.

Blunt wounds of the small intestine range from perforations and avulsions to intramural hematomas and serosal tears. Delayed perforation of such lesions up to 10 days after injury has been reported.[11] Injuries of the small bowel mesentery range from contusions and hematomas to avulsions. Rarely, laceration or avulsion of the major vessels occurs. Thrombosis of the mesenteric vessels is an unusual complication of blunt abdominal trauma and has been reported to cause delayed death.[12]

Jacobson et al, reported 7 cases of jejunal injury. [5] Only 2 cases showed free subphrenic air.Trapping of gas behind the transverse mesocolon was probably present in one case. Free fluid was seen at surgery in 6 cases and no detail concerning this in one case. Five cases showed nonspecific ileus, one case had no ileus and one case had air-distention of the stomach and the duodenum.

In conclusion:

1. Free air was seen only in 30% of cases of jejunal injury.
2. Free fluid was detected more , in 60% of cases, if the more sensitive examination for free fluid was used, e.g. ultrasonography, the percentage of this finding in the jejunal injury might be increased. If solid organs were not injured , the presence of free fluid should arouse the suspicion of bowel injury.
3. Normal gas pattern was present in 40% of cases.
4. Gastric gaseous dilatation was not associated with gastric injury.
5. Duodenal dilatation and rigidity of small bowel loop indicates injury to duodenum and small bowel loop respectively, however, the number of cases were small.
6. The paucity of positive findings in the roentgen examination of the abdomen does not exclude small bowel injury by blunt trauma.
7. The jejunal injury far from the fixed point was present in 50% of the cases.

REFERENCES

1. Dickinson SJ, Shaw A, Santulli TV. Rupture of the gastrointestinal tract in children by blunt trauma. Surg Gynecol Obstet 1970;130: 655-657
2. Kessler E, Chappell JS. Perforations of bowel associated with blunt abdominal trauma in children. S Afr Med J 1974; 48: 2396-2398
3. Robbs JV, Moore SW, Pillay SP. Blunt abdominal trauma with jejunal injury: a review. The Journal of Trauma 1980;20: 308-311
4. Poer DH, Woliver E. Intestinal and mesenteric injury due to non-penetrating abdominal trauma. JAMA 1942;118:11-15
5. Jacobson G, Carter RA. Small intestinal rupture due to non-penetrating abdominal injury: a roentgenological study. Amer J Roentgen 1955; 66: 52-64
6. Orloff MJ, Charters AC. Injuries of the small bowel and mesentery and retroperitoneal hematoma. Surg Clin North Am 1972;52(3):729-735
7. Williams RD, Yurko AA. Controversial aspects of diagnosis and management of blunt abdominal trauma. Amer J Surg 1966;111:477
8. Weiss M, Dreiling DA. Small bowel perforation in blunt trauma. Its relationship to previous laparotomy. Amer J Gastroent 1968; 50: 279
9. Williams RA, Sargent BA. The mechanism of intestinal injury in trauma. J Trauma 1963;3:288
10. Evans JP. Traumatic rupture of the ileum. Brit J Surg 1973; 60:119-121
11. Hicken WF, Carlquist JH. Traumatic rupture of the gastrointestinal tract by non-penetrating forces. Amer J Surg 1944; 64: 209
12. McCune WS, Keshishian JM, Blades BB. Mesenteric thrombosis following blunt abdominal trauma. Ann Surg 1952;135: 606

FOR MORE INFORMATION PLEASE CONTACT

PHILIPS MEDICAL SYSTEMS

- TEL. 745-4090 Ext. 3332
- FAX. 398-0792

Philips Electronics (Thailand) Ltd.
209/2 Sanpavuth Road, Prakanong, Bangkok 10260

PHILIPS

Let's make things better.

CT- GUIDED TRANSRECTAL DRAINAGE OF DEEP PELVIC COLLECTION

Komgrit TANISARO, M.D.

ABSTRACT

Postoperative deep pelvic collection was treated by transrectal catheter drainage under CT guidance in a 48 year - old female patient. The immediate result was dramatic. No procedure-related complications were seen. Long-term follow up was done by ultrasonography and revealed no residual or recurrent collection.

INTRODUCTION

Surgical drainage of the intraabdominal fluid collection is the conventional treatment of choice for a long time. Nowadays, radiologically interventional procedures are becoming popular. A case of transrectal drainage of pelvic abscess using the CT scan-guidance was reported.

CASE REPORT

A 42 years-old female with congenital spherocytosis was presented with hypersplenism and gallstones. Splenectomy and cholecystectomy were electively performed. Three days after the operation, she had hypovolumic shock and the second operation was done immediately. Bleeding at splenic artery stump was found and ligation was done. She still had fever and lower abdominal pain after the second operation. Transabdominal ultrasonography was performed (figure-1). The study revealed 8 cm.diameter collection at cul de sac and another 4 cm.diameter collection at left subphrenic region. Radiological intervention was offered, and the drainage procedures were followings;

1. The patient was placed in left lateral decubitus position on the CT table. Scanning was performed to locate the abscess.

2. Plastic introducer(tube) was inserted to rectum and repeated CT were obtained at the level of abscess to confirm the proper position (figure-2).

3. Without local anesthesia,16-G Chiba needle was then inserted via the plastic introducer and was directed toward the abscess by slight angulation of the needle-introducer assembly anteriorly (figure-3a,3b). The needle was advanced through the plastic introducer and the rectal wall to reach the abscess.

4. The inner stylet was removed and fluid aspiration was done to confirm the proper needle position. Foul-smell brownish fluid was obtained and sent for Gram stain. Numerous WBC and bacteria were found.

5. A 0.035 -inch guidewire were advanced through the needle and CT scanning were performed to verify the position of the guidewire (figure-4),then varying size of dilators were used to dilate the tract by Seldinger'technique before placing the 10-F Cope loop drainage catheter in the abscess cavity.

6. Suction and irrigation via the drainage catheter were done and the pigtail catheter was looped and taped to the buttock. Postprocedure CT scan was obtained (figure-5a ,5b).

Fever was subsided at the second day post drainage. The total pus contents was 200 ml. No bacterial growth was found on culture(may be

Department of Radiology, Hospital of Prince of Songkla University, Hatyai, 90112, Thailand.
e-mail ; tkomgrit@ratree.psu.ac.th

partially antibiotically treated). During placement of the catheter, the patient had normal life style.

Minimal residual collection was noted by ultrasonography performed on the 7th day post drainage. Left subphrenic collection was percutaneously aspirated using the ultrasound-guided method and non-infected fluid was obtained. The catheter was withdrawn on the 8th day post drainage and the patient could be discharged. No residual or recurrent abscess was seen at interval follow up by ultrasonography up to 5 months and the patient was asymptomatic.

Fig. 1 Preprocedural ultrasonography reveals 8 cm. diameter abscess in the cul de sac.

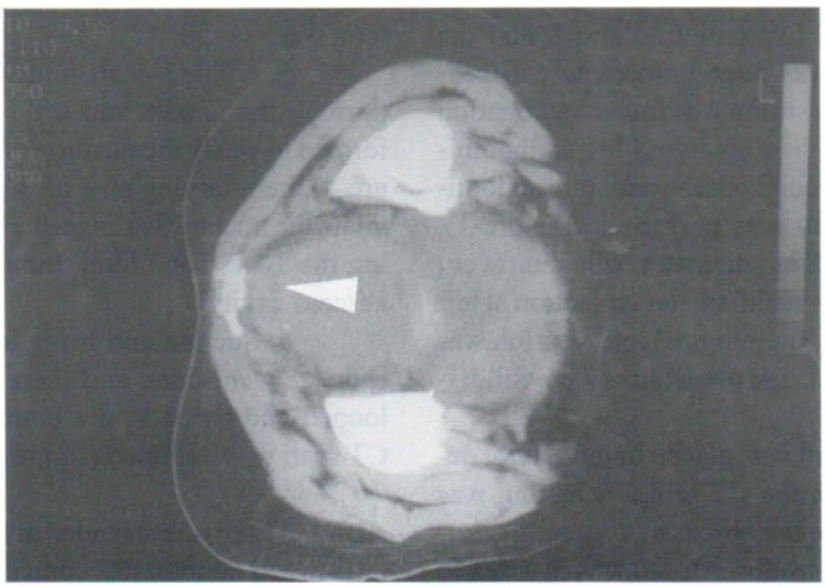

Fig. 2 Left lateral decubitus CT scan of the lower pelvis demonstrates plastic introducer in the rectum at the level of the abscess

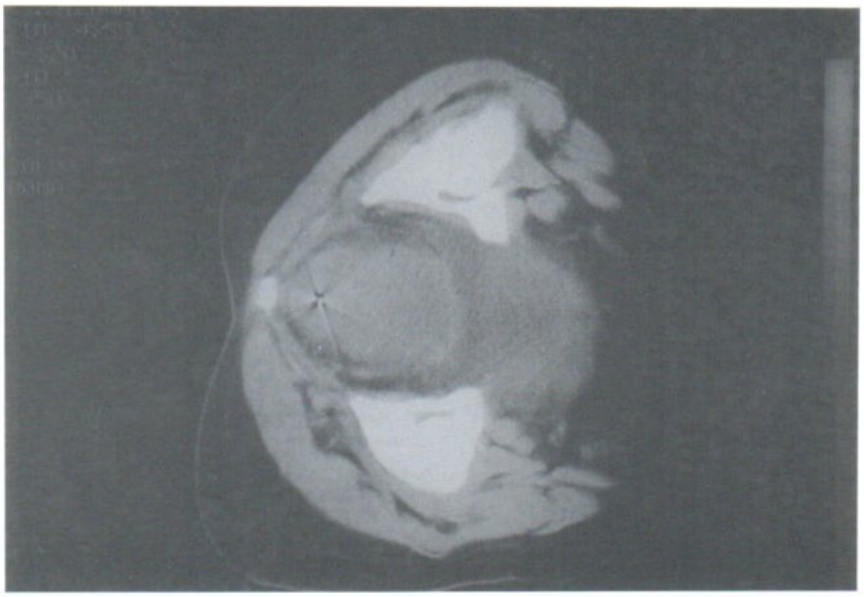

Fig. 3a. Left lateral decubitus CT scan of lower pelvis demonstrates 16-G trocar needle in the rectum at the level of the abscess.

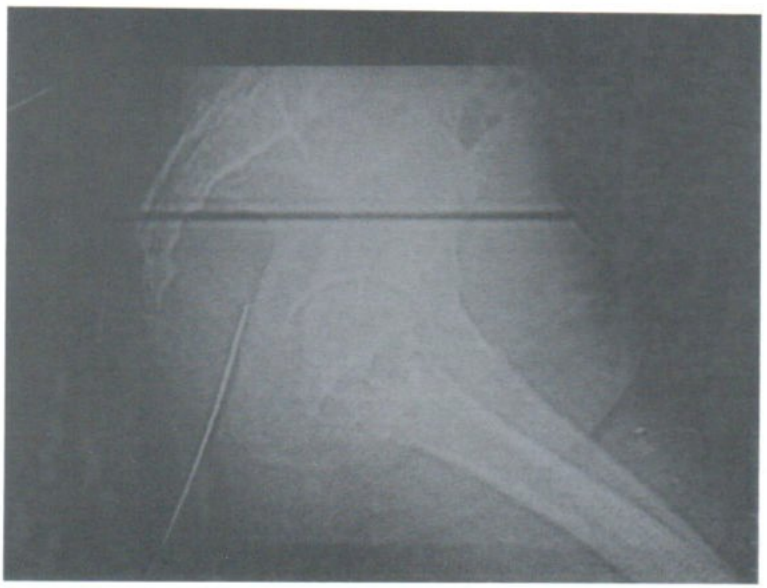

Fig. 3b. Scannogram shows the needle in the rectum before entering the abscess wall.

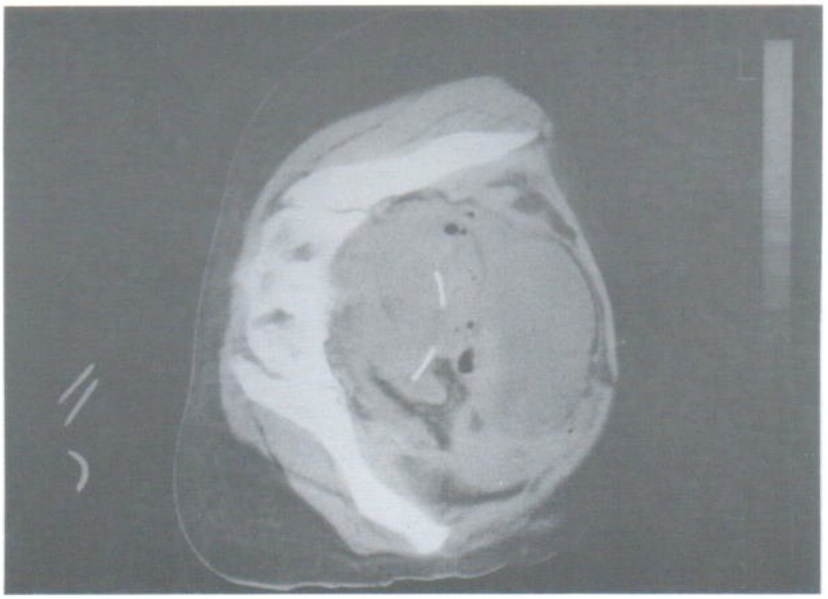

Fig. 4 After puncturing the abscess, the guidewire is inserted and was seen locating within the abscess.

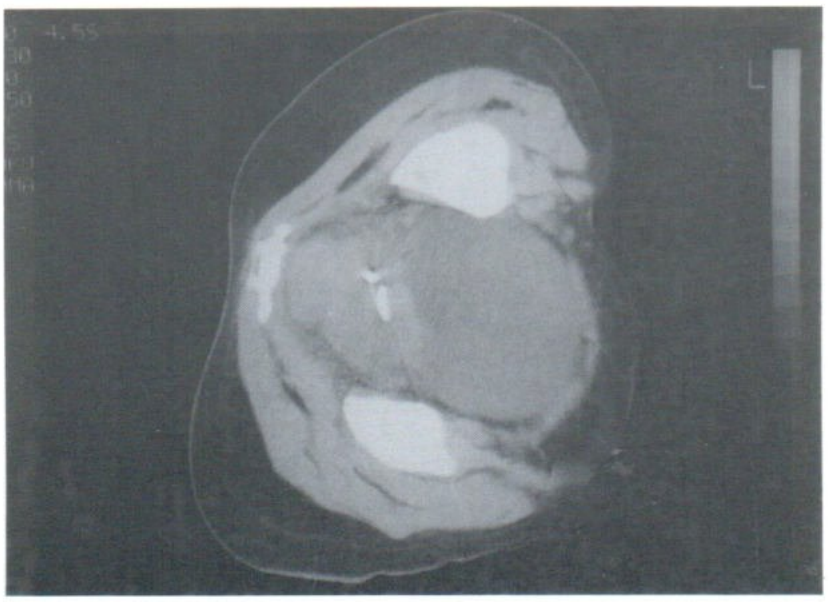

Fig. 5a. 10-F Cope type drainage catheter is shown within the abscess.

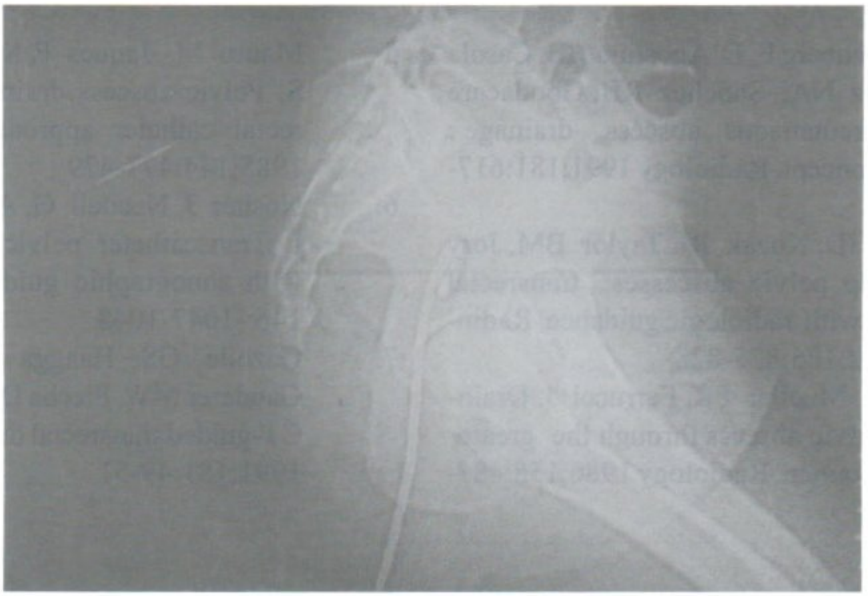

Fig. 5b. Scannogram is performed after placement of the drainage catheter in the abscess

DISCUSSION

Transcatheter drainage for abdominal and pelvic abscess is worldwide accepted to be effective and safe.[1] The anterior or anterolateral transabdominal approach is still preferred despite some of limitations.[2] Suitable access may be obstructed by bladder,neurovascular or osseous structures with the risk of intraperitoneal contamination.[3]

Butch et al.[4] reported severe pain using the posterior transgluteal approach with the risk of contamination of the muscle and fascial planes of the buttock. In addition,the greater sciatic foramen is an anatomically complex space for the passing of the sciatic nerve and the superior and inferior gluteal vessels.

Transrectal approach offers the shortest and the most direct access route to many of these collections. It has traditionally been performed by surgeons in cases of large collections which are palpable at rectal examination. Mauro et al.[5] described a technique for transrectal drainage under fluoroscopic guidance. Nosher et al.[6] described anterior transrectal drainage of palpable pelvic abscess under transabdominal ultrasono-graphic guidance. Bennett et al.[3] used combined transrectal ultrasonography and fluoroscopy for transrectal drainage of non-palpable pelvic abscess. The only one paper of CT-guided transrectal drainage has been reported by Gazelle et al.[7] and had the same technique as in this report. They found 100 % successful rate with no complication or recurrence.

CT provides accurate display of the anatomy and is not limited by the presence of bowel gas or surgical dressing. Small or deeply located abscess can be clearly visualized by CT images. Intraperitoneal and muscle contaminations can be avoided. The procedure is not painful and is well tolerated by the patient.

REFERENCES :

1. Pruett TL, Simmons RL. Status of percutaneous catheter drainage of abscesses. Surg Clin North Am 1988;68:89-105

2. vanSonnenberg E, D'Agostino HB, Casola G, Halasz NA, Sanchez RB, Goodacare BW. Percutaneous abscess drainage : current concept. Radiology 1991;181:617-626
3. Bennett JD, Kozak RI, Taylor BM, Jory TA. Deep pelvic abscesses: transrectal drainage with radiologic guidance. Radiology 1992;185:825-828
4. Butch R, Mueller PR, Ferrucci J. Drainage of pelvic abscess through the greater sciatic foramen. Radiology 1986;158:487-491
5. Mauro M, Jaques P, Mandell V, Mandel S. Pelvic abscess drainage by the transrectal catheter approach in men. AJR 1985;144:477-479
6. Nosher J, Needell G, Amorosa J, Krasna I. Transcatheter pelvic abscess drainage with sonographic guidance. AJR 1986; 146:-1047-1048
7. Gazelle GS, Haagga JR, Stellato TA, Gauderer MW, Plecha D. Pelvic abscesses: CT-guided transrectal drainage. Radiology 1991;181:49-51

CT FINDINGS OF CARCINOMATOSIS PERITONEI

Malai Muttarak,M.D., Kamonporn Wongwiwat,M.D.

ABSTRACT

OBJECTIVE 1. To illustrate the CT findings in 15 cases of carcinomatosis peritonei
2. To determine the suggestive signs of carcinomatosis peritonei.

Abdominal CT scans in fifteen patients with proven carcinomatosis peritonei were reviewed retrospectively. CT findings were evaluated for: 1) the presence, amount and distribution of ascites; 2) the morphologic appearance of the peritoneum, omentum, mesentery and bowel 3) the presence of lymphadenopathy and hepatosplenic involvement.

The peritoneum was thickened and enhanced after intravenous contrast in all cases. Ascites was present in fourteen patients and was large in eight patients. Loculation of the fluid occurred in seven patients. In three patients, despite generalized ascites; there was a notable lack of ascitic fluid in the cul-de-sac. Mesenteric infiltration was noted in twelve cases. Omental involvement was visible as soft tissue permeation of fat, enhancing nodules and/or extrinsic omental masses in nine cases. Bowel wall thickening was present in three cases. Masses in the cul-de-sac were found in five cases and were believed to represent drop metastases. Lymphadenopathy was present in four cases, liver metastasis in five cases and splenic metastasis in three cases.

Carcinomatosis peritonei should be suspected when there is enhancing peritoneal thickening accompanied by a large amount of ascites, mesenteric infiltration or omental involvement. Although not always present, bowel wall thickening, lymphadenopathy and hepatosplenic metastases also support the diagnosis.

INTRODUCTION

Abdominal computed tomography has been chosen recently as an imaging examination in patients with a wide variety of clinical symptoms. Many researchers have described various CT findings separately for each disease entity.[1-3] The purpose of our study is to illustrate the CT findings of carcinomatosis peritonei and to determine the suggestive signs for the diagnosis of the disease on the basis of our experience with fifteen patients.

MATERIALS AND METHODS

The abdominal CT findings of fifteen cases of carcinomatosis peritonei were reviewed at Maharaj Nakorn Chiang Mai Hospital. CT findings were evaluated for : 1) the presence, amount and distribution of ascites; 2) the morphologic appearance of the peritoneum, omentum, mesentery and bowel; 3) the presence of lymphadenopathy and hepatosplenic involvement. The fifteen patients were between

Department of Radiology, Faculty of Medicine, Chiang Mai University, Chiang Mai 50202 THAILAND

27 and 77 years old (mean 51 years old). Four were men and eleven were women. In nine patients, the site of primary carcinoma was known and in six, malignancy was diagnosed from fine needle aspiration biopsy of the peritoneal nodules or cytologic study of the ascites. Primary carcinoma in nine patients included two cases from the ovary and one each from the cecum, stomach, cervix, colon, breast and uterus. One case was from non-Hodgkin's lymphoma.

RESULTS

The most common CT findings of carcinomatosis peritonei were peritoneal thickening and enhancement (Fig 1A,2) present in all fifteen patients (100%). Thickening of the peritoneum could be either smooth, irregular or nodular and was detected along the anterior, lateral or posterior aspect of the peritoneum.

Ascites was the second most common CT finding (Fig.2) and was present in fourteen cases (93.3%). The amount was large in eight and loculation of the fluid occurred in seven. Absence of cul-de-sac fluid in the presence of generalized ascites was noted in three patients (Fig 1B).

Mesenteric infiltration was seen in twelve patients (80%) as soft tissue nodules in the mesentery, thickening of the mesenteric leaves or abnormal mesenteric configuration. (Fig 3,4)

Involvement of the greater omentum was present in nine cases (60%) and was manifest as soft tissue permeation of omental fat, enhancing nodules and/or an omental mass (Fig 2). Bowel wall thickening (Fig.4) was present in three patients (20%). Masses in the cul-de-sac were found in five patients (33.3%) and were believed to represent drop metastases. Lymphadenopathy was present in four patients (26.6%). Liver metastasis was seen in five patients (33.3%) and splenic metastasis in three patients (20%). Peritoneal tumor implant was calcified in one patient (6.6%)

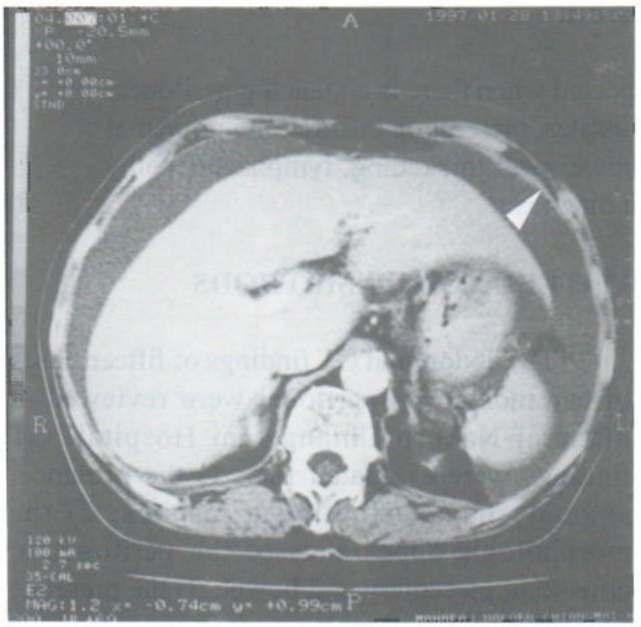

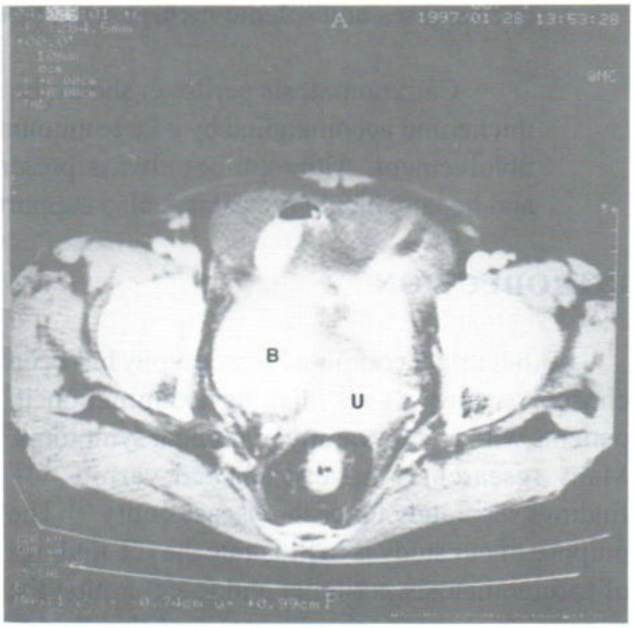

A 66 -year-old woman with carcinomatosis peritonei due to metastatic adenocarcinoma.

Fig 1A. Showing parietal peritoneal thickening and enhancement (arrow head) and ascites.

Fig 1.B. Showing absence of ascitic fluid in cul-de-sac in the presence of massive ascites. (B=urinary bladder, U = uterus)

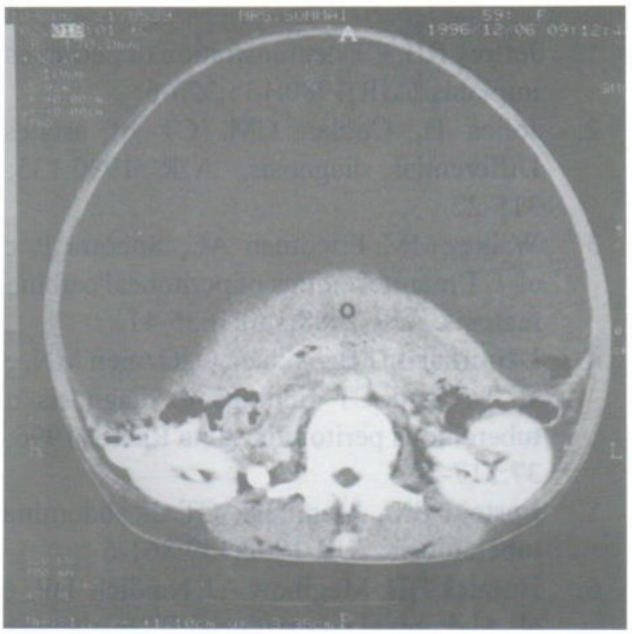

Fig 2. Carcinomatosis peritonei due to metastatic adenocarcinoma in 59-year-old woman. Contrast-enhanced CT scan shows massive ascites, omental cake (O) and thickened, enhanced parietal peritoneum (arrow).

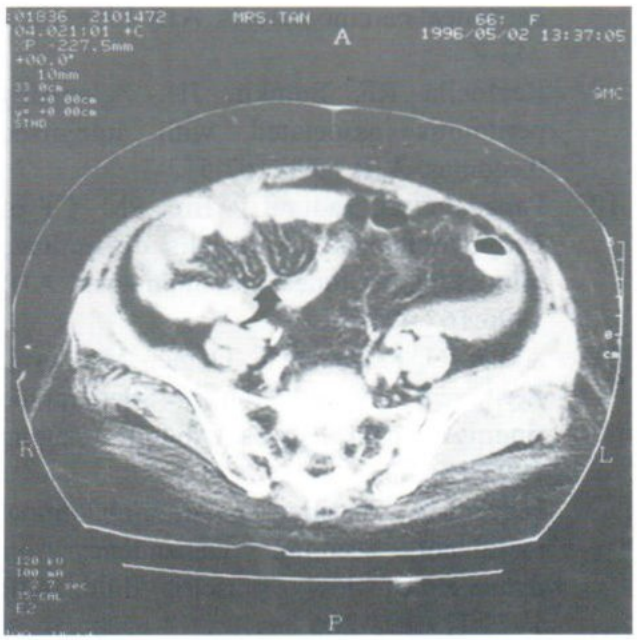

Fig 3. Contrast-enhanced CT scan demonstrates thickened mesenteric leaves (arrow).

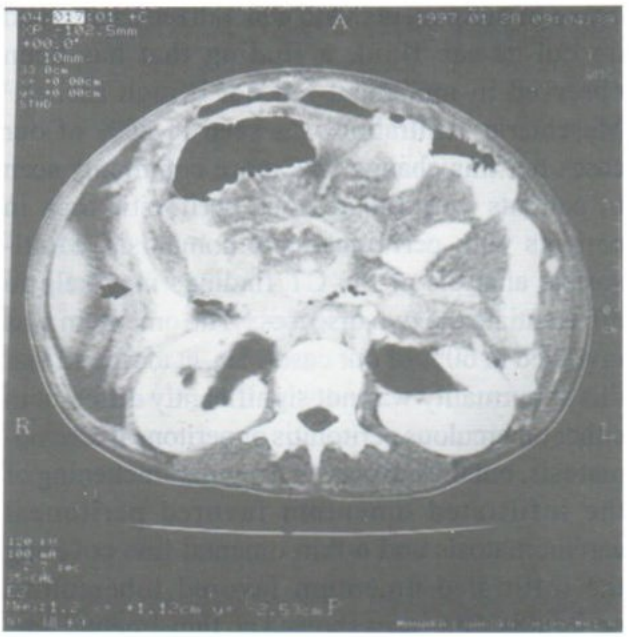

Fig 4. A 22-year-old woman with carcinomatosis peritonei due to disseminated NHL. Contrast enhanced CT scan shows thickened wall of ascending colon (arrow), ascites and thickened mesenteric leaves.

DISCUSSION

Thickening and contrast enhancement of the peritoneum were the most useful signs of malignancy.[1] However, this appearance is not specific and is known to occur in tuberculous peritonitis.[4-8] sclerosing peritonitis,[9] leiomyomatosis peritonealis disseminata,[10] and peritoneal mesothelioma.[11]

Ascites is common in many pathologic conditions ranging from abnormal cardiogenic, metabolic, inflammatory and neoplastic conditions. Although ascites alone is usually benign, ascites with co-existing mass can be either benign or malignant.[1,2,8,9] Tuberculous peritonitis is difficult to differentiate from peritoneal carcinomatosis. However, Ha, et al[8] reported that the amount of ascites in patients with tuberculous peritonitis was less than the amount in patients with peritoneal carcinomatosis. The amount of

ascites was large in more than half of our patients. Three of our patients with generalized ascites had no cul-de-sac fluid, a finding that has been observed in malignant but not benign ascites.[3] Mesenteric infiltration was seen in 80% of our cases but this change was more commonly seen in patients with tuberculous peritonitis than in patients with peritoneal carcinomatosis. Multivariate analysis of the CT findings may help to differentiate the two diseases.[8] The omentum was involved in 60% of our cases. Ha, et al[8] found that this abnormality was not significantly different in either tuberculous peritonitis or peritoneal carcinomatosis, but they observed irregular thickening of the infiltrated omentum favored peritoneal carcinomatosis and a thin omental line covering the infiltrated omentum favored tuberculous peritonitis. Our cases showed no thin omental line.

Bowel wall involvement was seen in three patients and was manifest by wall thickening without obstruction. One of these patients had NHL of the ascending colon. Masses in the cul-de-sac were found in five patients and were believed to represent drop metastases because the cul-de-sac is one of the four most common sites of malignant seeding in the peritoneum.[12] Lymphadenopathy, splenic and liver involvement were each found in less than half of the cases. Calcification of peritoneal tumor implant was seen in a case from a metastatic adenocarcinoma (primary unknown). This finding was not helpful in making a diagnosis because it can be mimicked by other conditions such as tuberculous peritonitis[8] or old intraperitoneal barium.[3]

CONCLUSION

CT findings in carcinomatosis peritonei include an enhanced thickened peritoneum, ascites, mesenteric infiltration, omental involvement, bowel wall thickening, lymphadenopathy and hepatosplenomegaly. Although most of the findings may overlap with other diseases, a combination of CT findings can make the diagnosis of carcinomatosis peritonei.

REFERENCES:

1. Jeffrey RB. CT demonstration of peritoneal implants. AJR;1980:135:323-6.
2. Jolles H, Coulan CM. CT of ascites: Differential diagnosis. AJR 1980;135:-315-22.
3. Walkey MM, Friedman AC, Sohotra P, et al. CT manifestations of peritoneal carcinomatosis. AJR 1988;150:1035-41.
4. Demirkazik FB, Akhan O, Ozmen MN, et al. US and CT findings in diagnosis of tuberculous peritonitis. Acta Radiol 1996;-37:517-20.
5. Epstein BM, Mann JH. CT of abdominal tuberculosis. AJR 1982;139:861-6
6. Hulnick DH, Megibow AJ, Naidich DP, et al. Abdominal tuberculosis: CT evaluation. Radiology 1985;157:199-204.
7. Zirinsky K, Auh YH. Knee land and JR, et al. Computed tomography, sonography, and MR imaging of abdominal tuberculosis. J Comput Assist Tomogr 1985;9:961-3.
8. Ha HK, Jung JI, Lee MS, et al. CT differentiation of tuberculous peritonitis and peritoneal carcinomatosis. AJR 1996;167:-743-8
9. Reginella RF, Sumkin JH, Sclerosing peritonitis associated with luteinized thecomas. AJR 1996;167:512-3.
10. Papadatos D, Taourel P, Bret PM. CT of Leiomyomatosis peritonealis disseminata mimicking peritoneal carcinomatosis. AJR 1996;167;475-6.
11. Akhan O, Kalyoncu F, Ozmen MN, et al. Peritoneal mesothelioma: Sonographic findings in nine cases. Abdom Imaging 1993;18:280.
12. Meyer MA. Distribution of intra-abdominal malignant seeding: Dependency on dynamics of flow of ascitic fluid. AJR 1973;119:198-206.

PERCUTANEOUS TRANSLUMINAL ANGIOPLASTY FOR RENOVASCULAR HYPERTENSION IN ARTERITIS ; EXPERIENCE IN THAILAND

PRABHASAVAT Krisdee M.D., VANAPRUKS Saroj M.D., KRUATRACHUE Chutakieat M.D., CHAITEERASUWET Somyot M.D., SUCHATO Nasuda M.D.

ABSTRACT

PURPOSE To evaluate the result of the treatment of the percutaneous transluminal angioplasty (PTA*) for renovascular hypertension in arteritis.

MATERIAL and METHODS There were 14 patients, 8 males, 6 females, age 18-53 years, mean 31 years. Five patients had bilateral renal artery stenosis. But PTA was performed in both renal arteries in only 1 case. The transfemoral route was used to treat 14 stenoses, except one patient who had complete aortic occlusion, transaxillary route was used. The PTA was performed, by exchange balloon catheter technique. Follow-up examination included blood pressure, renogram, and medication evaluation.

RESULTS Technical success rate was obtained in 14 lesions (93%) in 13 patients (93%). Only one failure occured in the very tight proximal stenosis of the renal artery. Clinical sucess rate was 88 % (improvement of hypertension, or discontinue medication). No complication was occured except there was temporary spasm/thrombosis of renal artery in one case (7%).

CONCLUSION The renal angioplasty in non-specific arteritis (Takayasu's arteritis) is effective and safe procedure. The results are good, and there is low acceptable complication. There is no long -term follow up examination.

PTA*= Percutaneous Transluminal Angioplasty

INTRODUCTION

In Thailand the non specific aortoarteritis or Takayasu's disease was not uncommon, especially in the young adult females, who were hypertensive. We diagnosed Takayasu's arteritis by clinical signs, and symptoms, such as headache, fever, hypertension, unequal, or absent peripheral pulse, abdominal bruit or abdominal pulsation, increasing erythrocyte sedimentation rate etc.. Then we performed an angioaortography to evaluate the entire aorta and its branches. It resulted in irregularity of the intima of endothelium, stenosis of artery, occlusion of aorta, or origin of its branches, and dilatation of the arterial lumen. Of all these, stenosis and occlusion were the most common ones, that involved abdominal aorta and renal arteries. When there was renal artery steno-

Department of Radiology,Faculty of Medicine, Siriraj Hospital,Bangkok 10700,Thailand.

sis, the patients eventually were hypertensive.

PATIENTS AND METHOD

Between January 1985 and January 1987, there were 14 patients, 8 males, 6 females, age range between 18-53 years, mean age was 31 years. All of them had the clinical diagnosis of renovascular hypertension caused by Takayasu's disease. Their aortography showed evidence of aortitis and/or arteritis especially in main arterial branches. The abdominal aorta were involved by irregularity, stenosis, and dilatation in 11 cases out of 14 cases, or 78.57% (Fig.1).

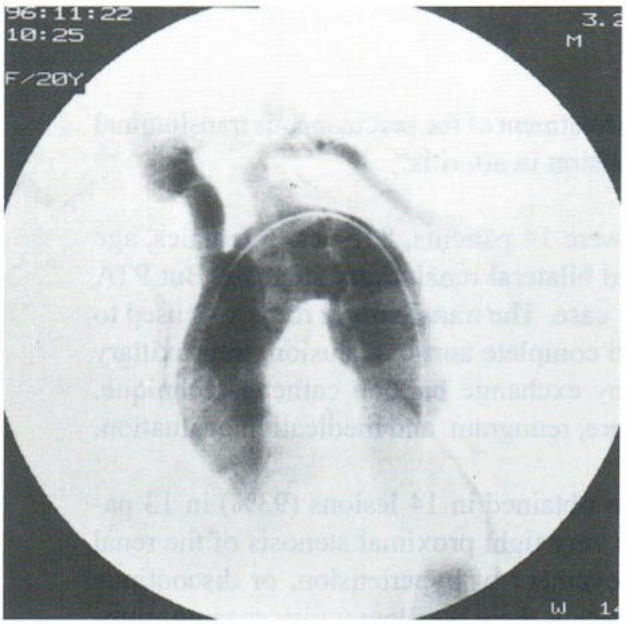

Fig. 1A

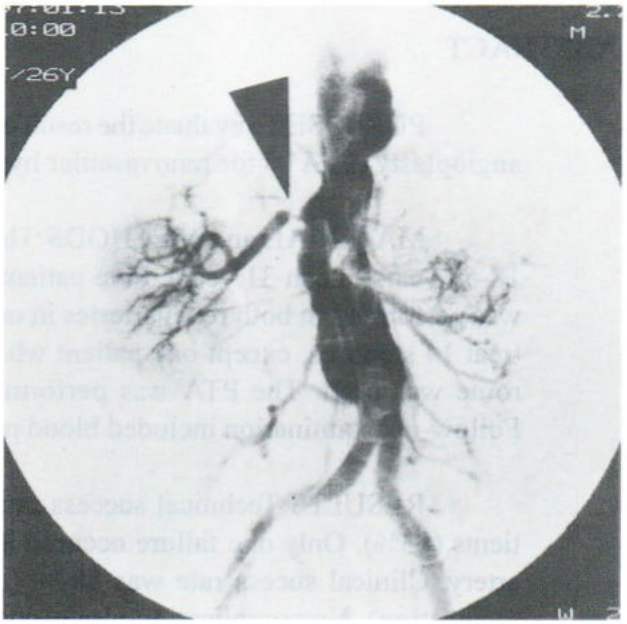

Fig. 1B

Fig. 1C

The patient was female , 20 years old.

Fig. 1A , B and C : Thoracic and abdominal aortography and ultrasonography showed that there were irregularities and aneurysmal dilatation of the entire aorta. There were also segmental narrowing of aorta .

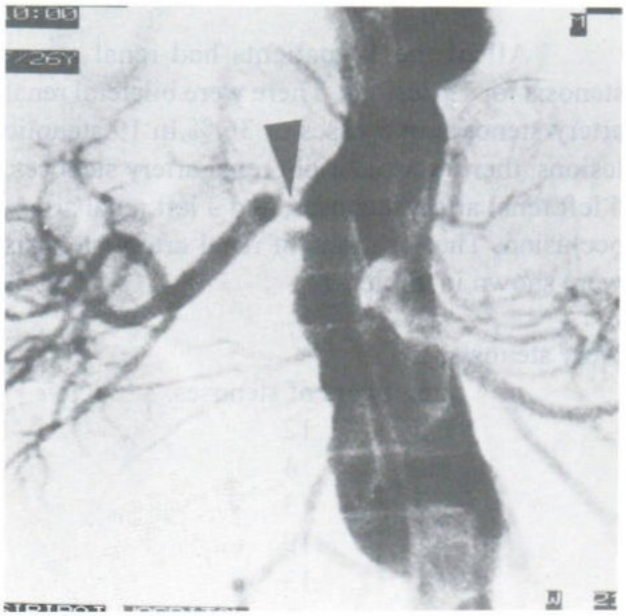

Fig. 1D

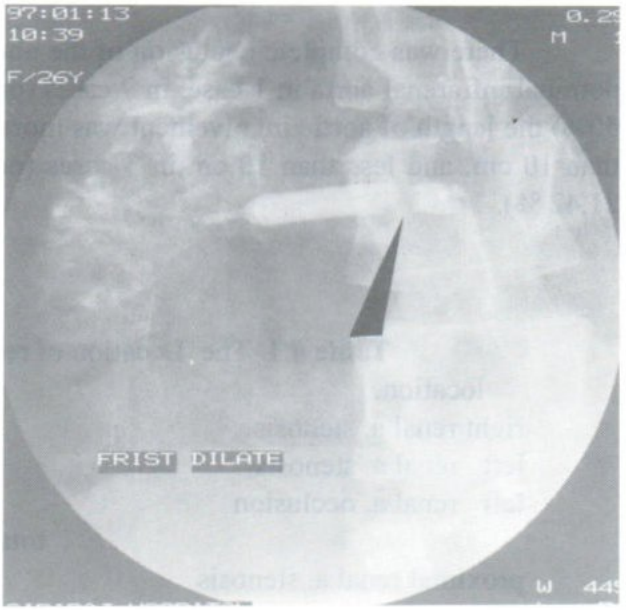

Fig. 1E

Fig. 1F

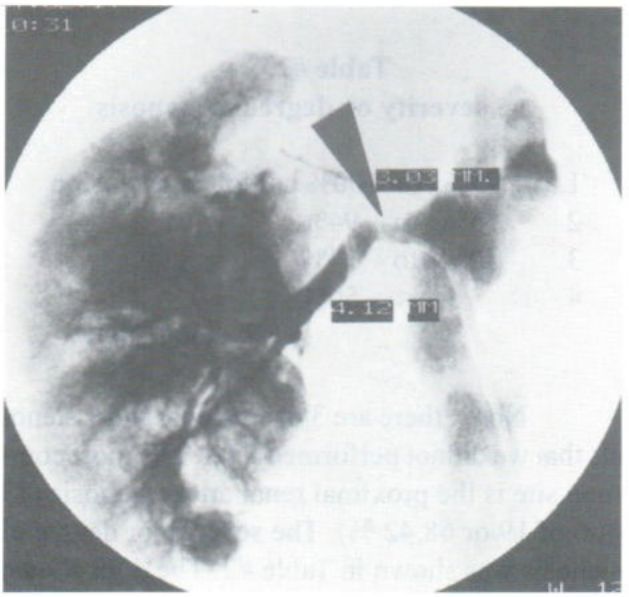

Fig. 1G

Fig.1 D There were 80% right renal artery stenosis, and complete occlusion of the left renal artery. And after PTA, fig.1 E,F showed there was reopening of the right renal artery, with minimal residual stenosis 25% ,fig 1G.

There was complete occlusion of the abdominal infrarenal aorta in 1 case. In 7 cases (or 50%) the length of aortic involvement was more than 10 cm. and less than 10 cm in 3 cases (or 21.42 %).

All of the 14 patients had renal artery stenosis for 19 lesions. There were bilateral renal artery stenoses in 5 cases or 36 %. In 19 stenotic lesions, there were 12 right renal artery stenoses, 4 left renal artery stenoses, and 3 left renal artery occlusion. The locations of renal artery stenosis were shown in Table #1.

Table # 1 The Location of renal artery stenosis.

location.	numbers of stenoses.
right renal a. stenosis	12
left renal a. stenosis	4
left renal a. occlusion	3
total	19
proximal renal a. stenosis	13
proximal and mid renal a. stenosis	3
mid renal a.stenosis	2
total	19

Table #2.

	severity or degree of stenosis	**No.# of stenoses** before PTA	after PTA
1.	> 95% to 100% complete occlusion	1	0
2.	75% to 94%	8	1
3.	50% to 74%	2	3
4.	< 50%	4	11
	total NO#	15	15

Note : there are 3 occlusions, and 1 stenosis that we didnot performed PTA. The most common site is the proximal renal artery stenosis (13 out of 19 or 68.42 %). The severity or degree of stenosis was shown in Table #2. The digit shown in percentage was the stenotic part of arterial lumen from the original normal lumen diameter. There were 12 renal artery stenoses (from total 19) and the degree of stenosis was more than 75%.

Fifteen renal angioplasty were performed in 14 patients. In 5 patients who had bilateral renal artery stenoses, the angioplasty was performed at both renal arteries in 1 case, and in 2 patients renal angioplasty was performed at the side where there was the most stenotic renal artery. In 3 patients who had complete left renal artery occlusion, the angiopasty was performed, at contralateral (right) stenotic renal artery.

Aspirin (300 mg) was administered orally on a daily basis beginning 2-3 days before, and at least 7 days after the PTA procedure. The transfemoral route was used to treat 14 renal artery stenoses. In 1 patient who had complete abdominal aortic occlusion just below the renal artery, transaxillary route was used, Fig.2.

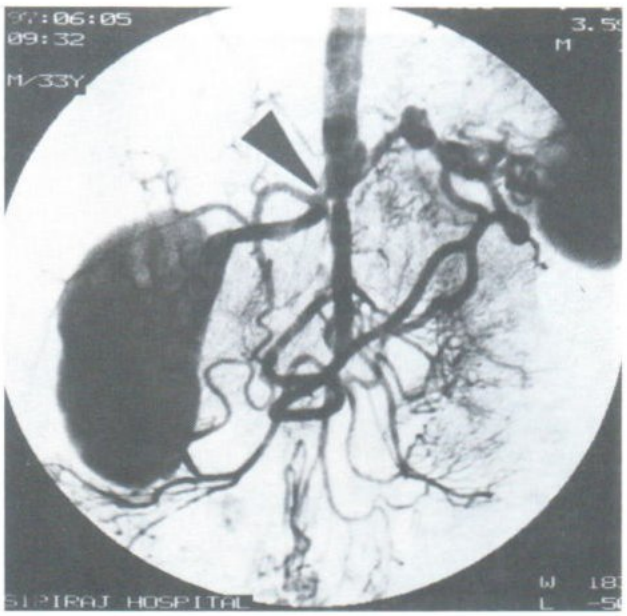

Fig. 2A

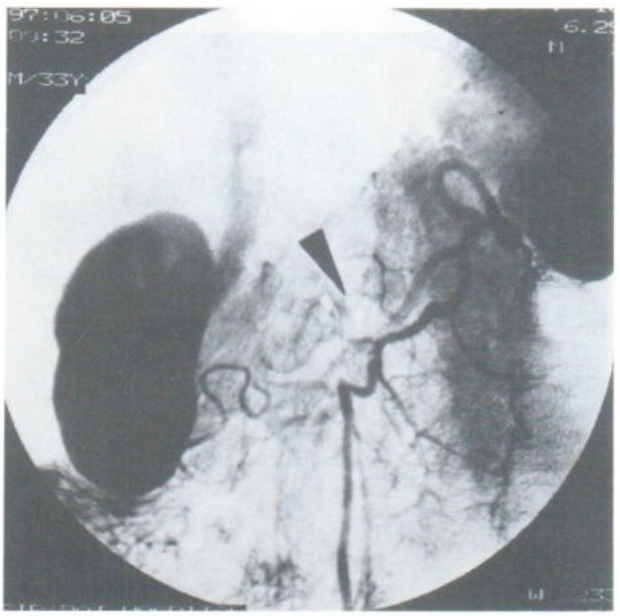

Fig. 2B

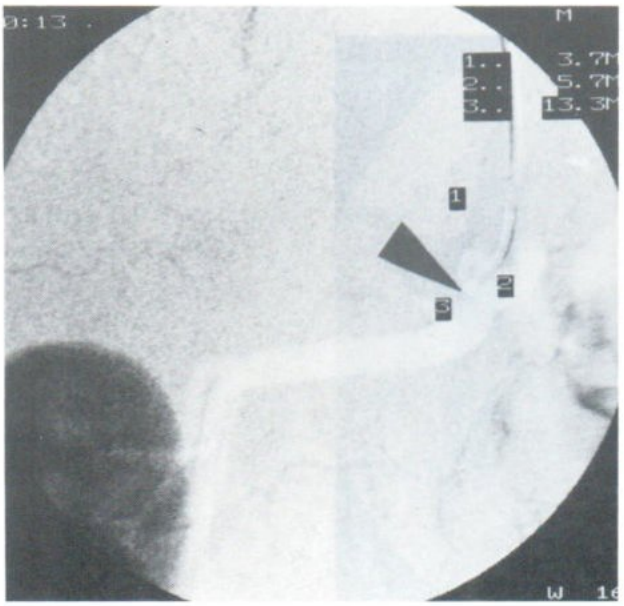

Fig. 2C

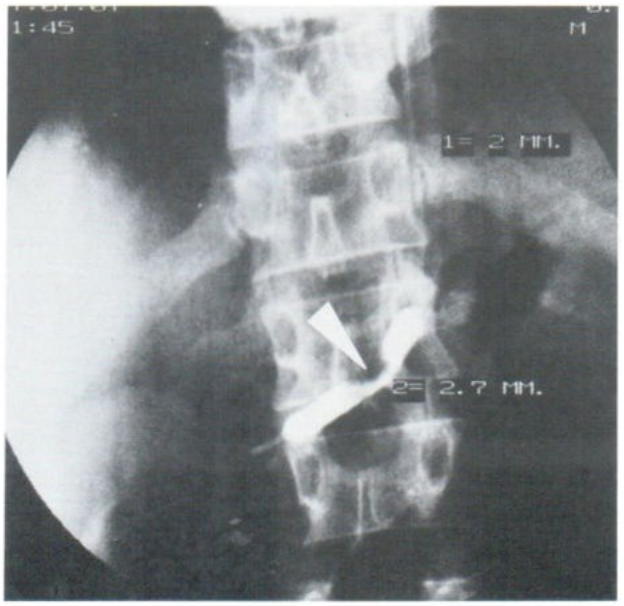

Fig. 2D

The patient was male, 33 years old.

Fig.2 A-B The abdominal aortography (from left axillary puncture) showed complete aortic occlusion at the infra renal level. There was right renal artery stenosis 60% (fig.2 C). During PTA, there was "waist" of the balloon at the stenosis (fig.2D).

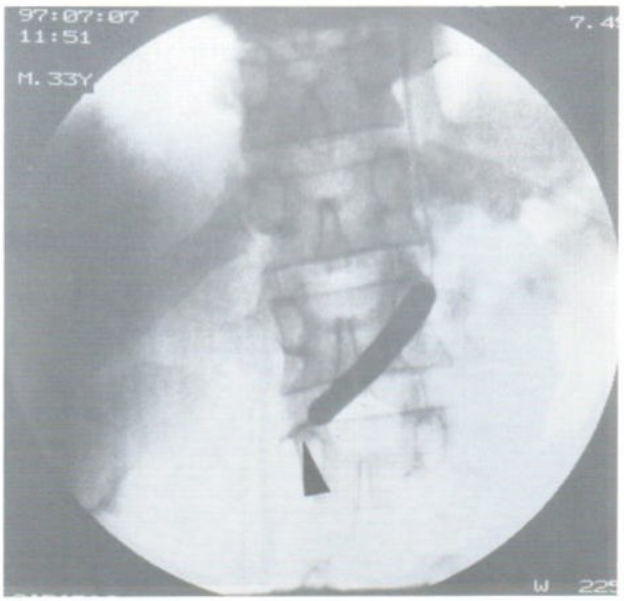

Fig. 2E

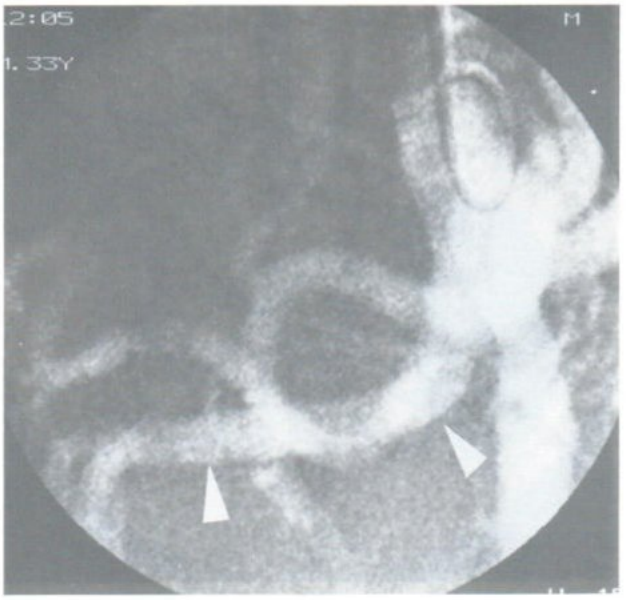

Fig. 2F

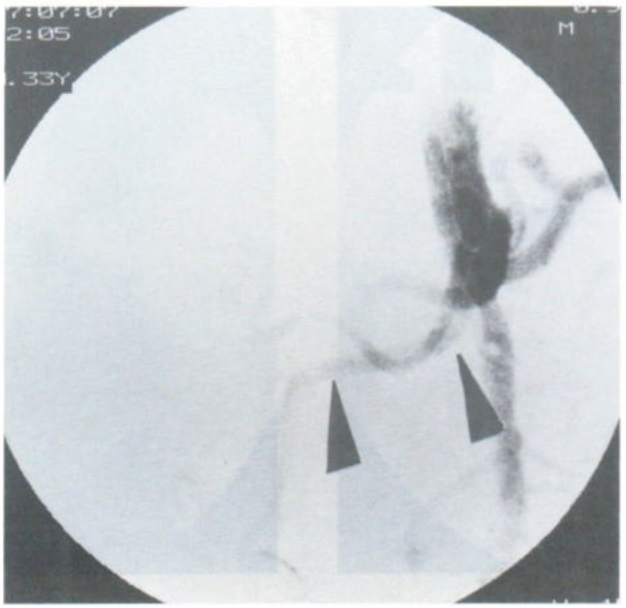

Fig. 2G

Fig. 2E After applying a high pressure by manual injection of contrast media 3-5 times, the stenosis disappeared substantially (fig 2 E). The right renal artery was normal in size without residual stenosis (fig.2F-G). The blood pressure of the patient before PTA was 180/110 and BP after PTA was 140/90 mm.Hg.

All of the 14 patients had aortography and captopril renogram studies on the day before the PTA was performed.

The balloon catheters were 5 french size,and the diameter of the balloons were 4 or 6 mm. depending on the actual size or corrected size of the patient's renal artery. The selective renal angiography was performed,by cobra-head catheter. Then the J-shape guide wire was placed in the stenotic renal artery and the PTA was performed by appropriate size balloon catheter by using standard exchange technique. When the balloon was in the appropriate position.The balloon was inflated by manual injection of contrast medium with 5 ml syringe,3-5 times, for 60 sec. each until the balloon "waist" disappeared substantially. The pressure in the balloon by this manual injection was raised to 12-15 atmospheric pressure. During 60 sec. of inflation of the balloon, we infused normal saline with 3,000 units of heparin into the renal artery through the lumen in the balloon catherter, for prevention of renal artery thrombosis. We did not use over-sized balloon catheters to avoid arterial rupture.In some cases, pethidine was injected intramuscularly to the patient who had "back pain" during PTA procedure. Immediately after the procedure, the angiography was obtained to access the adequacy of angioplasty. ECG and systemic blood pressure were monitored continuously throughout the procedure.

Angioplasty was considered as followings
1. technically suscessful ,if there is residual stenosis of renal artery lumen less than 30%, after PTA.
2. technically good improvement,if there is residual renal artery stenosis between 30-60%
3. technically mild improvement,if there is residual renal stenosis more than 60% or the postangioplasty renal arterial lumen is larger less than 15% from previous stenotic lumen.
4. technically a failure, if there is no significant change in stenosis.

The clinical results of angioplasty was judged as the followings.
1. cure, when the patient had normal blood pressure in 1month after PTA.
2. improved,when there is at least 15% reduction in diastolic blood pressure or diastolic blood pressure is between 90-110 mm.Hg. and the patient takes less antihypertensive medications.
3. failed,when there is no significant change in blood pressure after the procedure.

All patients who had been cured or improved were considered to have benefit from angioplasty. The follow up examination includes blood pressure, renogram, and medication evaluation.

RESULTS

Initial total technical success was achieved in 14 lesions out of total 15 lesions (93%) in 13 patients out of 14 patients (93%) shown in Table # 3.

Table No.3 Technical results.

	% Residual stenosis after PTA	No.# of renal a.
A. Good success	< 30%	6
B. Good improvement	30-60%	5
C. Mild improvement	> 60%	3
D. Fail	No significant change	1

Blood Pressure and,clinical results are shown in table # 4.

Table No.4	**No.# of patients.(total=14)**	
Diastolic pressure(mm.of Hg.)	before PTA	after PTA
> 110	5	2
90-110	9	5
80-90	0	7
Mean diastolic pressure	103	83 mm.Hg.
clinical results	**patients**	
cure	6	
clinical improvement	7	
fail	1	

The total clinical benefit from PTA is 13 cases out of 14 cases or 93 %. The mean blood pressure of these patients before PTA was 167/ 103 mm.Hg. and after PTA, mean BP was reduced to 130/83 mm.Hg. The number of antihypertensive drugs nesscessary to relieve hypertension before PTA was 3.1 types of medications (range 2-4), and after PTA the number of drugs was reduced to 1.8 (range 1-4).

There was no mortality but there was one technical failure (7%) because there was very tight stenosis at the origin of renal artery.

There was one complication in one case, who was 44 years old, female patient. There was renal artery spasm. The patient had severe aortitis and bilateral renal artery stenosis of more than 78%.

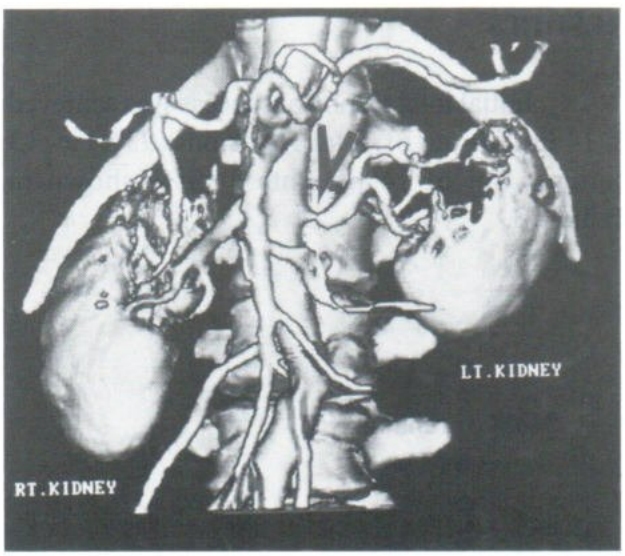

Fig. 3A

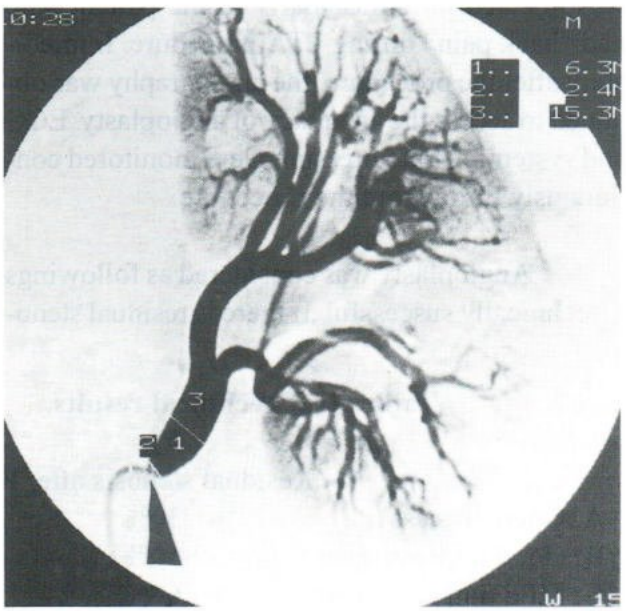

Fig. 3B

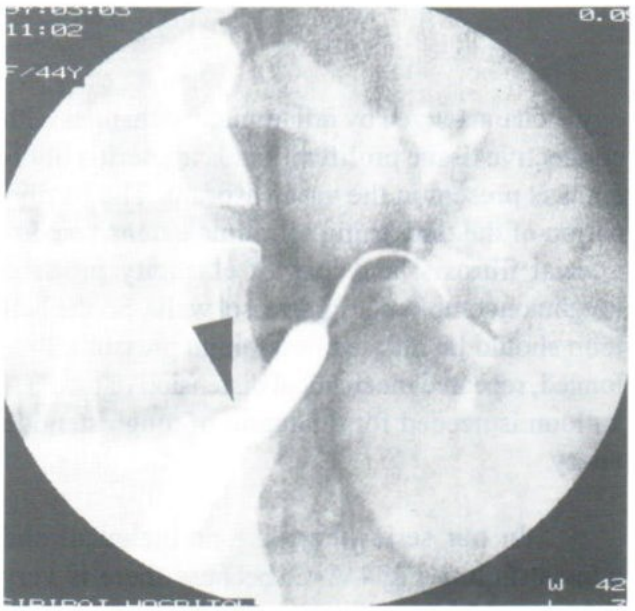

Fig. 3C

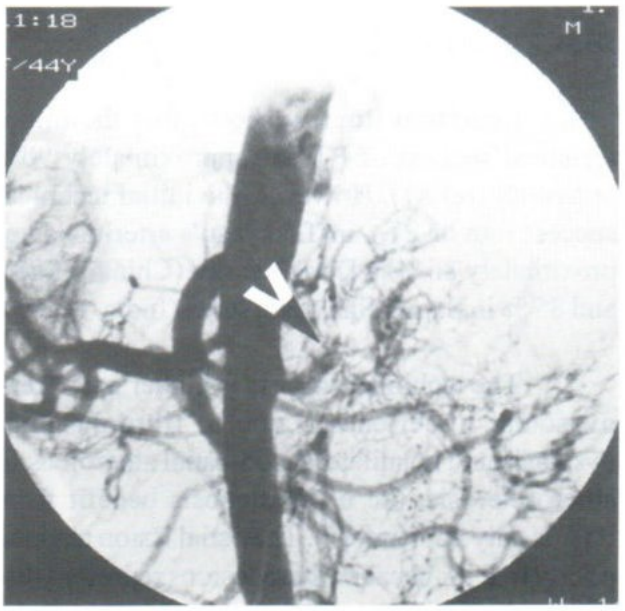

Fig. 3D

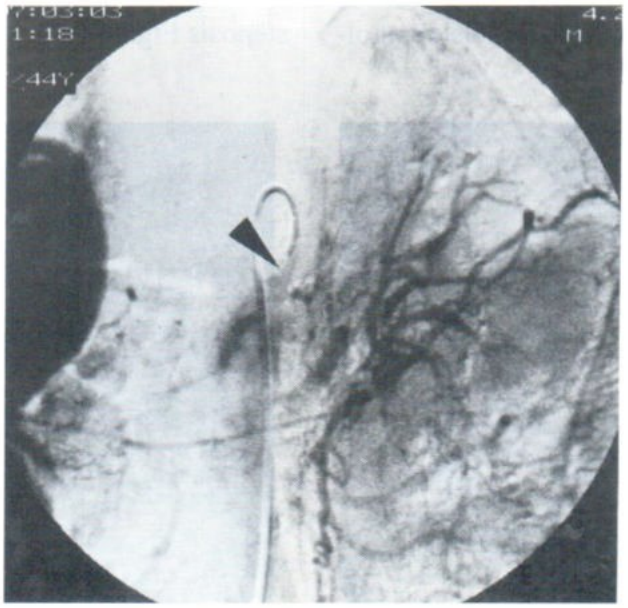

Fig. 3E

Fig. 3 A was a reconstrution of the computed tomoangiogram (CTA) of this patient and Fig.3 B was a selective left renal angiogram showed proximal renal artery stenosis. Immediately after PTA (fig.3 C), there was spasm of the left renal artery. Fig.3 D and E were early and late arterial phase and there was transient left renal ischemia. The conservative medical treatment without surgery obtained a good result.

One month follow up angiography study in 2 cases showed there is no evidence of recurrent renal artery stenosis.

DISCUSSION

Literature Review shows that the initial technical success of PTA is approximately 90% in overall (ref.#1). However, the initial technical success rate of PTA in Takayasu's arteritis is approximately 86 % in Dong's series (China-ref.#8), and 85 % in Sanjiv Sharma's series(India- ref #3).

The technical success is higher in the renovascular hypertension due to fibromuscular dysplasia,and in unilateral non-ostial atheromas.In atherosclerosis, the ostial stenosis benefit from PTA is only 25%(ref.#1). The ostial lesion respond poorly to PTA because these lesions represent disease in the aorta,and not in the renal artery. To be effective, angioplasty must be performed, with the balloon parallel to the direction of the involved vessel. In Takayasu's arteritis,there are panarteritis involving all layers of the vessels. Histopathology is characterized by inflammatory changes with connective tissue proliferation. Endarteritis obliterans is present in the vasa vasorum. The combination of the thickening of intima,extensive periarterial fibrosis, and loss of elasticity produce tough,noncompliant, rigid vessel walls. So the balloon should be inflated under high pressure. Prolonged, repeated mechanical distension of the PTA balloon is needed for dilatation of tough stenotic artery.

In our series,there is one technical and clinical failure Fig.4 A-C. because there is very tight stenosis at the origin of renal artery and there is involvement of abdominal aorta.The .032 guide wire can pass through the stenosis but the 5F balloon catheter cannot pass through the very tight stenosis Fig.#4 C.

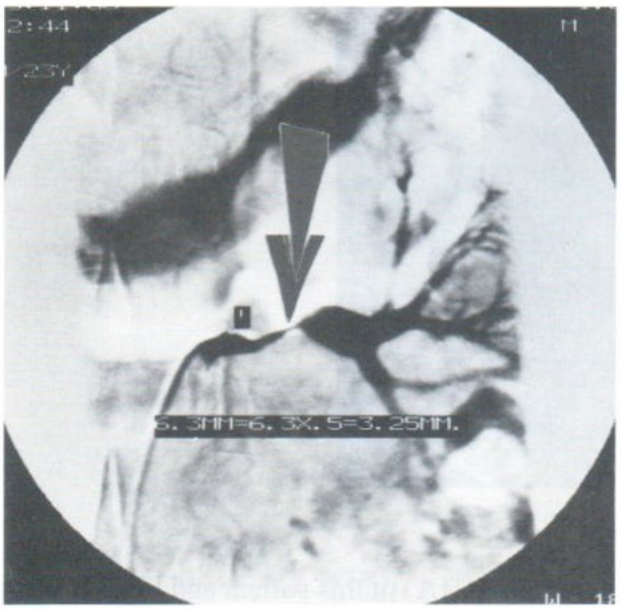

Fig. 4A

A 33 year -old –man.

Fig.4A The selective left renal angiogram showed the tight proximal stenosis (98%) of left renal artery.

Fig. 4B

Fig. 4B The MRA showed normal right renal artery but there was no signal from the stenotic part of the left renal artery be cause there was tight stenosis.

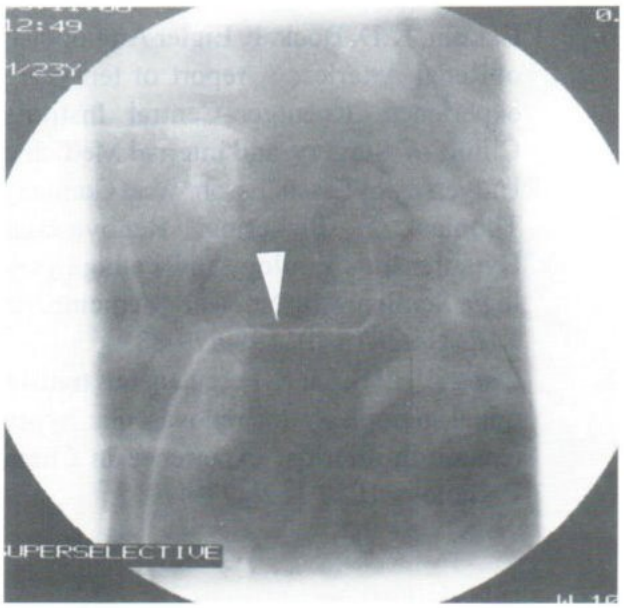

Fig. 4C

Fig .4C showed the guide wire can be passed through the stenosis but the 5F.catheter cannot be passed through the stenosis.

However, there was another case who had severe proximal right renal artery stenosis more than 95% but we can pass 028 guide wire through the stenosis and we used thin wall 4F catheter for exchange to 035 guidewire. After that 5F balloon catheter can pass through the stenosis and PTA was sucessful with very good result. The residual stenosis was reduced from 95% to 15% or about of normal size renal artery.

The value of PTA in the management of renovascular hypertension caused by Takayasu's arteritis has been described infrequently in the literature. In China, Dong (ref.#8) reported the experience with PTA in 30 patients, of these 22 patients were Takayasu's disease. The PTA was sucessful in treating hypertension in 86% and there were 7 complications (excessive bleeding in 3 patients, pseudoaneurysm in 1,occlusion of renal artery in 2 and dissection of renal artery in 1). In India, Sanjiv Sharma (ref.#3) reported that the PTA in Takayasu's arteritis technically sucessful in treating 28 lesions (85%) in 17 patients(85%). Clinical cure, or improvement was achieved in 14 (82%) of these 17 patients. There was only one major complication that nessitated emergency surgery due to rupture of renal vein in one patient. They described technical failure related to the unfavorable angiography. The diseased renal artery arose from a stenoses or tortuous segment of aorta, and showed tight proximal stenosis.

CONCLUSION

In our experiences, the renal angioplasty in renovascular hypertensive patient, caused by Takayasu's arteritis, is an effective and safe procedure. The technical, and clinical results are very good (93%). There is low and acceptable minor complication (7%) from renal arterial spasm. The PTA of renal artery stenosis is the best method of treating renovascular hypertension.

REFERENCES

1. Carl Tack, Thomas A. Sos Radiologic Diagnosis of Renovascular Hypertension and Percutaneous Transluminal Renal Angioplasty. Seminars in Nuclear Medicine, vol XIX, No.2 (April),1989:89-100.
2. Jan klinge, Willem P.T.M.Mali, Carl B.A.J.Puijlaert. Percutaneous Transluminal Renal Angioplasty: intial and long-term results. Radiology 1989;171:501-506.
3. Sanjiv Sharma, Anita Saxena ,Kewal K. Talwar et al Renal Artery Stenosis Caused by Nonspecific arteritis (Takayasu's disease): Results of treatment with Percutaneous Transluminal Angioplasty. AJR 158;417-422,February,1992

4. Guy E.Wilms, Albert L. Baert, Antoon K. Amery. Short-term Morphologic Results of Percutaneous Transluminal Renal Angioplasty as determined with Angiography Radiology 1989;1019-1021.

5. Philippe Cluzel, Alain Raynaud, Bernard Beyssen Stenoses Of Renal Branch Arteries in Fibromuscular Dysplasia: Results of Percutaneous Transluminal Angioplasty. Radiology 1994;193:227-232

6. E. Lohr, K.D. Bock, F. Eigler Angioplasty of Renal Arteries: A report of ten year's experience. Roentgen-Central Institute. Clinic of Surgery and Internal Medicine. University of Essen, Essen. West Germany.

7. Thomas G. Pickering. Renovascular Hypertension: Etiology and Pathophysiology. Seminars in Nuclear Medicine, vol XIX, No.2(April), 1989:79-88.

8. Dong ZJ, Li S, Lu X. Percutaneous transluminal angioplasty for renovascular hypertension in arteritis: experience in China. Radiology 1987;162:477-479.

MULTIPLE DURAL ARTERIOVENOUS MALFORMATIONS

Pipat CHIEWVIT[1], Orasa CHAWALPARIT[1], Anchalee CHUROJ[1], Suthisak SUTHIPONGCHAI[1], In Sup CHOI[2].

ABSTRACT

Four cases of multiple dural arteriovenous malformations (DAVMs) including base of skull are reported. Two of them have a DAVMs involving the cavernous sinus and separate AVMs in base of skull.The third patient has the symptomatic DAVMs involving straight sinus and the last patient has DAVMs involving torcular and both also have the second DAVMs involving superior sagittal sinus. All of the second DAVMs are incidentally detected by cerebral angiography. Reviewing of previous reports of this occurrence and the vascular anomalies that can association with dural AVMs are discussed.

INTRODUCTION

Dural arteriovenous malformations (DAVMs) account for 10-15 % for intracranial malformations. These lesions may occur within any dural structures but usually occur in the transverse sinus, sigmoid sinus and cavernous sinus. 35% of DAVMs are located in the posterior fossa. The DAVMs are generally considered as acquired lesions which may evolve from organization and revascularization of a previously thrombosed sinus.[2,4,5,9] Recent studies both angiographically and histologically[7,8] considered the site of fistula located within the sinus wall. The natural history of dural AVMs is highly variable. The most common clinical presentation are bruits, headache, intracranial hemorrhage, however, these depend mainly on the location of shunt, direction and route of the venous drainage of dural arteriovenous malformations.[2,3,14] Venous drainage is usually through the dural sinus and / or other dural and leptomeningeal venous channels. Retrograde leptomeningeal venous drainage is oftenly developed tortuous, variceal and frankly aneurysmal which associated risk of aggressive behavior such as intracranial hemorrhage or neurodeficits.[6,8] Spontaneous regression or thrombosis is not uncommon,[11,12,13] however, it should not be occurred in patients with high flow lesions, cortical venous drainage, or in children.[10]

As previously mentioned, DAVMs are relatively rare conditions and report of patients in case of multiple dural AVMs are very rare. We report four cases of dural AVMs associated with separate another dural AVMs. Two of them have a dural AVMs involving cavernous sinus and another separate arteriovenous malformations in right jugular bulb in one and left mastoid region in the other ones. The third patient has a symptomatic dural AVMs in posterior fossa and separate incidentally detected dural AVMs involving SSS. The fourth patient has a symptomatic dural AVMs of the torcular and the second dural AVMs draining into the SSS. Those are well demonstrated by diagnostic angiography.

(SSS = Superior Sagittal Sinus)

[1] Department of Radiology, Siriraj Hopital, Mahidol University, BKK 10700, Thailand.
[2] Department of Radiology, Massachusetts General Hopital, Harvard University, Boston, MA 02114, USA.

CASE REPORTS

CASE 1

Clinical course: A 55-year-old woman had a history of a red eye for two years. She experienced a severe bifrontal headache. The pain was across the eyes and sometimes extended down to the maxillary sinus region. Approximately two years ago she suddenly started having the redness of the left eye. Approximately three months ago she started having a double vision and proptosis of the left eye. She had been managed conservatively for five months without any improvement. She was referred for evaluation and possible endovascular treatment.

Examination: The neuro-opthalomological examination revealed mild to moderate engorgement of the conjunctival vessels, slight proptosis, asymmetrical intraocular pressure and slight engorged retinal veins on the left eye. No detectable bruit. The extraocular muscles revealed minimal limitation of abduction in the left eye.

The angiographic study was performed and demonstrated a rapid dural arteriovenous shunting at the posteromedial aspect of the left cavernous sinus. Arterial blood supply was mainly by clival branches from neuromeningeal trunk of left ascending pharyngeal artery as well as small dural branches of C5 segment of both internal carotid arteries. Venous drainage was mainly into the left cavernous sinus appeared in aneurysmal fashion approximately 10 mm. in diameter. Further retrograde venous drainage was into a large posterior fossa vein which drain further into multiple cerebellar cortical veins as well as superiorly through anterior pontomesencephalic vein into basal vein of Rosenthal. Venous drainage anteriorly from left cavernous sinus into the left opthalmic veins was also documented. Another arteriovenous malformation was detected at anterior aspect of the right jugular bulb which mainly fed by superior and middle pharyngeal branches of pharyngeal trunk of ascending pharyngeal arteries bilaterally. The venous drainage of this dural malformation was via right jugular vein. The patient was treated endovascular route with GDC coils packing in the aneurysmal dilatation of the left cavernous sinus. The result is impressive.

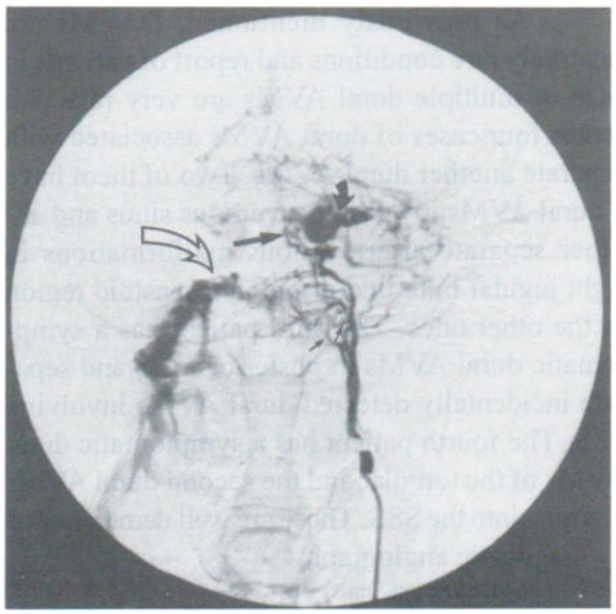

Fig. 1 A

Fig. 1 Case 1. A. Anterosuperior (AP) view of left ascending pharyngeal artery demonstrates left dural carotid-cavernous sinus malformations (curve arrow ➲) and fed by clival branches (arrow ➧) from neuromeningeal trunk. The separate DAVMs in right jugular fossa (curve open arrow ➲) is fed by left pharyngeal branches (small arrows ➧) of ascending pharyngeal artery pass through anastomosis to contralateral sided branches to the AVM and draining to the right jugular vein.

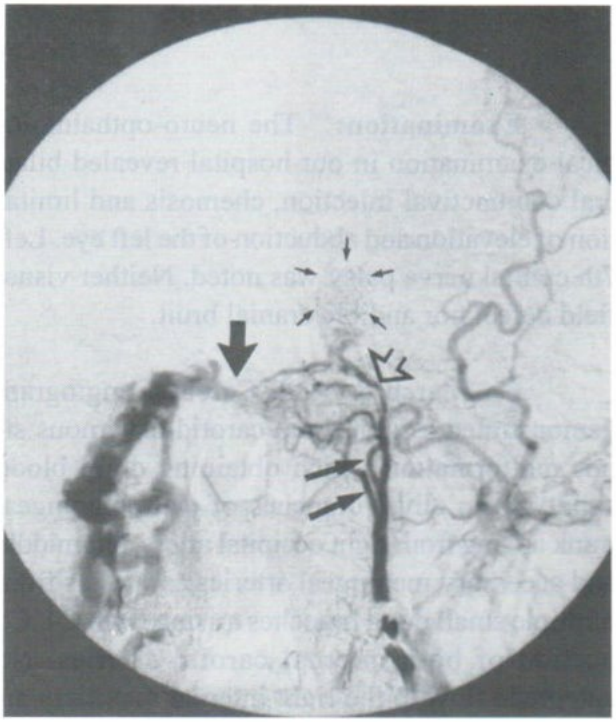

Fig. 1 B. AP view Control angiography of left ascending pharyngeal artery (open arrow ⇧) immediately after embolization of left dural AVMs with GDC coils (small arrows ▲) reveals no longer presence of abnormal venous drainage. The right jugular fossa AVM (large arrow ⬆) is fed by superior pharyngeal and middle pharyngeal (arrows ⬆) branches.

Fig. 1 B

Fig. 1 C

Fig. 1 D

Fig. 1 C and D. AP and Lateral views during right ascending pharyngeal artery injection show a silent AVM at right jugular fossa (open arrow⇧) fed by pharyngeal branch (small arrows▲) and neuromeningeal branch of left ascending pharyngeal artery (curve arrow ➲). The venous drainage is into the right jugular vein (large arrow ⬆).

CASE 2

Clinical course: A 77-year-old woman who first noticed a tinnitus on the right sided of her head in September 1994, approximately nine months after a history of facial trauma. The symptoms then progressed into redness of her left eye, double vision and eventually proptosis of the eye. She underwent cerebral angiogram on October 1994. This study was interpreted as bilateral carotid-cavernous sinus fistula with a small associated parasellar arteriovenous malformation. She was underwent two endovascular treatment attempts which included right external carotid artery embolization with polyvinyl alcohol (PVA) particles on December 30, 1994 and left external carotid artery embolization with PVA particles on February 1, 1995. The patient had some relief of her ocular symptoms such as her double vision, proptosis of left eye. She was referred on March 2, 1995 for evaluation and possible further endovascular treatment.

About the past history of trauma on December 1993, she was falling on her face while walking. She reported no blood loss or any surgical treatment needed.

Examination: The neuro-opthalmological examination in our hospital revealed bilateral conjunctival injection, chemosis and limitation of elevation and abduction of the left eye. Left 7th cranial nerve palsy was noted. Neither visual field defect nor audible cranial bruit.

On March 8, 1995 Cerebral angiogram demonstrated a right dural carotid-cavernous sinus malformation which obtaining dural blood supply from clival branches of neuromeningeal trunk arising from right occipital artery, left middle and accessory meningeal arteries as well as from multiple small dural branches arising from C4, C5 portion of both internal carotid arteries. No antegrade flow to the right internal maxillary artery due to status post previous embolization. The right internal maxillary artery was reconstituted via infraorbital artery and buccal branches of facial artery. Early venous drainage was demonstrated at right cavernous sinus with retrograde filling to the right opthalmic vein and simultaneously antegrade to right inferior petrosal sinus. Another separate arteriovenous malformation was demonstrated at the base of skull in the inferior aspect of left mastoid temporal bone.

Fig. 2 A

Fig. 2 B

Fig. 2 Case 2, A and B. AP and Lateral view during right external carotid arteriography reveal right dural carotid-cavernous sinus malformations fed by clival branches of neuromeningeal trunk (arrow⬆) from occipital artery. No demonstrable of right internal maxillary artery due to previous embolization, however, filling of infraorbital artery from facial artery via buccal branches (open arrows ⇧) is documented. The venous drainage is into cavernous sinus and inferior petrosal sinus (small arrows ↑) as orderly.

Fig. 2 C

Fig. 2 C. AP view of left external arteriography shows right dural carotid-cavernous malformations fed by left middle meningeal artery (arrows ⬆) and distal internal maxillary artery (open arrows ⇧). The venous drain age is into right cavernous sinus (small arrows ↑). The separate AVM opacified at left occipital area (curved arrows ↄ).

Fig. 2 D

Fig.2 D. AP view of left common carotid arteriography after platinum fibered coils (open arrow ⇧) embolization of anterosuperior compartment of right cavernous sinus demonstrates residual AVMs draining into posteroinferior compartment of cavernous sinus and to inferior petrosal sinus (arrows ⬆). Opacification of separate AVM at basal skull of left occipital bone is noted (small arrows ↑).

CASE 3

Clinical course: A 63-year-old right handed man had a symptoms of headache with nausea and vomiting on November 1995. He was subsequently worked up and disclosed of acute subarachnoid hemorrhage and intraventricular hemorrhage on Computerized tomography scan. The cerebral angiography was underwent from other hospital and demonstrated a posterior fossa dural arteriovenous malformation along the inferior surface of straight sinus which mainly supplied by right occipital artery via transmastoid and transcalvarial branches as well as C5 tentorial branches from bilateral internal carotid arteries. The right and left middle meningeal artery were recruited into the dural AVM via right occipital, squamosal and left parieto-occipital, temporo-occipital and sqaumosal branches respectively. The right ascending pharyngeal artery was involving in this particular case as well. Early venous drainage was well defined in superior vermian vein with further drainage into inferior vermian vein as well as superiorly through posterior mesencephalic vein into the vein of Galen and straight sinus, and anteriorly through lateral mesencephalic, anterior

pontomesencephalic vein and basal vein of Rosenthal into superficial middle cerebral vein.

Another dural AVM was incidentally detected by right internal carotid arteriography and demonstrated dural AVM in superior sagittal sinus (SSS) supplying by right anterior falx artery arising from right anterior ethmoid artery of right opthalmic artery. Early venous drainage was into SSS.

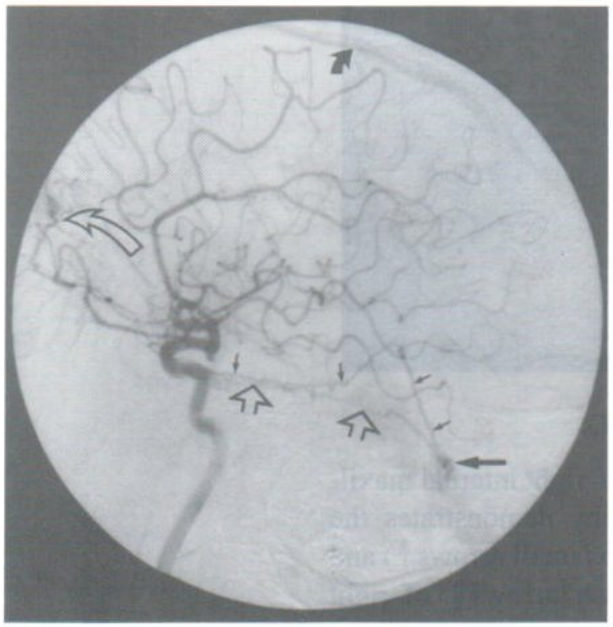

Fig. 3 A

Fig. 3 B

Fig. 3 Case 3, A. Lateral view of right internal carotid arteriography demonstrates multiple dural AVMs, one is fed C5 branches of internal carotid artery as marginal tentorial artery (small arrows ↟) and basal tentorial artery (open arrows ⇧) direct fistulas (arrow ⬆) into the posterior fossa veins and the other is in anterior cranial fossa (curved open arrow ⤺) draining into superior sagittal sinus (curved arrow ↱).

Fig. 3 B. Oblique view of right internal carotid arteriography clearly demonstrates silent dural AVMs (small arrows ↟) supplied by anterior falx artery (arrow ⬆) and draining into the superior sagittal sinus (open arrows ⇧). The tentorial branches from C5 portion of internal carotid artery are noted (large arrows ⬆).

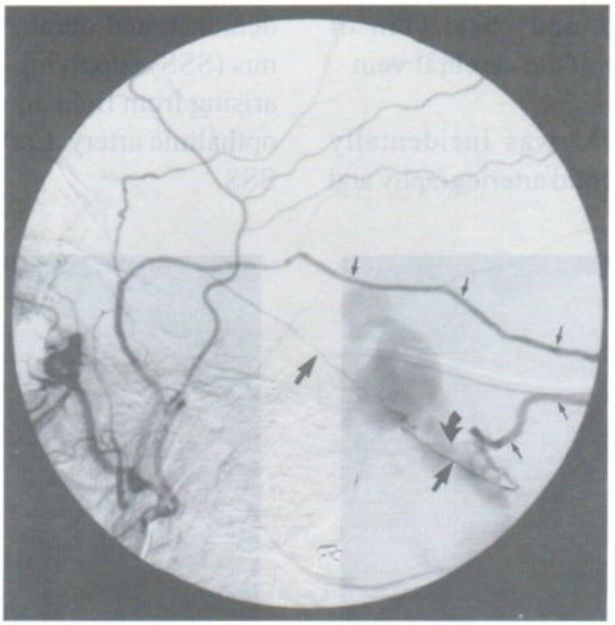

Fig. 3 C

Fig. 3 C. Lateral view of right internal maxillary arteriography demonstrates the occipital branch (small arrows ↑) and squamosal branch (arrows ⬆) of right middle meningeal artery supplying the dural AVMs and draining into the superior vermian vein (curved arrow ↷).

CASE 4

Clinical course: A 27-year-old right handed man who had a car accident in July 1989 with resultant severe closed head injury and coma of four to five weeks. The patient was stable with residual cognitive and gait difficulties. Over the last several months there was a decline in both cognitive and physical functioning. A follow up MRI showed an arteriovenous malformations. The cerebral angiogram demonstrated the multiple dural AVMs, the extensive one involving the torcular and peritorcular regions which supplying by bilateral occipital arteries via transmastoid branches, posterior meningeal branches of right vertebral artery, dural branches of posterior cerebral arteries, the tentorial branches from right internal carotid artery and petrosal branches of bilateral middle meningeal arteries. The venous drainage was into the torcula, left transverse sinus, left sigmoid sinus in orderly fashion. There was severe venous hypertension seen after injection of internal carotid arteries and vertebral arteries as shown by the prominence of cortical veins without filling of the deep venous system. The second dural AVMs was a small arteriovenous shunting at SSS which fed by superficial temporal artery and drained into SSS directly.

Fig. 4 A

Fig. 4 B

Fig. 4 Case 4, A. AP view of right occipital arteriography shows extensive supply of right occipital artery via transmastoid branches (small arrows ↑) and draining into torcular (arrow ⬆).

Fig. 4 B. Lateral view of left external carotid arteriography demonstrates multiple dural AVMs, symptomatic one (open arrow ⇧) is fed by squamosal branches (arrow ⬆) of middle meningeal artery. The second dural AVMs involving SSS curved open arrow ⤴) is fed by superficial temporal artery (arrowhead ▲).

DISCUSSION

Anomalous communication between dural arteries and venous system occurring in the absence of significant trauma have been described by a number of authors as dural arteriovenous malformations. Approximately 10-15% of intracranial arteriovenous malformations were in dural origin [1]. Mostly located in the cavernous sinus and transverse-sigmoid sinuses. In large series of Aminoff, et al. (1973) the lesion located in the former area in 12% and the latter in 62% as well as Lasjuanias, et al. (1986) reported 191 cases with cavernous lesion in 19% and lateral sinus in 67%. The etiology of dural arteriovenous malformations (DAVMs) is not exactly known. The convincing evidences that have recently been presented and suggested at least some of them are acquired in origin resulting from the dural venous sinus thrombosis.[2,4,5,9] We reported four cases of multiple dural AVMs. Two of them had dural AVMs occurring in cavernous sinus and associated with separate AVM in the basal skull. Both of them presented to us as classical cases of dural AVMs of carotid-cavernous sinus region that occurred in elderly woman with neuro-opthalmological signs and symptoms of slow-flow low-pressure shunting such as conjunctival hyperemia, proptosis, and double vision.[10,15-17,19-21,23-25] According to the angiographically classification proposed by Barrow, et al. (1985), which classified[1] carotid-cavernous sinus fistula into 4 categories and the most

common type is type D which obtaining meningeal supply from both external and internal carotid arteries.[16] Our patients, both of them were in type D as described in CCFs of Barrow & classification. The first patient had received conservative treatment for five months before comimg to hospital. It was probably reasonable to conservative treatment at that time because of mild symptoms and possibilities of spontaneous regression. The incidence of spontaneous regression or cure was varied from series to series such as 3 of 20 cases (15%) in Vinuela & series, 5 of 14 cases (36%) of Barrow & series, and 3 of 37 cases (8%) in Debrun & series [15-17]. Although, there was no clinical signs and symptoms of hazardous CCFs, we decided to treat this patient immediately due to her angiographic features associated with risk of morbidity and mortality. Those features were aneurysmal dilatation of left cavernous sinus and venous drainage into cortical veins of posterior fossa which can produce aggressive neurological deficits. Multimodalities in treatment dural CCFs have been reported.[15-20,22,24-27] Surgical approaches in treatment dural CCFs were arterial feeders ligation, placement of thrombogenic material into the sinus to promote thrombosis and closure.[18,19,22] Recently, transarterial embolization have been described for alleviation symptoms or even cure lesions.[15-17,20,27] Manual compression therapy have been reported as a safe technique in selected cases with cure rate 17% in direct CCFs and 30% in indirect CCFs.[24] More recently transfemoral transvenous embolization has been used as primary method for cure dural CCFs and other dural AVMs.[25,26] We chose GDC coils as embolic material in this patient due to its opacity, thrombogenicity, accurate disposition in proper site and no movement of coils during detachable. The results both angiographically and clinically are impressive to us.

Considering vascular anomalies that associated with Dural AVMs, it is somewhat rare and was reported in the literatures as multiple DAVMs,[2,9,27-31] cerebral AVM,[32,38,39] Rendu Osler Weber disease,[10] arterial aneurysm.[10] In term of multiple DAVMs it is surprising that there are only seven reports with nine cases of multiple DAVMs documented.[2,9,27-31] In our study, we present four cases of multiple DAVMs which occurred in different locations such as cavernous sinus, straight sinus, torcular, SSS, and base of skull which varying from case to case. Basically, they can occur anywhere along the dura mater. The pathophysiology, natural history and treatment of which are similar to the usual DAVMs. It is considered to be an acquired lesion originating from recanalized blood clot clarifying by histological sections[9] and some cases do have a spontaneous regression [28]. The association of a dural AVM and a brain AVM was first reported by Tamaki in 1971. In that patient, Tamaki described AVM involving the scalp as well as dura, retina, cerebrum and posterior fossa.[32] Then, two additional reports were followed by Willinsky[36] and Schlacter.[37] The Dural AVM was also noted in patient with Rendu Osler Weber disease.[10] The Rendu Osler Weber disease is charactered by a triad of mucocutaneous and visceral telangiectasia, recurrent epitaxis and familial history.[33] The central nervous system involvement in this disease is common causing by pulmonary arteriovenous fistula (cerebral hypoxemia, septic emboli and brain abscess), vascular malformations of the brain, spinal cord and porto-systemic encephalopathy respectively.[34,35] Another disease that having separate AVMs involved central nervous system is retinocephalic vascular malformations (Wyburn-Mason sydrome). The Wyburn-Mason sydrome composed of arteriovenous malformations of one or both sides of midbrain with ipsilateral or bilateral arteriovenous malformation of the retina and cutaneous nevi. Brain AVMs in this disease usually follow the optic tracts and optic nerves.[38,39] As previously mentioned, Tamaki reported one case of AVM involving scalp, dura, retina, cerebrum and posterior fossa which possibility of unilateral retinocephalic disease is considered. Dural AVM also associated with arterial aneurysm.[10] This study presents four additional cases of multiple AVMs,

CCFs = Carotid-Cavernous Fistulas

two cases of those which has a dural AVM associated with a second dural AVMs occupying in the base of skull, one is in the anterior aspect of right jugular foramen and the other is in the base of skull of left occipitomastoid bone. These cause no symptoms with incidentally found during cerebral angiographic procedures. We have never seen dural AVM associated with separate AVMs in the base of skull areas.The other two cases have the second silent DAVMs in the superior sagittal sinus. All cases are unrelated to any known disease processes or familial preponderance. We believe that multiple DAVMs found in the same patients without associated vascular disease are rare and very interesting.

REFERENCES

1. Newton TH, Cronqvist S. Involvement of dural arteries in intracranial arteriovenous malformations. Radiology 1969;93:1071-1078.
2. Houser OW, Baker HL, Rhonton AL, Okazaki H. Intracranial dural arteriovenous malformations. Radiology 1972;-105:55-64.
3. Aminoff MJ, Kendall BE. Asymptomatic dural vascular anomalies. British Journal of Radiology 1973;46:662-667.
4. Thoraff MS, David GK. The surgical approach to arteriovenous malformations of the lateral and sigmoid dural sinus. J Neurosurg 1983;59:32-39.
5. Houser OW, Campbell JK, Campbell RJ, et al. Arteriovenous malformation affecting the transverse dural sinus-an acquired lesion. Mayo clin Proc 1979;54:651-661.
6. Award IA, Little JR, Akrawi WP, et al. Intracranial dural arteriovenous malformations: factor predisposing to an aggressive neurological course. J Neurosurg 1990;-72:893-850.
7. Nishijima M, Takaku A, Endo S, et al. Etiology evaluation of dural arteriovenous malformation of lateral and sigmoid sinus based upon histopathological examinations. J Neurosurg 1992;76:600-606.
8. Barnwell SL, Halbach VV, Dowd CF, et al. A variant of arteriovenous fistula within the wall of dural sinus: Result of combined surgical and endovascular therapy. J Neurosurg 1991;74:199-204.
9. Graeb DA, Dolman CL. Radiological and pathological aspect of dural arteriovenous fistulas. J Neurosurg 1986;64:962-967.
10. Lasjuanias P, Berenstein A. Endovascular treatment of Craniofacial lesion, Surgical Neuroangiography 2. Berlin; London: Springer-Verlag, 1987:273-315.
11. Hansen JH, Sogaard I. Spontaneous regression of extra - and intracranial arteriovenous malformation. Case Report. J Neurosurg 1976;45:338-341.
12. Magidson MA, Weinberg PE. Spontaneous closure of dural arteriovenous malformation. Surg Neurol 1976;6:107-110.
13. Olutola PS, Eliam M, Molot M, et al. Spontaneous regression of dural arteriovenous malformation. Neurosurg 1983;-12:687-690.
14. Lasjuanias P, Chiu M, Terbrugge K. Neurological manifestation of intracranial dural arteriovenous malformation. J Neurosurg 1986;64:724-730.
15. Vinuela F, Fox AJ, Debrun GM, Perless SJ, Drake CH. Spontaneous carotidcavernous fistulas: clinical, radiological, and therapeutic considerations. Experience with 20 cases. J Neurosurg 1984;60:976-984.
16. Barrow DL, Spector RH, Braun IF, Landman JA, Tindall SC, Tindall GT. Classification and treatment of spontaneous carotid-cavernous fistulas. J Neurosurg 1985;62:248-256.

17. Debrun GM, Vinuela F, Fox AJ, Davis KR, Anh HS. Indications for treatment and classification of 132 Carotid-Cavernous fistulas: Experimental and clinical studies. Neurosurg 1988;22:285-289.
18. Samson D, Ditmore QM, Beyer CW. Intravasular use of Isobutyl 2-Cyanoacrylate: Part 2: Treatment of carotid-cavernous fistulas. Neurosurg 1981;8:52-55.
19. Mullan S. Treatment of carotid-cavernous fistulas by cavernous sinus occlusion. J Neurosurg 1979;50:131-144.
20. Peeters FLM, Kroger R. Dural and direct cavernous sinus fistulas. AJR 1979;132:-599-606.
21. Graf CJ. Spontaneous carotid-cavernous fistula. Arch Neurol 1965;13:664-672.
22. Hosobuchi Y. Electrothrombosis of carotid-cavernous fistula. J Neurosurg 1975;-42:76-85.
23. Halbach VV, Higashida RT, Heishima GB, Reicher M, Norman D, Newton TH. Dural fistulas involving the transverse and sigmoid sinuses. Results in 30 patients. Radiology 1987;163:437-442.
24. Halbach VV, Hieshima GB, Higashida RT, Reicher M. Carotid cavernous fistulae: indication for urgent treatment. AJR 1987;149:587-593.
25. Halbach VV, Higashida RT, Hieshima GB, Hardin CW, Pribram H. Transvenous embolization of dural fistulas involving the cavernous sinus. AJNR 1989;10:377-383.
26. Halbach VV, Higashida RT, Hieshima GB, Hardin CW. Transvenous embolization of dural fistulas involving the Transvenous and sigmoid sinuses. AJNR 1989;10:385-392.
27. Aminoff MJ. Vascular anomalies in the intracranial dura mater. Brain 1973;96:-601-612.
28. Kataoka K, Taneda M. Angiographic disappearance of multiple dural arteriovenous malformation. J Neurosurg 1984;-60:1275-1278.
29. Newton TH, Weidner W, Greitz T. Dural arteriovenous malformation in the posterior fossa. Radiology 1968;90:27-35.
30. Nakagawa H, Kubo S, Nakajima Y, Izumoto S, Fujita T. Shifting of duralarteriovenous malformation from cavernous sinus to the sigmoid sinus to the transverse sinus after transvenous embolization-a case of left spontaneous carotid-cavernous sinus fistula. Surg Neurol 1992;37:30-38.
31. Kawayama N, Takaku A, Nishijima M, Endo S, Hirao M. Multiple dural arteriovenous malformations-report of two cases. J Neurosurg 1989;71:932-934.
32. Tamaki N, Fujita K, Yamashita H. Multiple arteriovenous malformations involving the scalp, dura, retina, cerebrum, and posterior fossa. J Neurosurg 1971;34:95-98.
33. Perry WH. Clinical spectrum of hereditary hemorrhagic telangiectasia (Osler- Rendu-Weber disease). Am J Med 1987;82:989-997.
34. Roman G, Fisher M, Perl DP, Poser CM. Neurological manifestations of hereditary hemorrhagic telangiectasia (Rendu-Osler-Weber disease). Report of 2 cases and review of the literatures. Ann Neurol 1978;4:130-144.
35. Sobel D, Norman D. CNS manifestations of hereditary hemorrhagic telangiectasia. AJNR 1984;5:569-573.
36. Willinsky RA, Lasjuanias P, Burrow P. Multiple cerebral arteriovenous malformations (AVMs). Review of our experience from 203 patients with cerebral vascular lesions. Neuroradiology 1990;32:207-210.
37. Schlacter LB, Fleischer AS, Faria MA, Tindall GT. Multifocal intracranial arteriovenous malformations. Neurosurg 1980;-7:495-499.
38. Theron J, Newton TH, Hoyt WF. Unilateral retinocephalic vascular malformations. Neuroradiology 1974;7:185-196.
39. Wyburn-Mason R. Arteriovenous aneurysm of mid brain and retina, facial naevi and mental changes. Brain 1943;66:12-203.
40. Malik GM, Pearce JE, Ausman JI, et al. Dural arteriovenous malformation and intracranial hemorrhage. Neurosurg 1984;-15:332-339.

STEREOTACTIC INSTRUMENT IN CT GUIDED BIOPSY

Anuchit RUAMTHANTONG M.D., Thiti THATRINARANONTASIN Tech Gd.
Krisdee PRABHASAVAT M.D., Suwana JITBANCHUEN B.Sc.
Panida CHARNCHAOWANICK B.Sc., Supawadee KARUWANARINT B.Sc.
Venus WISESTSANG B.Sc.

ABSTRACT

We have designed a basic and simple instument for CT-guided biopsy, attached to the CT-table. The instrument is easy to be used and can be learned how to use in a short time. We use this instrument for CT-guided biopsy in 6 cases with good accuracy of 100 % and no major complications

We believe that the procedures with this instrument when used as an aid to the CT-biopsy would improve the safety, accuracy and the value of percutaneous biopsy in the radiology department.

INTRODUCTION

Computed tomographic guided needle biopsy is a well established useful procedure with a high yield of tissue diagnosis without the need for open surgery. It has the advantage over ultrasound in its ability to detect a small resolving lesion and identification of needle tip. This increases the yield of tissue diagnosis as sampling is accurately within the lesion. Its disadvantages include lack of real time imaging, expensiveness, and risk of exposure to radiation. The procedure is also time consuming, taking one to two hours per case in comparison with 45 minutes in ultrasound guided biopsy. The duration of the procedure is influenced by many factors such as radiologist's skill, type of CT machine (continuous or spiral) and characteristi of the lesion (localized or diffused, whether easily approached, etc.) All these may contribute to longer duration of the procedure.

The use of our apparatus that would aid in the localization and enhance the accuracy of needle angulation and depth of needle puncture would greatly improve CT guided biopsy procedures and as such would be of benefit to the patient. This diagnostic aid would reduce procedure time, radiation exposure and the patient discomfont. Also increasing the accuracy of every needle tip positioning would lead to lesser unnecessary needle movements and puncture and as such lower incidence of procedure related complications.

OBJECTIVE

The objective of this study is to introduce a new instrument, simple, cheap and which does not require much expertise to operate, and which would help shorten the time in the performance of CT guided biopsy.

MATERIALS AND METHODS

Steps for CT guided fine needle biopsy:

1. Simple scanning, select the area of

* Department of Radiology, Siriraj Hospital, Dhonburi, Bangkok, Thailand.

solid or confluent tissue with contrast enhancement around the necrotic area.

2. Place the skin marker on selected area above the lesion, then make single cut with CT scan.

3. From the monitor , select the skin entry point and measure the angulation of the needle and the depth of the mass from the skin.

4. Use the instrument with the needle attached which would direct the advancement of the needle to the desired position, then proceed with the actual needle puncture.

5. Rescan to see the tip of the needle making 3 cuts , 10 mm. apart ;above, at and below the tip of the needle.

6. With the needle in correct position, remove the patient from the scanner and do the biopsy.

7. After biopsy, remove the needle and rescan the patient to detect any acute complication (hemorrhage) that might occur.

8. Observe the patient in sitting position for 2 - 4 hours before sending home.

DESIGN OF INSTRUMENT

This instrument was designed to be used in 3 - dimensions (in the x-y-and z-axis) for the purpose of shortening the time of the procedure. We used the property of the opposited angle in the parallel lines of the same triangle in the same direction. (Fig.1,2,3)

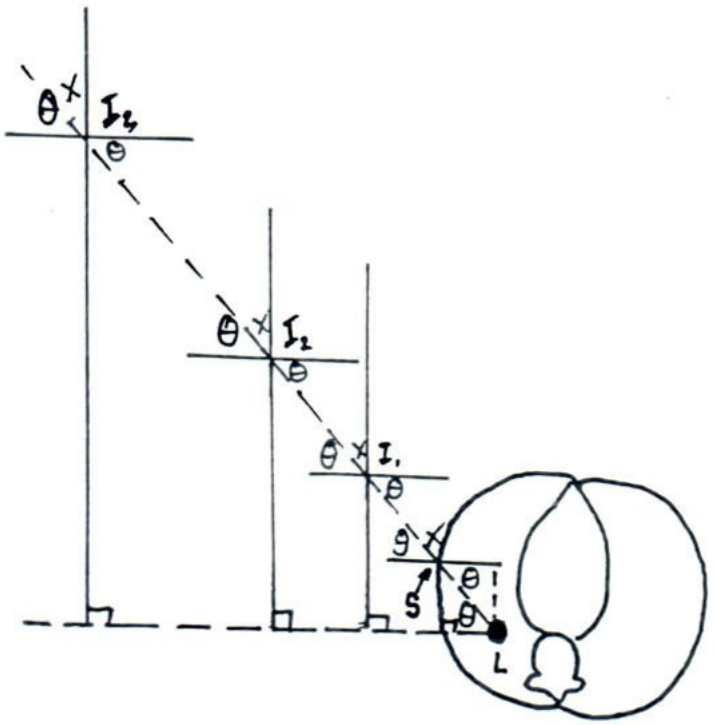

Fig. 1 Diagram of the property of the opposited angle in the parallel lines.

Θ = defined from an angle between the parallel axis and a line from center of the mass (L) to the skin marker (S).

I_1 ; I_2 ; I_3 = Imaginary points outside the patient having the same angulation (Θ)

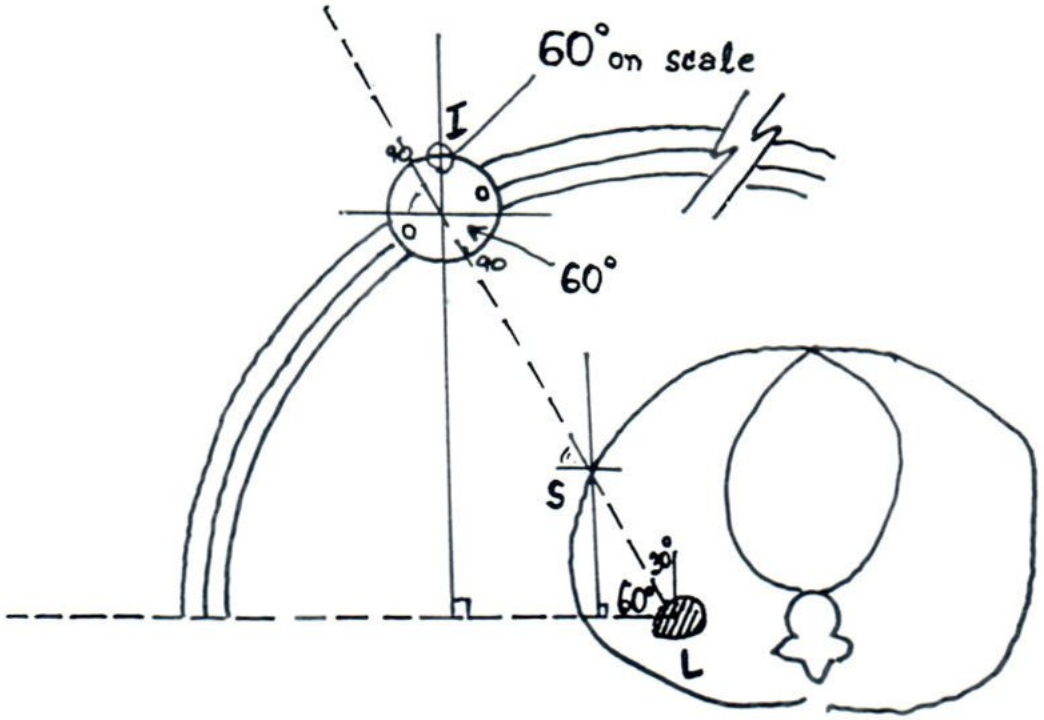

Fig. 2 After using the water - level instrument at the imaginary-point(I); adjusting to get the angulation [60°] from I to S (Skin marker).

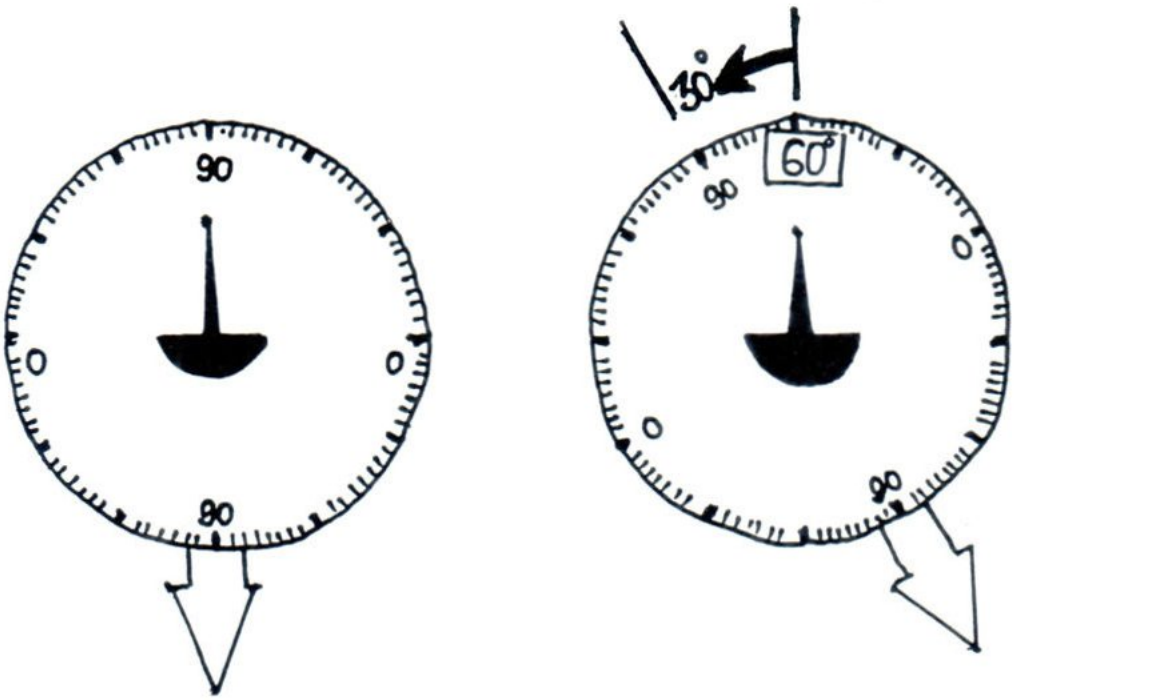

Before Adjusting Counter Clock-wise Rotation

Fig. 3 Close-up view of the scale in Fig. 2

THE INSTRUMENTS ARE COMPOSED OF

1. Clamper to hold the semi-circular frame to the CT-table.

2. Semicircular frame which used to make the extra-axial point angulated with the skin marker in the same degree to the lesion.

3. Water-level instrument (used by the carpenter) for measuring the angle from the semicircular frame.

4. Sliding-ruler to hold and to measure the depth for the needle puncture with scale. (Fig.4)

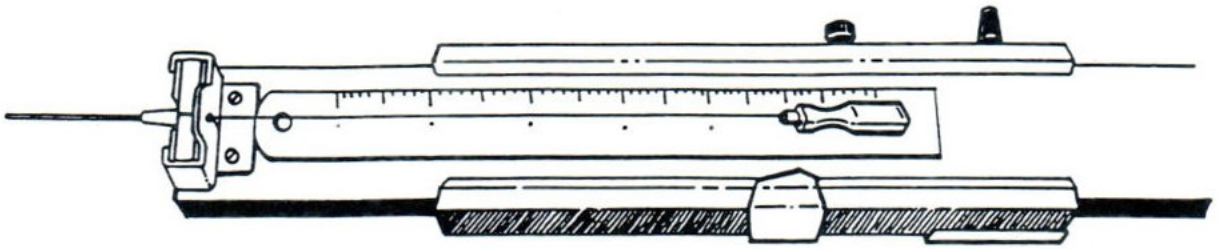

Fig. 4 Sliding-ruler with puncture-needle.

STEPS IN THE PROCEDURES

1. Select the slice of serial scans which found the lesion and may be propable to puncture and avoid the vital organ from the direction of puncture.

2. Re-scan with the skin marker at the same slice.

3. Choose the puncture point from the skin-marker ("A") to the lesion ("B") ;
At the monitor of the CT-scan we should know.

@ depth of the direction to puncture

@ angulation with the parallel level (X-axis)

4. Using sterile technique at the puncture point.

5. Construct the instrument.

6. Adjust the angle of the instrument to be the same angle seeing from the monitor (which acquired from the first scan) ; by the water-level instrument. (Fig.5)

7. Puncture with sliding-ruler.

8. Re-scan again to evaluate the complication of the procedure.

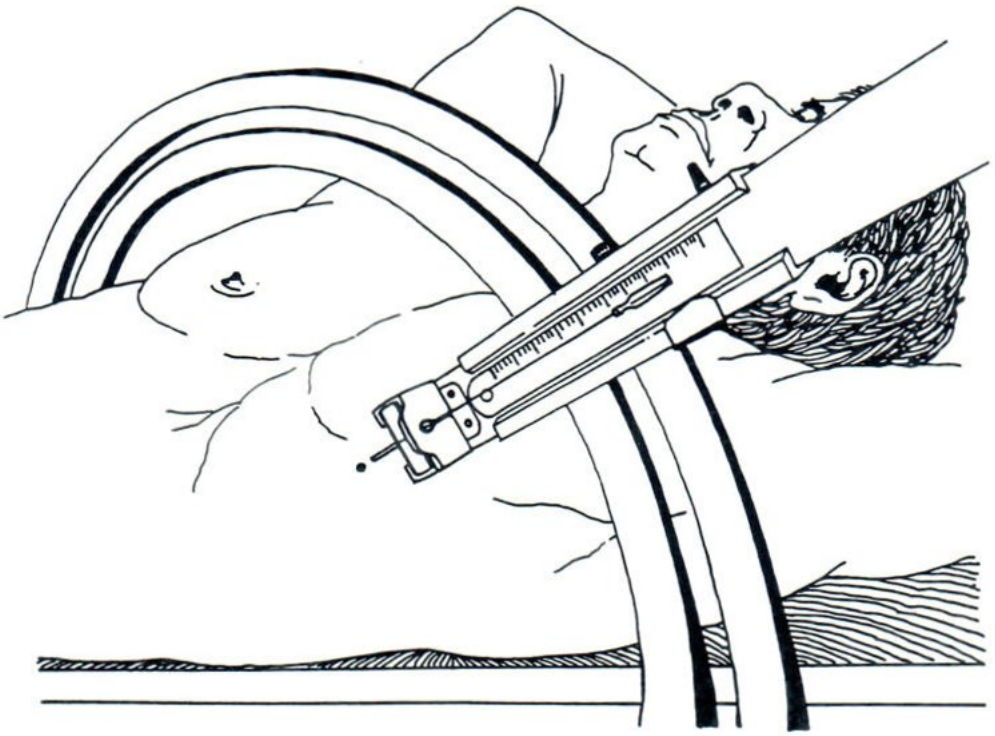

Fig. 5 Illustration of stereotactic instrument above the patient.

RESULT

In our preliminary report of 6 cases using this instrument with CT-guided biopsy, we can manage the needle to enter the mass in every case and could get enough tissue to give diagnosis by the cytologist. Only 2 cases had minor complications of pneumothorax who were admitted in the hospital for 24 hours and were discharged next day without the complication. After having some experiences, we can reduce the time in the CT-guided biopsy. In the first three cases we spent about one and a half hour per case as a learning stage in the use of this instrument. But in the latter three cases we spent not more than 45 minutes per case.

DISCUSSION

The value of a diagnostic aid to a procedure is based on its contribution to the accuracy, diagnostic yield, shortening of examination time, lowering of complication rate and attributable to patient's comfort. In percutaneous biopsy, accuracy and diasnostic yield is higly dependent on the amount of tissue sample and accuracy of biopsy sampling within a given lesion. There are two very important points that should be first and foremost for anyone performing per cutaneous biopsy. One is the exactness of the point of needle puncture and angulation which should always be the prime goal as this may be together avoiding additional or a second puncture, secondly

decreasing the time of the examinations, possible complications and enhancing patient comfort during the biopsy, likewise, accurate needle position within the lesion garantees representative histological sampling of the mass.

Our instrumental design tries to enhance the biopsy procedure by complementing the accuracy of needle puncture in depth and angulation , thereby fulfilling the other requisities for an accurate diagnosis.

It has been designed to resolve the limited angle of puncture; decreasing time for re-scan and facilitate the accuracy of the direction of puncturing.

This instrument may be openned to further improvement for use with the CT scan (conventional type) or for spiral . However cost and high radiation doses are to be considered in spiral CT .

REFERENCE

1. Andy adam, MRCP, FRCR & Robert N. Gibson, FRACR, DDU : Practical Interventional Radiology of The Hepatobiliary System And Gastrointestinal Tract; Chapt. 7 "Computed Tomographic-guided and Ultrasound-guided intra-abdominal biopsy and abcess drainage" by Eugene Y. Yeugn; p 100-117
2. Joseph T. Ferruci, Jr., M.D. & Jack Wittenberg, M.D. : Interventional Radiology of The Abdomen; Chapt. 4 Percutaneous Tumer Biopsy p. 115-155
3. Stuart G.Silverman, David A. Bloom et al. Needle-Tip Localization During CT-Guided Abdominal Biopsy : Comparison of Conventional and Spiral CT. AJR 1992; 159 : 1095 - 1097
4. Gary Onik, M.D., Eric R. cosman, PhD. et al. : CT-guided Aspirations for the Body: Comparison of hand Guidance with Stereotaxis : Radiology 1986;160:389-394
5. Gary Onik, M.D., Philip Costello et al. CT Body Stereotaxis : An Aid for CT-Guided Biopsies. AJR 1986;146;163-168
6. Eric van Sonnenberg, Jack Wittenberg et al : Triangulation Method for Percutaneous Needle Guidance : The Angled Approach to Upper Abdomen Masses : AJR 1981; 137; 757 - 761
7. Phillip R. Frederick, M.D., Thomas H. Brown, M.S., C.S. et al A Light-Guidance System to be Used for CT-Guided Biopsy: Radilology 1985;154(2):535-536
8. Joseph T. Ferrucci, Jr., M.D. & Jack Wittenbery, M.D. : CT Biopsy of Abdominal Tumors : Aids for Lesion Localization: Radiology 1978;129:739-744

ENDOVASCULAR TREATMENT OF TRAUMATIC ANEURYSM INVOLVING HEAD AND NECK REGION

Suthisak SUTHIPONGCHAI,M.D., Orasa CHAWALPARIT,M.D., Pipat CHIEWVIT,M.D., Anchalee CHUROJANA,M.D.

ABSTRACT

Endovascular treatments of 21 traumatic vascular diseases with intracranial aneurysms and aneurysms of head and neck are reported. Fourteen cases with epistaxis were treated by detachable balloon occlusion and thirteen cases of aneurysms were successfully occluded. Five of this group had associated carotid cavernous fistulas (CCF) and successfully occluded in four cases. One case of non-epitaxis had CCF with aneurysm of internal maxillary artery and was treated by Gelfoam embolization. Two cases of cervical internal carotid aneurysms were treated successfully in the same setting of associated CCF. The other two cases of cervical carotid and one of common carotid aneurysms were treated by surgery. One hemiplegia from thromboemboli and one blindness from unavoided occlusion of the ophthalmic origin were found as the complication.

Key Words : Traumatic aneurysm; head and neck; endovascular treatment.

Traumatic processes of vessels could bring about either hemorrhage, thrombosis, fistula or aneurysm.

Traumatic aneurysms are not uncommon; most of them involve the large basal arteries. The assumption of a traumatic origin is usually based on the close temporal injury and local relationship between a head injury and the later manifestation of the aneurysm.

The treatments of the aneurysms depend on location and size of the lesion. Herein we report our experiences in treatment of the various locations and sizes of the traumatic aneurysms in the head and neck region by endovascular approaches.

MATERIALS AND METHODS

From 1992 to1996, twenty-one cases came to our department for endovascular treatment of the traumatic vascular diseases associated with aneurysm. There were 16 males and 5 females with the range of age from 16 to 60 years old. Nineteen patients had a history of car accident and two had had previous head injury from other causes. Of all patients, 14 patients presented with epitaxis mostly moderate to severe degree. The first episode of epitaxis occured within 5 days to 6 months after injury. The other 7 cases without epitaxis came with sign and symptom of the carotid-cavernous fistula and aneurysms were incidental findings.

Four cases had two aneurysms and all had history of epitaxis. In the group of patients with epitaxis, 18 aneurysms were found and 5 cases

Neuroradiology Section,Diagnostic Division, Department of Radiology, Siriraj Hospital,Faculty of Medicine, Mahidol University, Bangkok, Thailand.

were associated with carotid-cavernous fistula (CCF). The location of the aneurysms are shown in Table I.

In 7 cases without epitaxis, all were diagnosed clinically to be CCF and angiographically proven to have the fistula. The location of the aneurysms are shown in Table II.

ENDOVASCULAR TREATMENTS

The angiographic examination includes four-vessels and bilateral external carotid angiography to exclude additional vascular lesion, appropiate views of the aneurysms and a cross-compression study to assess the competency of the circle of Willis. Embolization is done at the same or the second setting under neuroleptic analgesia with anesthesist in attendance. A thin-walled No.7 or 8 French introducer catheter (Ingenor) is placed in the involved internal carotid artery by transfemoral approach. Continuous perfusion of the introducer catheter is done by heparinized saline. Systemic heparinization is administered by using 3000-4000 units of heparin intravenously before introducing of the balloon.

Gold valve balloon No.9 (If only CCF is found) or No.16 (If associated or only aneurysm of the cavernous portion is found) is used to occlude the CCF and/or the neck of the aneurysm. In the case of aneurysm in cavernous portion, sacrifice of the internal carotid artery is usually the aim. Once the balloon is inflated, the internal carotid artery is arbitrarily occluded for 15-20 minutes under careful clinical monitoring to detect any neurological deficit. In occlusion of the artery, if the patient cannot tolerate, the balloon should be deflated immediately. When tolerance test is successful, sacrifice of the internal carotid artery is done at the cavernous portion with occlusion of the fistula and aneurysmal neck. The stumpectomy of the sacrificed artery is followed by using No.16 GVB at the origin just above the bifurcation. Heparinization is reversed after embolization is completed.

Particulate embolic material such as Gelfoam or Ivalon is used for embolization of the small aneurysm of external carotid artery. There is only one case in our series which is an aneurysm of internal maxillary artery and we used Gelfoam to occlude the aneurysm.

Surgery is the first choice for the treatment of false aneurysm in the cervical portion if it is not occluded in the balloon embolization for treatment of CCF.

RESULTS

In epitaxis group, 14 of 21 patients, sacrifice of the involved internal carotid artery with successful controlling of the bleeding were successfully treated by endovascular mean in 13 out of 14 patients. Ten cases were treated sucessfully in the first setting of embolizaiton. Of the other 3 cases, one with CCF and aneurysm at the cavernous portion, the internal carotid was first sacrificed with 4 more balloons in the aneurysm. The angiogram after 3 months follow up showed filling of the aneurysm. In 8 months follow up angiogram, no aneurysm is seen.

Another case with aneurysm at the cavernous portion was first occluded only the aneurysm neck. Follow up study showed recurrent aneurysm with the first balloon displacement into the aneurysm, so we sacrificed the internal carotid artery in the second setting.

The third case of epitaxis group with two aneurysms at the cavernous part, the internal carotid artery was sacrificed in the first setting but the smaller aneurysm was still seen. After 10 days follow up, no more filling of the aneurysm was shown.

The last patient with severe head injury and carotid-cavernous fistula had one aneurysm at the supraclinoid portion and one at the cavernous portion. The supraclinoid aneurysm was trapped by surgery. Balloon embolization was tried to occlude the internal carotid artery but the balloon was ruptured possibly from bony spicule. The patient had severe epitaxis after the procedure. So emergency ligation of the artery was done by the surgeon.

In the non-epitaxis group,2 of the 4 cervical internal carotid aneurysm, the artery was sacrificed in the same setting for the treatment of the CCF. The other two cervical aneurysms were treated by surgery. One case with common carotid aneurysm at the same site as the CCF, the internal carotid artery was sacrificed for treatment of the CCF. The aneurysm was treated by surgery. Another case of CCF with aneurysm at the anterior choroidal artery was treated only the CCF. The anterior choroidal aneurysm is small and is referred to the surgeon.

The patient with internal maxillary aneurysm was embolized by Gelfoam via 5 French catheter and well occluded.

All patients whose internal carotid arteries were sacrificed have tolerated such occlusion. In one case with supraclinoid aneurysm and severe epitaxis, the ipsilateral eye is blind after the internal carotid artery was sacrificed. One case with CCF and cavernous portion of internal carotid aneurysm has hemiplegia after the treatment, possibly from thrombus emboli to the middle cerebral artery. The other cases have no severe complication.

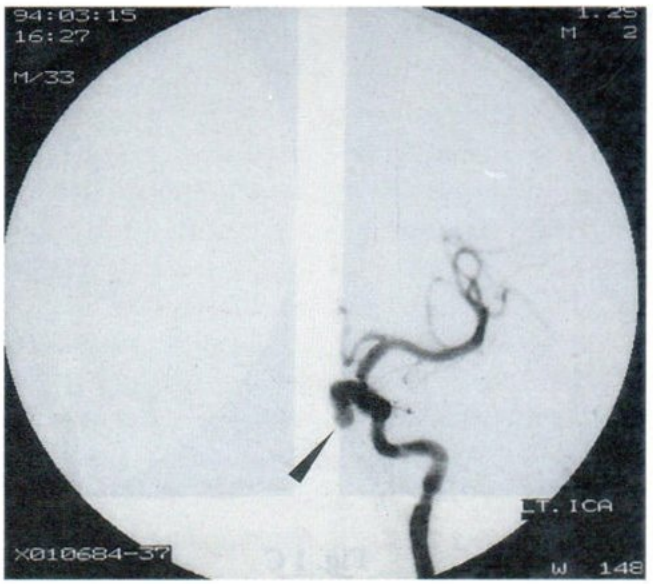

Fig. 1 A

Fig. 1 Traumatic aneurysm of cavernous portion of left internal carotid artery (arrow in A.).

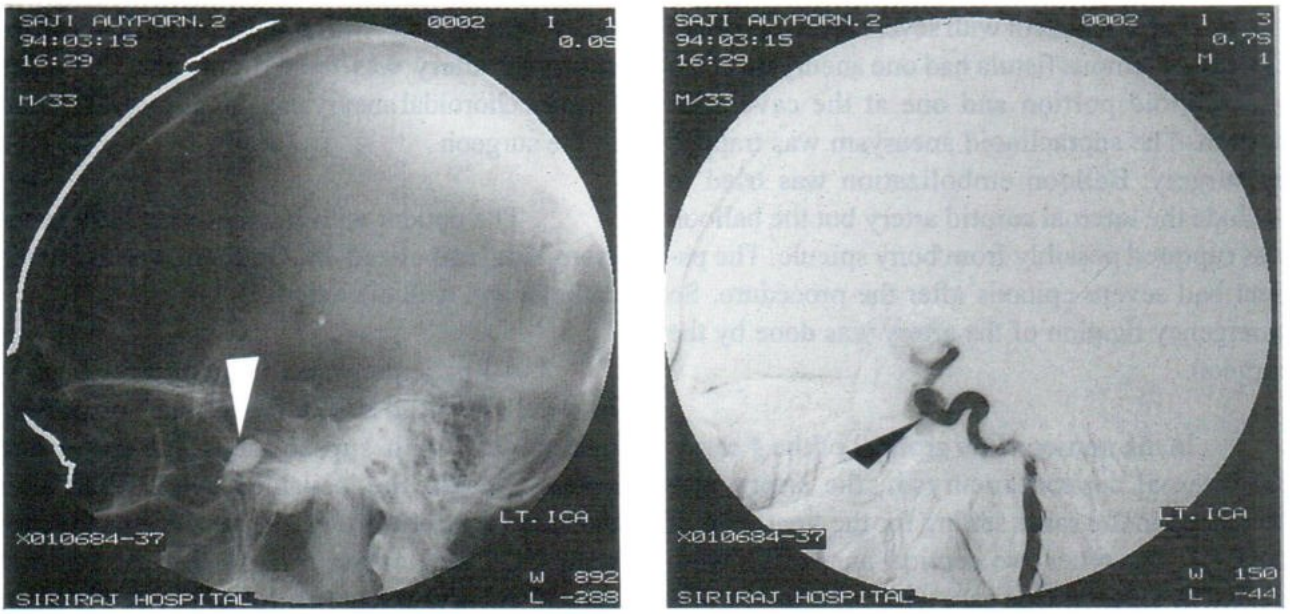

Fig. 1 B

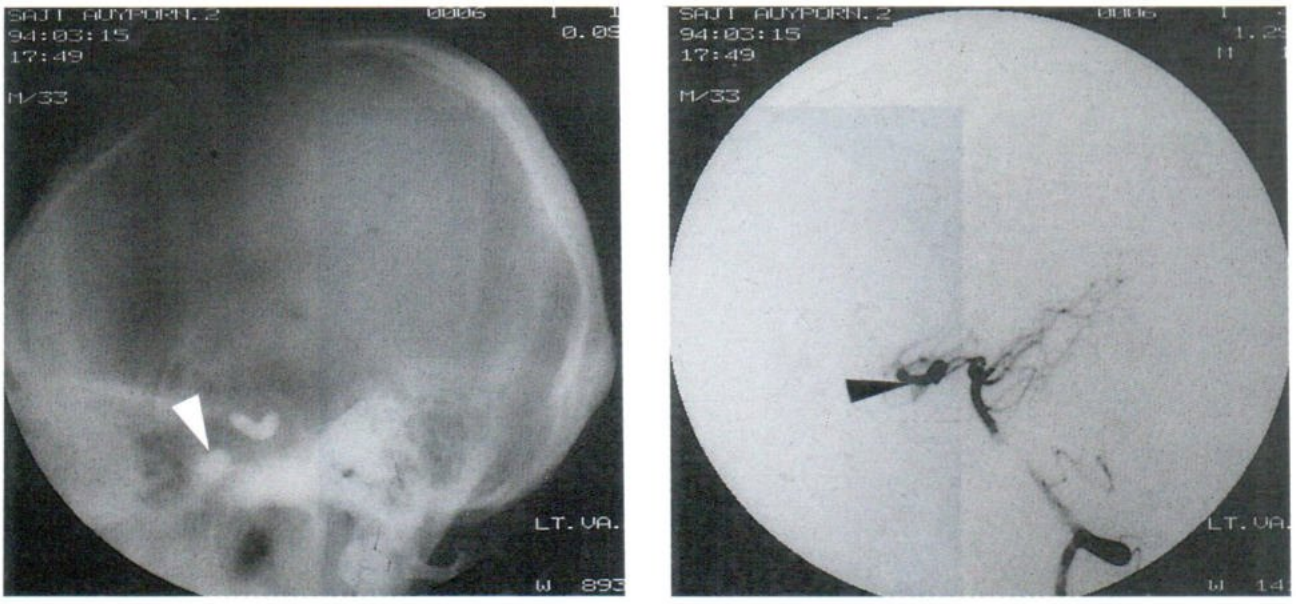

Fig. 1 C

Fig. 2 The first balloon was placed at the aneurysm neck but displaced into the aneurysm (B). Sacrificed left ICA. was done (C).

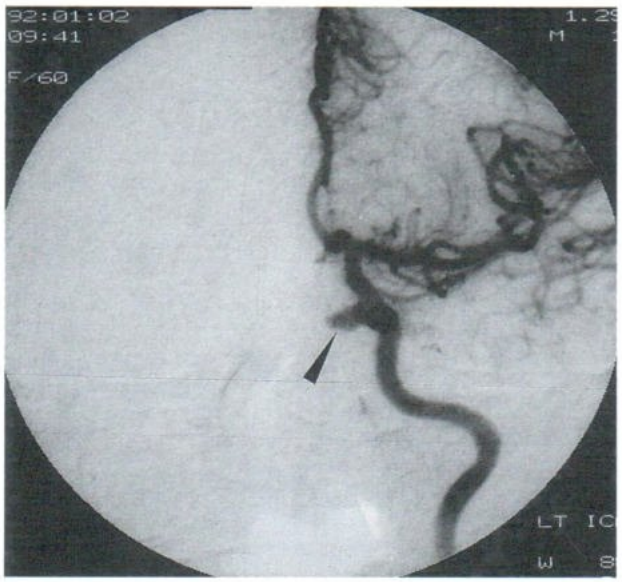

Fig. 2 A

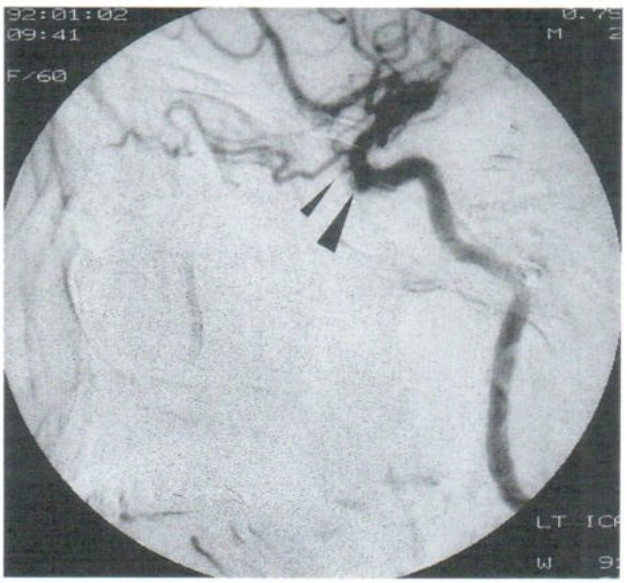

Fig. 2 B

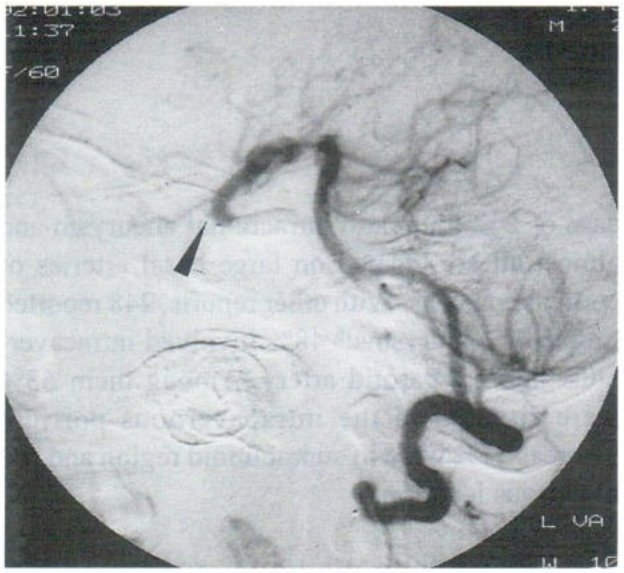

Fig. 2 C

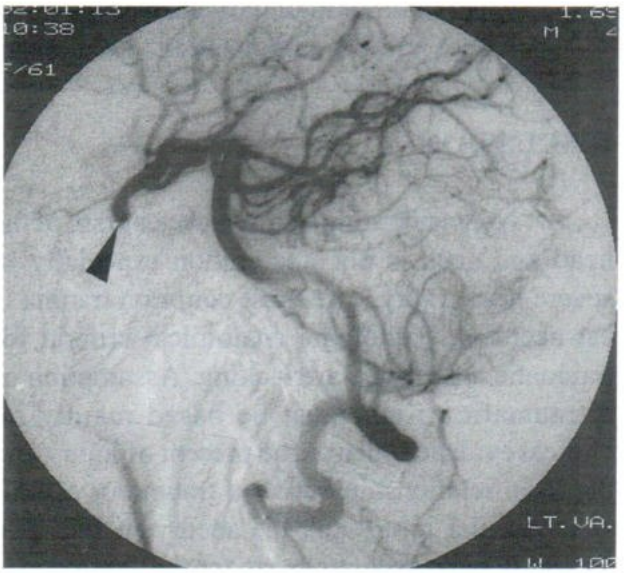

Fig. 2 D

Fig. 2 Two traumatic aneurysm of cavernous portion of left ICA. (arrows in A and B). After sacrificed left ICA, the smaller aneurysm was still seen (arrow in C) . Following up angiogram shows no more aneurysm (D).

Fig. 3 A

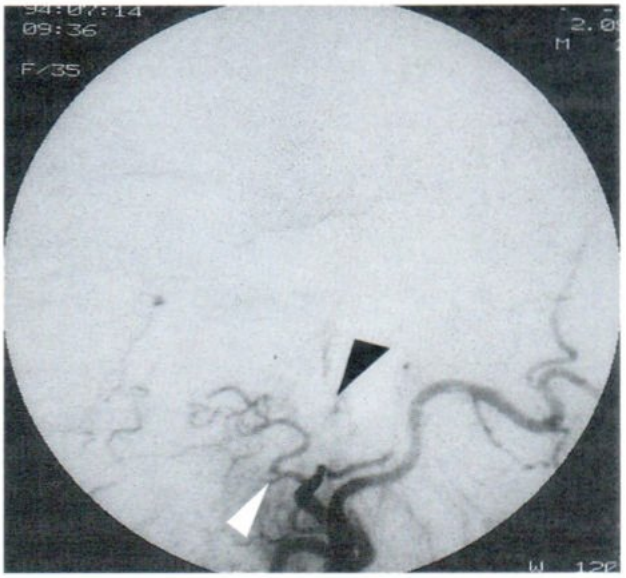

Fig. 3 B

Fig. 3 Right internal maxillary aneurysms (arrows in A). After Gelfoam embolization, no more aneurysm (B).

DISCUSSION

Nonpenetrating traumatic aneurysm of the head and neck is not uncommon especially in severe head injury. The most common trauma is car accident. Pathologic anatomical criteria for traumatic aneurysms are lacking. Assumption of a traumatic origin must be based mainly on clinical evidence such as the present of injury and the local relationship between trauma or associated vascular injury and the aneurysm site. The patient may be asymptomatic for the aneurysm if it is not ruptured especially at the area out side the skull base or cranium such as cervical region. However, in the case of skull base fracture, severe vascular injury does often occur, and the cavernous portion of the internal carotid artery is the most vulnerable to injury. Since the anatomical small space and close relationship to the bone around the cavernous sinus, injury to the vessel by bony spicule or fragment is usually severe. These patients are all symptomatic. Fox[7] listed the case of 242 traumatic intracranial aneurysm and almost all are located on large basal arteries or cortical branches. With other reports, 248 reported traumatic aneurysms[16] 48% involved intracavernous internal carotid artery. Among them 63% were situated in the intracavernous portion, whereas 31% were in supraclinoid region and 6% of petrous location.

Most traumatic intracavernous internal carotid aneurysms present with rupture into the sphenoid sinus had medial tear.[2,9,14,17] In our cases, we have one case of supraclinoid internal carotid and two cases of ophthalmic aneurysms ruptured into the sphenoid sinus as well. All of these cases had history of epitaxis usually delayed and gradually severe in later episodes. The mortality of this condition is 30-50%.[17] The classical triad of unilateral blindness, orbital fractures and massive epitaxis may alert the surgeon to the present of

pseudoaneurysm and emergency treatment may be needed.[9] The mortality rate and recurrent hemorrhage for surgical treatment are still high in most reports.[4,8,14,18] Recent series reported better outcomes of balloon embolization.[1,6,10] Scattered case reports also showed application of the technique in other traumatic aneurysms presenting epitaxis.[15,2,9] In our experiences, balloon occlusion can be easily and readily accomplished under local anesthesia with neurological status continuously monitored. The aneurysm at neck has to be occluded in the arterial side to avoid recurrent opening. Since the fragile aneurysmal wall, the balloon should be aware of propagation into the sac. Sacrificed main artery is suggested. When the internal carotid artery must be sacrificed,[6] the GVB No.16 is recommended because of its elongated shape. The balloon should be placed and occlude the opening of the aneurysm and the entire cavernous segment, there by controlling the branches of C_4 and C_5 segments of the artery which represents the source of recanalization the thrombosed segment.[11] The other balloon for stumpectomy is needed to prevent thrombus embli retrogradely slipping to the supraclinoid cerebral arteries.

Y. Masana[12] reviewed and reported 10 cases of CCF associated with aneurysms. He found correlated ratio of location of the aneurysms with that of aneurysms without CCF. In his report, only direct surgical approach was successful in completely obliterating the CCF and aneurysms. In our 5 patients of cavernous internal carotid aneurysms with CCF. had epitaxis. Four of them were successfully treated with detachable balloon. The last one is the one we tried to sacrificed the artery but ruptured balloon occured and the patient was emergency ligated the artery (as described above). We still recommended that the treatment of choice for such case is detachable balloon occlusion. Both CCF. and aneurysm can be occluded in the same setting. Only one of our five cases had partial occlusion of the aneurysm. Delayed thrombosis and disappearance of the aneurysm was noted after follow up angiogram. Decreasing flow or partial occlusion is also gives some benefit.[1]

Treatment of choice of the cervical carotid aneurysm may be surgery. We try to keep the internal carotid artery for treatment of CCF. and leave the aneurysm for the surgeon. The aneurysm is occluded only in the case that sacrifice of the internal carotid artery for CCF cannot be avoided.

Small aneurysm of the external carotid branches can be treated by many ways such as particulate embolic material and histoacryl. Because of anatomical anastomosis of internal and external carotid system, the particle should not be smaller than 100 um. In our case, we used handcut Gelfoam and injected through the 4-F catheter. The aneurysm was occluded successfully with no complication.

Complications associated with endovascular treatment do occur and are primarily related to distal emboli, either thromboemboli or unwanted embolization of the normal cerebral artery and subsequent strokes. The risk of the procedure is largely related to the careful approach, adequate heparinization, and knowledge of the anatomical vessels and used instruments. One of our cases had hemiplegia possible from thromboemboli. The other one had blindness which could not be avoided because of the near ophthalmic origin of the supraclinoid aneurysm. In order to stop bleeding of severe epitaxis and save the patient life, we had to place the balloon and occlude the ophthalmic origin. In some of our cases which the aneurysm is near the ophthalmic artery, if the artery also has the blood supply from external-carotid system, the vision can be spared.

With the experiences of these cases, we can conclude that endovascular treatment is indicated in traumatic aneurysms of head and neck especially in the area that surgical approach is difficult such as base of skull. Urgent treatment is

needed in the case with epitaxis and detachable balloon occlusion to sacrifice the internal carotid artery and aneurysm is recommended.

Table I (A) Site of aneurysms in epitaxis (aneurysm/case)

	No CCF	With CCF
Cavernous ICA	9/7	5/5
Supraclinoid ICA	1/1	1/1
Opthalmic	2/2	-
Total	12/10	6/6

NB : ICA = Internal carotid artery
ICA = Carotid - cavernous fistula
Four cases with two aneurysms in each patient.

Table I (B) Site of aneurysms in 4 cases with double aneurysms

Case I	:	2 aneurysms at cavernous ICA.
Case II	:	2 aneurysms at cavernous ICA,
Cases III	:	1 aneurysm at cavernous ICA, 1 at supraclinoid ICA.
Cases IV	:	1 aneurysm at cavernous ICA, 1 at ophthalmic origin

Table II Site of aneurysms in nonepitaxis (case)

Cervical ICA	4
Common CA	1
Anterior choroidal	1
Internal maxillary	1

ICA = Internal carotid artery.

Table III Treatment of aneurysms in epitaxis.

Sacrificed ICA	13
Surgery	1

Table IV Treatment of nonepitaxis

Detachable balloon occlusion (Sacrificed ICA)	2	(Cervical ICA)
Gelfoam	1	(IMA)
Surgery	4	

REFERENCE

1. Bernstein A, Ransohoff J., Kupersmith M, et al: Transvascular treatment of giant aneurysms of the cavernous carotid and vertebral arteries : Functional investigation and embolization. Surg Neurol 21:3-12,-1984.
2. Crow WN, Bruce AS, Faustino CGJ., et al : Massive epitaxis due to pseudoaneurysm : Treated with detachable balloons. Arch Otolaryngol Head Neck Surg 118:-321-324, 1992
3. Debrun G, Fox A., Drake C : Giant unclippable aneurysms Treatment with detachable balloons. AJNR 2:167-173,1981
4. Drake CG ; Giant intracranial aneurysms: Experience with surgical treatment in 174 patients. Clin Neurosurg 26:12-95,1979
5. Enomoto H., Shibata T., Ito A., it al : Traumatic aneurysm of the supraclinoid internal carotid artery : report of a case. Neurosurgery 15:700-702,1984
6. Fox AJ.Vinuela F., Pelz DM, et al : Use of detachable balloonsfor proximal artery occlusion in the treatment of unclippable cerebral aneurysms. J. Neurosurg 52:1-10,1980
7. Fox. JL : Intracranial aneurysms. New York : Springer - Verlag, 1983
8. Giannotta SL, Mc Gillicuddy JE, Kindt GW : Gradual carotid artery occlusion in the treatment of inaccessible internal Carotid artery aneurysm. Neurosurg. 5:417-421,1979
9. Han MH, Sung MW, Chang KH, et al : Traumatic pseudoaneurysm of the intracavernous ICA presenting with massive epitaxis : Imaging diagnosis and endovascular treatment. Laryngoscope 104:370-377,1994
10. Higashida RT, Halbach VV., Dowd CF., et al : Intracranial neurovascular treatment with detachable balloons - Results in 215 cases. Radiology 178:633-670,1991

11. Lasjaunias P. (With collaboration of Berenstein A.) : Craniofacial and upper cervical arteries. Vol. Baltimore : Williams & Wilkins, 1981
12. Masana Y, Taneda M : Direct approach to a traumatic gian internal carotid artery aneurysm associated with a carotid-cavernous fistula : Case report J. Neurosurg 76:-524-527,1992
13. Parkinson D, West M.: Traumatic intracranial aneurysms J. Neurosurg 52:11-20,-1980
14. Saim L, Rejab E., Hamzah M, et al : Massive epitaxis from traumatic aneurysm of the internal carotid artery. Aust. N.Z.J. Surg 63:906-910, 1993
15. Simpson RK., Harper RL., Bryan RN : Emergency balloon occlusion for massive epitaxis due to traumactic carotid - cavernous aneurysm : Case report. J Neurosurg 68:142,1988
16. Steinmetz H , Heip E., Mironov A. : Traumatic giant aneurysms of the intracranial carotid artery presenting lung after head injury. Surg Neurol 30:305-310,1988
17. Wang AN, Winfield JA, Gucer G. : Traumatic internal carotid artery aneurysm with rupture into the sphenoid sinus. Surg Neurol 25:77-81,1986
18. Worthington BS, Kean DM, Hawks RC, et al : NMR imaging in the regonition of giant intracranial aneurysms. AJNR 4:835-836,1983

QUALITY ASSURANCE IN RADIOTHERAPY BY IN VIVO DOSIMETRY ; ENTRANCE DOSE MEASUREMENT

L. TUNTIPUMIAMORN,M.Sc,[1] V. POLVATSATIAN,B.Sc,[1]
B. CHAORUNGRIT,B.Sc,[2] P. SUKPRASERT,B.Sc,[2]

ABSTRACT

Quality assurance in radiotherapy by in vivo dosimetry was performed at the Division of Radiation Oncology, Department of Radiology,Siriraj Hospital during August 1996 to January 1997. The entrance doses of a total number of 467 treatment set-ups (182 cancer patients)undergoing radiation therapy with Cobalt-60 Teletherapy unit were measured with semiconductor detectors. From the study , the global results of the percentage ratios of the measured dose and calculated dose showed a Gaussian frequency distribution which a mean and one standard deviation value were 99.2+3.34 %. This meaned that the uncertainty caused by a systematic and random errors in the treatment delivery were 0.8% and 3.34% respectively. Eighty-seven percents of all treatment set-ups are reliable due to the dose delivered fitted in ±5% of the prescribed dose while the treatments with a large error (2SD) were found in 2.99%. Source of the uncertainties in this study arised from incorrect dose calculation , contour irregularities, human mistakes in treatment setting-up , insufficient immobilization and erroneous in the entrance dose measurements themselves.

INTRODUCTION

The outcome of radiation therapy ,local control and complication, is closely related to the dose delivered to the clinical target volume and surrounding normal tissue. A small change in the absorbed dose can give rise in failure of tumour control and complication probabilities[1]. Especially, when the prescribed total dose are closed to the tolerance of the surrounding normal tissues, it is critical to deliver the accurate prescribed dose to the target volume. ICRU in its report No.24 recommended the actual dose delivered to the clinical target volume should be within ±5% of the prescribed dose[2]. WHO in 1988 also published the guidebook of the quality assurance programme in radiation therapy to urge the radiotherapy centers all over the world to control thier treatment quality[3]. In this study ,we aim to investigate the dose accuracy delivered to the patients undergoing radiation therapy with Cobalt-60 Teletherapy unit at the Division of Radiation Oncology,Siriraj Hospital, Mahidol University by in vivo dosimetry.

MATERIAL AND METHOD

The semiconductor detector Rainbow type 30-490-80 (suitable for photon in the energy range of Cobalt-60 to 4 MV x-rays) connected with electrometer was selected in this study due to its main advantage of no time delay between measurements and results. First, it was calibrated with 0.6 cm^3 NE Farmer Dosemeter type 2570/1 . The calibra-

[1] Division of Radiation Oncology, Department of Radiology, Faculty of Medicine, Siriraj Hopital, Mahidol University, Bangkok 10700, Thailand
[2] Department of Radiological Technology, Faculty of Medical Technology, Mahidol University, Bangkok 10700, Thailand

tion was performed with the four diodes in calibration disk positioned on the surface of a solid water phantom (30cmx30cmx30cm) at the center of 15cm x15 cm field at 80 cm SSD with Cobalt-60 Teletherapy unit. (Fig 1)

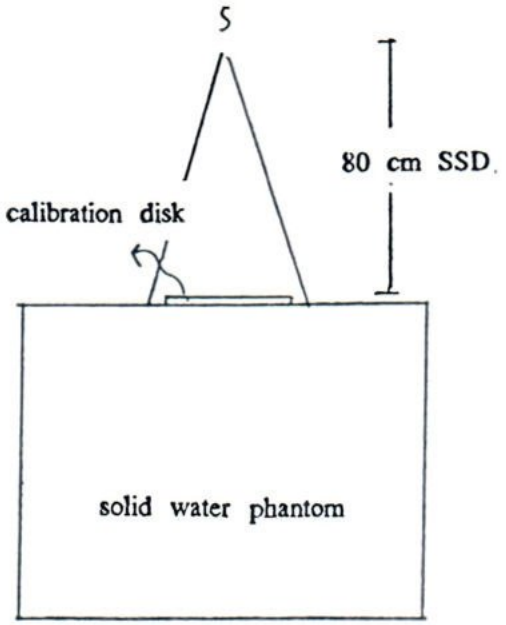

Fig. 1 The calibration geometry of semiconductor diodes

Since four diodes were used in this study, so the calibration factor (F_{cal}) was determined for each individual . The entrance dose calibration will be determined as the ratio of the absorbed dose measured with ionization chamber (D_{IC}) at depth of maximum dose (0.5 cm) and the reading gained by semiconductor(R_{SC}). Therefore, the calibration factor of each diode was

$$F_{CAL} = \frac{D_{IC}}{R_{SC}}$$

MEASUREMENT ON PATIENTS

Having been calibrated completely, the diode will be positioned in the center of the treatment field on the skin of the patient after the treatment set-up was performed as usual from the radiological technologist. The signal from the electrometer will be evaluated at the end of an irradiation and was converted to the measured entrance dose. Correction factors due to irradiation geometry differed from the reference geometry such as collimator openning, tray, source-skin distance (SSD) also have to be determined and applied to the following equation.[4]

$$\text{MEASURED ENTRANCE DOSE} = SC\ SIGNAL\ X\ F_{CAL}\ X\ C.F_{FIELDSIZE}\ X\ C.F_{TRAY}\ X\ C.F_{SSD}$$

Then the data of measured entrance dose will be evaluated as percentage of the ratios of measured and expected (or calculated) entrance dose(% MD/ED). Expected entrance dose is manually calculated from the dose at depth of maximum of the prescribed dose. Because of the importance of having sufficient data for statistical analysis, in this study the data will be received from making a few measurements on many patients as suggested from Dobbs HJ,et al.[5]

MD = Measured entrance dose

ED = Expected (or calculated) entrance dose

RESULTS

From the entrance dose measurements on the total number of 182 cancer patients undergoing radiation therapy at the Division of Radiation Oncology, Siriraj Hospital, the distribution of the patients receiving measurement are classified as in Table 1.

Table1. Distribution of the patients receiving entrance dose measurements

Group of patients	No. of patients	No.of measurements	No.of measurements/patient
Head & Neck	96	261	2.72
Mediastinal	23	36	1.56
Breast	32	118	3.69
Spine	6	16	2.66
Pelvic	25	36	1.44
Total	182	467	2.56

The data of the entrance dose measurements were plotted as the frequency distribution of the ratios of measured dose and expected dose in percentage (%MD/ED). N was the number of treatment set-ups measured, the mean value (X) and one standard deviation (SD) were also calculated from the data.

GLOBAL RESULTS OF ENTRANCE DOSE MEASUREMENT

The overall results of the total number of 467 treatment set-ups showed a distribution of % MD/ED with a mean value of 99.20% and one relative standard deviation of 3.34% as presented in Fig. 2 The discrepancy between the measured and the expected mean value was 0.8%.

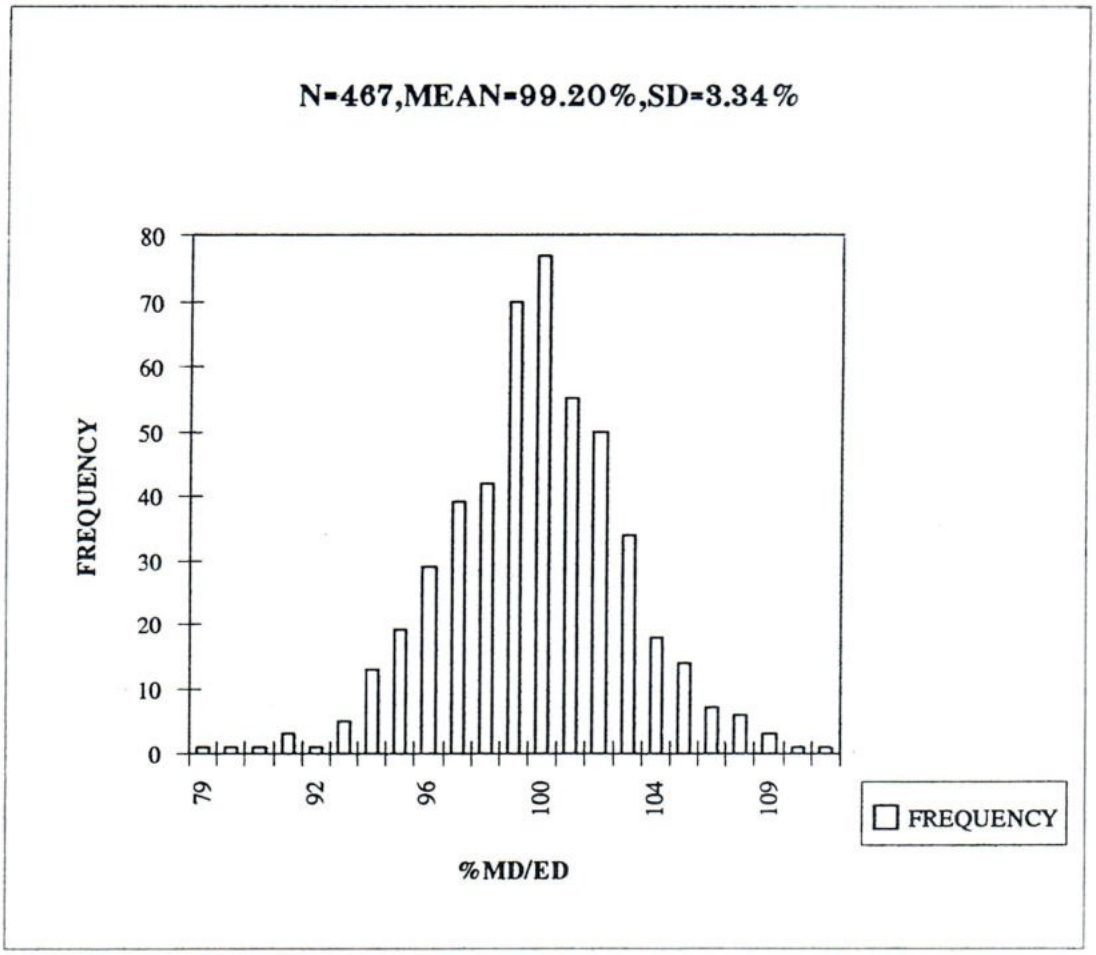

Fig.2 Frequency distribution of overall results of entrance dose measurement

RESULTS OF ENTRANCE DOSE MEASUREMENT ON PATIENTS TREATED FOR HEAD AND NECK MALIGNANCY

Radiation treatment technique in head and neck malignancy are two -paralleled opposing fields and one anterior cervical split field. The entrance dose measurement was performed on lateral field only because it cannot be measured correctly on central-blocked field such as anterior split field. Total number of 261 lateral field treatment set-ups (96 patients) were measured and the mean value of %MD/ED in this group of patients was 98.84% and one standard deviation of 2.98% as shown in Fig 3.

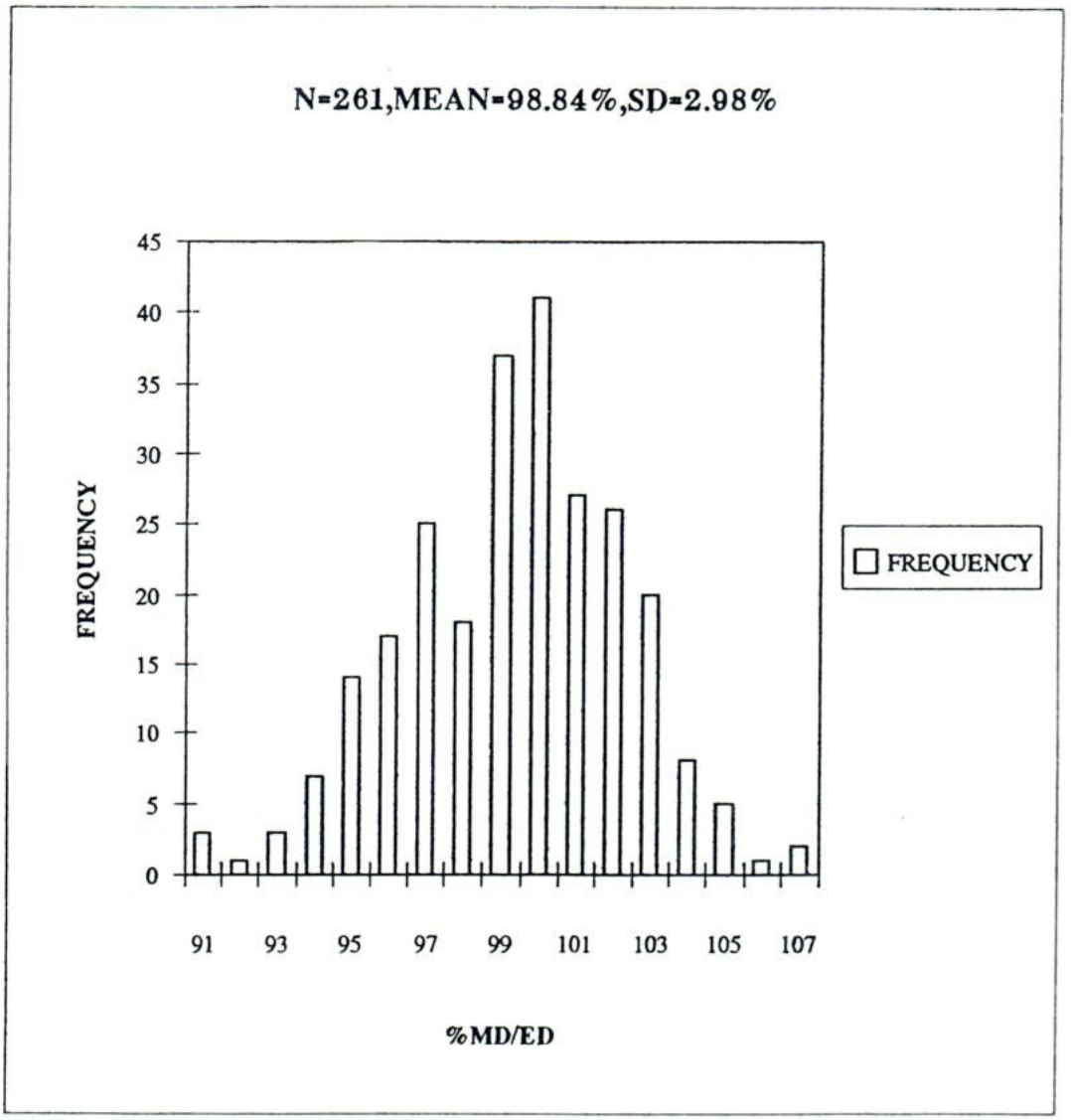

Fig. 3 The histogram showed frequency distribution of % MD/ED in head and neck malignancy patients

RESULTS OF ENTRANCE DOSE MEASUREMENT ON BREAST CANCER PATIENTS

Most of patients received radiation therapy with the Quadrate Technique. Entrance dose measurement was performed on all treatment fields (Internal mammary chain, Supraclavicular-axillary and Tangential fields) and the ratios of % MD/ED were plotted in Fig 4. The total number of measurements performed was 118 measurements on 32 patients. The mean and one relative standard deviation value of % MD/ED was 100.43±3.86. It can be seen that the frequency spread of the results in breast cancer was broader than the head and neck malignancies.

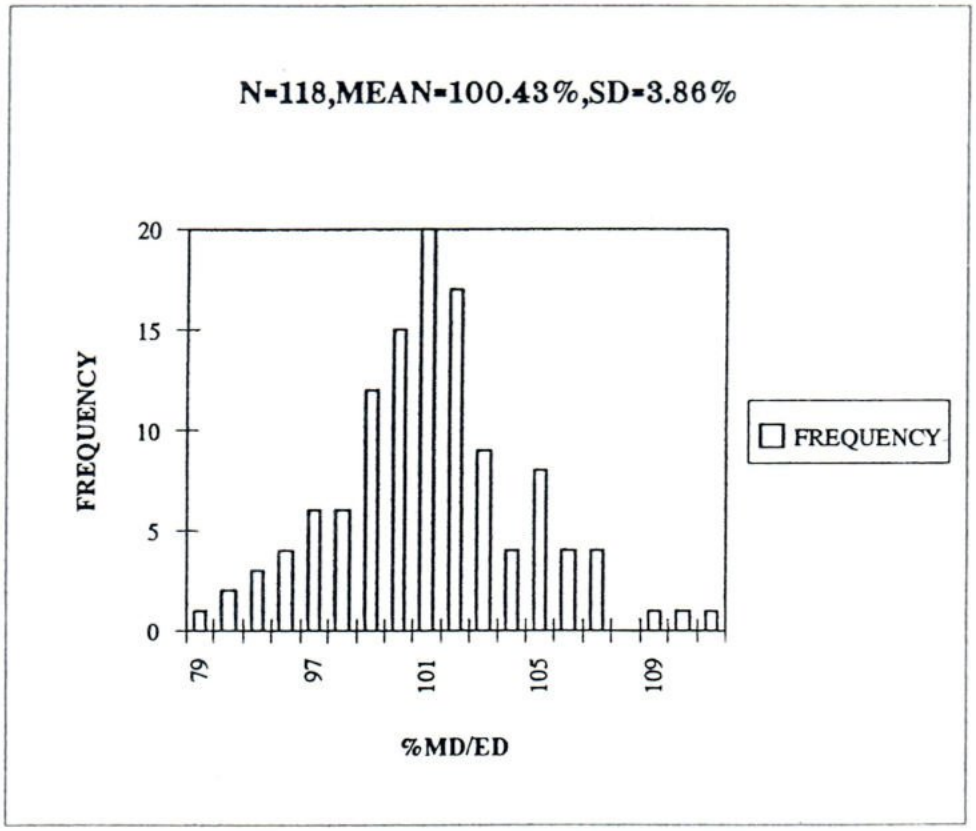

Fig 4. The histogram showed frequency distribution of % MD/ED in breast cancer patients

Results of entrance dose measurement on other treatment sites such as mediastinum, pelvic and spines, were not plotted in histogram due to a small number of data in each site. The results of the mean and one standard deviation of % MD/ED in all treatment sites are summarized in Table 2.

Table 2 Mean (X) and one relative standard deviation (%SD) of %MD/ED in all treatment sites

Treatment Sites	No. of Measurements (N)	Mean	% SD
Head & Neck	261	99.84	2.98
Breast	118	100.43	3.86
Medistinum	36	97.33	3.00
Pelvic	36	98.90	2.15
Spines	16	100.68	4.35

DISCUSSION

From the global results of entrance dose measurement , the percentage ratios of measured and calculated dose (%MD/ED) have a mean and one standard deviation equal to 99.2 ± 3.34 %.

The discrapancy between measured and calculated dose 0.8% implied to the systematic error found in our treatment delivery. This kind of error arised from poor measurement and calibration process including poor initial adjustment. As well as the standard deviation value 3.34% indicated to the random error caused by human mistakes in patient setting-up such as setting up of the machine parameters, patient positioning and patient immobilization.[6]

In this study, both of the systematic and the random error founded were reasonably acceptable because they were in good agreement with the studys of Leunens G[4] and Mijnheer et al[7] that concluded the uncertainty associated with dose delivery should be less than ± 3.5% ,expressed as one relative standard deviation. And from the calculations of Goitein[8] the 5% accuracy requirement as proposed by the ICRU should be considered as 1.5 SD. In our investigation 86.94% of all treatment set-ups are fitted in this requirement. Large error that defined as a discrapancy between measured and calculated dose in + 2SD have also been detected in 2.99% of all meaurements. Source of errors came from incorrect dose calculation, contour irregularities, insufficient immobilization and also an errorneous in entrance dose measurement themselves due to the measurement geometry differing from the calibration geometry such as the measurement on Tangential breast irradiation.

For breast cancer dose measurement, the results showed a broader of standard deviation in %MD/ED than in head and neck malignancy. When 118 data of entrance dose were analyzed, we found that 83 measurements performed on Internal mamary chain and Supraclavicular-axillary field has a mean + SD of % MD/ED equal to 99.32+2.7%, while the other 35 measurements performed on Tangential field was 100.26±5.03%. These data coincided with the study of Leunens G, et al[9] that reported the treatment error was found 15% in Tangential breast irradiation in Cobalt-60 Machine without automatic verification system compared to treatment error of 2.3% in Mevatran Siemen linear accelerator when this system was available.

Results of entrance dose measurement on spinal irradiation also has a large standard deviation (4.35%). However, having a small number of data therefore we cannot make any discussion here.

CONCLUSION

It could be concluded from the study that the quality of whole treatment chain, that means dosimetry, dose calculation ,treatment techniques using in our treatment delivery, would be in a satisfactory level as well as improvement in treatment techniques such as effective immobilization and reproducibility, machine with auto-verification system, should be provided to minimize the incidence of random error.

REFERENCES

1. Herring DF, Compton DMJ. The degree of precision required in the radiation dose delivered in cancer therapy. BJR suppl 5, 1971:51
2. ICRU Determination of absorbed dose in a patient irradiated by beams of X or Gamma rays in radiotherapy procedures. Report 24, ICRU, Washington 1976.

3. World Health Organization. Institue of Radiation Hygience, Federal Health Office, Neuherburg, Federal Republic of Germany. Quality assurance in radiotherapy. England, 1988
4. Leunens G, Van Dam J, Dutriex A, Van Der S. Quality assurance in radiotherapy by in vivo dosimetry. 1. Entrace dose measurements, a reliable procedure. Radiotherapy and Oncology, 1990;17:141-151
5. Dobbs HJ, Dutriex A, Johansson KA, Leunens G. Treatment preparation and in vivo dosimetry. Regional seminar for Asia and the Pacific on Radiotherpy Dosimetry. Bangkok, Thailand, 28 Nov-1 Dec 1995
6. Dutriex A. When and how can we improve precision in radiotherapy?. Radiotherapy and Oncology, 1984;2:275-292
7. Mijnheer BJ, Battermann JJ, Wambersie A. What degree of accuracy is required and can be achieved in photon and neutron therapy?. Radiother. Oncol, 1987;8:237-252
8. Goitein M. Calculation of uncertainty in the dose delivered during radiation therapy. Med Phys, 1985;12:608-612
9. Leunens G, Verstraele J, Van Dam J, Dutriex A, Van Der Schueren E. Experience in in- vivo dosimetry investigation in Leuven. Radiother Oncol, 1991:283

THE FIELD SIZE AND DEPTH DEPENDENCE OF WEDGE TRANSMISSION FACTOR FOR HIGH ENERGY PHOTON BEAMS

Nisakorn MANATRAKUL M.Sc.[1]
Chumpot KAKANAPORN M.Sc.,[2] Yaowapa PISUTTISUP B.Sc.[3]

The wedge transmission factors (WTF) usually were assumed to be used for clinical treatment planning system by independence on field size and depth of measurement. For this study, the field size and depth dependence of the in phantom WTF has been determined for Co-60 teletherapy unit and three Linear Accelerator energies of 6, 10 and 15 MV X-ray beam, containing 15°-60° lead, brass and alloy wedge filters. All measurements were made with a cylindrical ionization chamber in water or solid water phantom with a source-skin distance of 80 cm or 100 cm. Field sizes varied from 4x4 cm^2 up to a maximum allowable size for each wedge filter. Several depths of measurement were selected: d_{max}, 5 cm (AAPM TG-21 calibration depth), 10 cm and 15 cm.The results show that use of single wedge WTF measured for 10x10 cm^2 field introduces error less than 3% for field size not exceeding than 15x15 cm^2 for all energies, but for a 22x22 cm^2 field size, the error is up to 5%, 5.5%, 6% and 4.5% for Co-60, 6, 10 and 15 MV respectively. Moreover, for a 25x25 cm^2 field size the error is up to 7.6% and 5.7% for 6 and 15 MV respectively . For the depth dependence study, we conclude that the WTF at depth for Co-60 differ not exceeding 3.5% from the determined values at TG-21 calibration depth and for 6, 10 and 15 MV X-ray there are about 4.4%, 2% and 2.8% difference respectively. In this paper we have attempted to show that there is a definite dependence of WTF on field size and depth. Therefore a WTF measurement for a reference field size and depth may not be valid for all field sizes and depths.

INTRODUCTION

The use of wedge filters to obtain desirable dose distributions in external beam treatment planning is well established technique in radiation therapy. This is used to optimize dose distributions with high energy photon beams. The wedge transmission factor (WTF) in dosimetry calculation are very common, but various methods have been used in measuring this factor. Conventionally, it is recommended that the reference field size and the reference depth be used instead of the dose maximum for these kinds of measurements to avoid the influence of contaminating electron in the beam.[1] The WTF used for clinical treatment planning system is generally assumed to be independent on field size and depth of measurement. We intended to investigate the field size and depth dependence of WTF for various beam energies. This paper reveals our findings which effects the accuracy of dose calculations for patients treatments .

Presented at the World Congress on Medical Physics and Biomedical Engineering, 14-19 September 1997, Nice, France.

[1] Division of Radiation Oncology, National Cancer Institute, Bangkok, Thailand
[2] Division of Radiation Oncology, Siriraj Hospital, Bangkok, Thailand

MATERIALS AND METHODS

The WTFs were determined in water phantom or solid water phantom, using a Farmer type 0.6 cm^3 ion chamber with a Farmer type 2570/1 electrometer for cobalt -60 gamma rays from a Theratron 780C (manufactured by Theratronix International Limited), 10 MV X-rays from a ML-15M linear accelerator (manufactured by Misubishi), 6 MV and 15 MV X-rays from MD and KD Mevatron linear accelerators (manufactured by Siemens Medical System). Measurements were taken by varying field sizes from 4x4 cm^2 up to a maximum allowable sizes for each wedge filter containing 15° - 60° lead, brass and alloy wedges. Measurement were also taken at the beam center of each machine (80 cm or 100 cm SSD): for the depth of d_{max}, the calibration depths recommended by the AAPM protocol TG 21 (5 cm: Cobalt-60, 6, 10 and 15 MV);[2] the recommended depth of 10 cm for wedge angle specification (ICRU);[3] and another depth, of 15 cm, relevant of treatment planning considerations of deep tumors. To confirm that the wedge was centered, measurements were performed with the two possible wedge positions and various collimator orientations. The WTFs were then calculated by taking the ratio of the central axis ionization reading with wedge filter in place to the open field reading for the same field size and depth of measurement. Results were further shown with WTF normalized to 10x10 cm^2 field for the field size dependence study in table I-IV in the term of relative wedge factor (RWFa).

RWFa = WTF (d, a) / WTF (d, 10x10)

Furthermore, the results for the depth dependence study were shown with WTF for 10x10 cm^2 field normalized to the TG-21 calibration depth in table V-VIII in the term of relative wedge factor (RWFd).

RWFd = WTF (d) / WTF (d 5 cm)

RESULTS

The WTFs were found to be similar for each energy: for the field size dependence, the WTF increased with increasing field sizes and for the depth dependence, the WTF increased with increasing depths. Table I-IV showed the relative wedge factors as a function of field size normalized to the field size 10x10 cm^2 for each energy. For cobalt-60 (Table I) there was a small percentage difference for the field size not more than 15x15 cm^2, the maximum values were 1.3%, 1.7%, 2.3% and 3% at the depth of d_{max} , 5 cm , 10 cm and 15 cm respectively. But for the field size greater than 15x15 up to 22x22 cm^2, the maximum percentage difference were 5.0%, 4.6%, 4% and 3.7% at the depth of d_{max}, 5 cm, 10 cm and 15 cm respectively.

TABLE I. Relative Wedge factors for cobalt-60 teletherapy unit. Factors normalized to the field size 10x10 cm ^{2}

Wedge angle	Measurement position (depth)	Side of equivalent square field (cm) 5	6	8	9	10	12	15	18	20	22
	d_{max}	0.992	0.994	0.9970	0.999	1.000	1.006	1.012			
15°	5.0 cm	0.992	0.993	0.997	0.997	1.000	1.006	1.006			
	10.0 cm	0.991	0.991	0.997	0.998	1.000	1.006	1.014			
	15.0 cm	0.985	0.985	0.996	0.999	1.000	0.998	0.998			
	d_{max}	0.999	0.998	0.999	0.999	1.000	1.003	1.008			
30°	5.0 cm	1.001	1.001	1.003	1.002	1.000	1.005	1.006			
	10.0 cm	0.995	0.994	0.997	0.997	1.000	1.001	1.005			
	15.0 cm	0.993	0.984	0.994	0.999	1.000	0.988	0.991			
	d_{max}	0.991	0.992	0.995	0.997	1.000	1.004	1.012			
45°	5.0 cm	1.000	1.009	1.007	0.998	1.000	**1.017**	1.006			
	10.0 cm	0.995	0.992	0.997	0.999	1.000	1.008	1.016			
	15.0 cm	0.991	0.990	1.005	1.008	1.000	1.010	1.008			
	d_{max}	**0.987**	0.989	0.994	0.997	1.000					
60°	5.0 cm	0.983	0.986	1.006	0.991	1.000					
	10.0 cm	**0.977**	0.981	0.988	0.995	1.000					
	15.0 cm	**0.970**	0.970	0.985	0.986	1.000					
	d_{max}	0.994	0.995	0.997	0.998	1.000	1.004	1.011	1.019	1.026	1.031
30°	5.0 cm	0.997	0.998	0.997	0.997	1.000	1.004	1.007	1.020	1.023	1.028
	10.0 cm	0.993	0.990	0.997	0.997	1.000	1.002	1.007	1.014	1.016	1.020
	15.0 cm	1.000	0.992	0.995	0.997	1.000	0.992	0.996	1.001	1.016	1.020
	d_{max}	0.991	0.990	0.997	0.996	1.000	1.020	1.019	1.033	1.041	**1.050**
25°	5.0 cm	0.992	0.990	0.996	0.997	1.000	1.008	1.013	1.033	1.038	**1.046**
	10.0 cm	0.986	0.988	0.996	0.997	1.000	1.004	1.015	1.026	1.032	**1.040**
	15.0 cm	0.992	0.985	1.004	0.997	1.000	1.004	1.005	1.019	1.009	**1.037**

TABLE II. Relative Wedge Factors for 6 MV photon beam. Factors normalized to the field size 10x10 cm^2.

Wedge angle	Measurement position (depth)	Side of equivalent square field (cm) 4	5	6	8	10	12	15	17	20	22	25
	d_{max}	1.002	1.005	1.000	1.002	1.000	1.000	1.004	1.008	1.013	1.015	1.025
15°	5.0cm	1.002	1.000	1.001	0.998	1.000	1.001	0.999	1.003	1.006	1.012	1.016
	10.0cm	1.024	1.023	1.024	1.023	1.000	1.019	1.017	1.017	1.018	1.027	1.032
	15.0cm	1.002	0.999	0.998	1.002	1.000	0.994	0.998	0.995	0.998	1.005	1.008
	d_{max}	1.000	1.006	1.006	1.006	1.000	1.005	1.010	1.018	1.028	1.032	1.042
30°	5.0cm	1.000	0.996	0.999	0.995	1.000	1.002	1.002	1.009	1.017	1.022	1.034
	10.0cm	1.022	1.025	1.019	1.018	1.000	1.019	1.018	1.023	1.031	1.038	1.040
	15.0cm	1.009	1.008	1.006	1.008	1.000	1.003	1.001	1.004	1.007	1.011	1.020
	d_{max}	0.987	0.993	0.995	0.995	1.000	1.002	1.012	1.021	1.036	**1.048**	**1.076**
45°	5.0cm	1.010	1.006	1.005	0.995	1.000	1.008	1.012	1.031	1.043	**1.055**	**1.073**
	10.0cm	1.016	1.018	1.015	1.018	1.000	1.014	1.019	1.027	1.041	**1.055**	**1.068**
	15.0cm	1.016	0.987	1.008	0.998	1.000	1.012	**1.018**	1.008	1.028	1.029	**1.049**
	d_{max}	0.992	0.999	0.999	0.997	1.000	1.000	**1.017**	1.025	1.037		
60°	5.0cm	1.000	1.003	1.000	0.997	1.000	1.006	**0.987**	1.025	1.035		
	10.0cm	1.028	1.027	1.022	1.021	1.000	1.023	**1.026**	1.032	1.020		
	15.0cm	1.013	1.001	1.010	1.002	1.000	1.008	1.011	1.014	**1.031**		

TABLE III. Relative Wedge factors for 10 MV photon beam. Factors normalized to the field size 10x10 cm^2.

Wedge angle	Measurement position (depth)	Side of equivalent square field								
		5	6	8	10	12	15	17	20	22
15°	d^{max}	0.988	0.986	0.993	1.000	1.006	**1.023**	1.029	1.051	**1.060**
	5.0 cm	0.989	0.994	0.995	1.000	1.006	**1.021**	1.031	1.041	**1.045**
	10.0 cm	0.991	0.992	0.995	1.000	1.006	**1.018**	1.025	1.033	**1.039**
	15.0 cm	0.997	0.997	0.998	1.000	1.007	**1.017**	1.023	1.030	**1.039**
30 °	d_{max}	0.994	0.997	0.999	1.000	1.007	1.017	1.021	1.038	1.045
	5.0 cm	0.989	0.991	0.995	1.000	1.002	1.013	1.020	1.030	1.034
	10.0 cm	0.992	0.993	0.995	1.000	1.006	1.013	1.018	1.027	1.033
	15.0 cm	0.988	0.989	0.993	1.000	1.003	1.012	1.014	1.022	1.028
45°	d_{max}	0.996	0.994	0.995	1.000	1.004	1.011	1.016	1.034	1.041
	5.0 cm	0.989	0.993	0.996	1.000	1.003	1.013	1.020	1.031	1.032
	10.0 cm	0.992	0.992	0.994	1.000	1.005	1.012	1.017	1.025	1.031
	15.0 cm	0.990	0.991	0.992	1.000	1.000	1.008	1.010	1.018	1.024
60 °	d_{max}	0.996	0.990	0.994	1.000	1.004	1.012	1.016		
	5.0 cm	0.991	0.993	0.995	1.000	1.003	1.013	1.018		
	10.0 cm	0.992	0.993	0.996	1.000	1.005	1.014	1.023		
	15.0 cm	0.989	0.989	0.994	1.000	1.007	1.016	1.024		

TABLE IV. Relative wedge factors for 15 MV photon beams. Factors normalized to the field size 10x10 cm^2.

Wedge angle	Measurement position (depth)	Side of equivalent square (cm)										
		4	5	6	8	10	12	15	17	20	22	25
15 °	d_{max}	1.004	1.006	0.999	0.998	1.000	1.002	1.004	1.003	1.004	1.010	1.011
	5.0 cm	0.997	1.000	1.003	1.005	1.000	1.009	1.012	1.011	1.013	1.012	1.017
	10.0 cm	1.006	1.007	1.010	1.001	1.000	0.991	1.000	0.995	1.005	1.000	1.017
	15.0 cm	0.995	0.994	0.989	1.002	1.000	1.002	0.999	0.999	1.002	1.005	1.010
30 °	d_{max}	0.992	0.991	1.003	0.999	1.000	1.000	1.005	0.997	1.005	1.012	1.021
	5.0 cm	0.995	0.993	0.997	0.992	1.000	1.003	1.009	1.013	1.007	1.004	1.011
	10.0 cm	0.994	0.989	0.999	0.983	1.000	0.996	1.003	1.004	1.000	1.017	1.022
	15.0 cm	0.994	0.993	0.994	1.001	1.000	1.017	1.012	1.014	1.023	1.014	1.026
45°	d_{max}	0.980	**0.976**	0.992	0.993	1.000	0.993	1.003	1.008	1.004	1.023	**1.039**
	5.0 cm	0.993	0.988	1.001	0.995	1.000	**1.014**	1.021	1.025	**1.034**	1.026	**1.042**
	10.0 cm	1.002	1.001	1.009	0.993	1.000	1.007	**1.017**	1.025	1.043	**1.045**	**1.056**
	15.0 cm	0.989	**0.979**	0.980	0.984	1.000	1.001	1.008	1.018	1.027	**1.041**	**1.057**
60°	d_{max}	0.993	0.996	1.002	1.002	1.000	1.004	1.001	1.005	1.015	**1.027**	1.035
	5.0 cm	0.992	0.986	0.996	0.989	1.000	1.004	1.010	1.018	1.026	1.020	1.032
	10.0 cm	1.000	0.997	1.002	0.995	1.000	1.005	1.013	1.020	1.027	1.037	1.047
	15.0 cm	0.984	0.986	0.998	0.999	1.000	0.999	1.005	1.013	1.021	1.034	1.048

TABLE V. Relative Wedge factors for 10x10 cm^2, a cobalt-60 teletherapy unit. Factor normalized to 5 cm depth.

Depth (cm)	Wedge angle					
	15°	30°	45°	60°	30°	25°
d_{max}	0.993	0.994	1.000	**0.972**	1.000	0.997
5	1.000	1.000	1.000	1.000	1.000	1.000
10	1.000	1.013	1.001	**1.032**	1.007	1.008
15	1.013	1.024	1.013	**1.035**	1.015	1.008

TABLE VI. Relative wedge factors for 10x10 cm^2, 6 MV photon beam, Factor normalized to the 5 cm depth.

Depth (cm)	Wedge angle			
	15°	30°	45°	60°
d_{max}	0.986	**0.977**	0.982	0.979
5	1.000	1.000	1.000	1.000
10	0.987	1.010	1.021	**1.023**
15	1.017	1.023	**1.044**	1.042

TABLE VII. Relative wedge factors for 10x10 cm^2 , 10 MV photon beam. Factor normalized to the 5 cm depth.

Depth (cm)	Wedge angle			
	15°	30°	45°	60°
d_{max}	0.990	**0.988**	0.997	0.996
5	1.000	1.000	1.000	1.000
10	0.997	0.990	0.998	**0.980**
15	1.006	1.006	**1.015**	1.000

TABLE VIII. Relative wedge factors for 10x10 cm^2, 15 MV photon beam. Factor normalized to the 5 cm depth.

Depth (cm)	Wedge angle			
	15°	30°	45°	60°
d_{max}	0.993	0.992	1.007	**0.972**
5	1.000	1.000	1.000	1.000
10	0.999	0.999	1.001	**0.996**
15	1.017	0.997	**1.018**	1.005

For the 6 MV X-rays (Table II) there were a small percentage difference for the field not exceeding 15x15 cm^2, the maximum values were 1.7%, 1.3%, 2.6% and 1.8% at the depth of d_{max}, 5 cm , 10 cm and 15 cm respectively. But for the field sizes greater than 15x15 up to 22x22 cm^2, the maximum percentage differences were 4.8%, 5.5%, 5.5% and 3.1% at the depth of d_{max}, 5 cm, 10 cm and 15 cm respectively.

For the field size 25x25 cm^2 the maximum percentage differences were 7.6%, 7.3%, 6.8% and 4.9% at the depth of d_{max}, 5 cm, 10 cm and 15 cm respectively. For the 10 MV X-rays (Table III) there were a small percentage differences for the field size not exceeding 15x15 cm^2, the maximum values were 2.3%, 2.1%, 1.8% and 1.7% at the depth of d_{max}, 5 cm, 10 cm and 15 cm respectively. But for the field sizes greater than 15x15 up to 22x22 cm, the maximum percentage differences were 6.0%, 4.5%, 3.9% and 3.9% at the depth of d_{max} 5 cm, 10 cm and 15 cm respectively.

For the 15 MV X-rays (Table IV) there were a small percentage differences for the field size not exceeding 15x15 cm^2, the maximum values were 2.4%, 1.4%, 1.7% and 2.1% at the depth of d_{max}, 5 cm, 10 cm and 15 cm respectively. But for the field size greater than 15x15 up to 22x22 cm^2, the maximum percentage differences were 2.7%, 3.4%, 4.5% and 4.1% at the depth of d_{max}, 5 cm, 10 cm and 15 cm respectively. But for the field size of 25x25 cm^2, the maximum percentage differences were 3.9%, 4.2%. 5.6% and 5.7% at the depth of d_{max}, 5 cm, 10 cm and 15 cm respectively.

For the depth dependence study, the variation of relative wedge factors were shown in table V-VIII. Table V- VIII present the relative wedge factor as a function of depth normalized to TG-21 recommendation depth (5 cm) for the field size of 10x10 cm^2 for each energy.

For cobalt-60 (Table V), the maximum percentage differences were 2.8%, 3.2% and 3.5% at the depth of d_{max}, 10 cm and 15 cm respectively.

For 6 MV X-rays (Table VI), the maximum percentage differences were 2.3%, 2.3% and 4.4% at the depth of d_{max}, 10 cm and 15 cm respectively.

For 10 MV X-rays (Table VII), the maximum percentage differences were 1.2%, 2.0% and 1.5% at the depth of d_{max}, 10 cm and 15 cm respectively.

For 15 MV X-rays (Table VIII), the maximum percentage differences were 2.8%, 0.4% and 1.8% at the depth of d_{max}, 10 cm and 15 cm respectively.

DISCUSSION

This study supports previous report by the others. Jatnitor R et al[4] had studied with 4 and 6 MV X-rays measuring the variation of wedge factor for various field sizes. In their experiments, the variation of wedge factors with a 60° wedge, the use of single wedge factor measure for 10x10 cm^2 field introduced errors of up to 3.5% and 7% for a 16 cm and 20 cm wide field respectively. McCullough et al[5] showed a change in wedge factors of less than 2% for a 30° wedge filter at depth down to 10 cm. For deeper depths and larger wedge angles, greater changes were found up to 5%. Since there was no data for supporting the cobalt-60 machine and 15 MV high energy photon beams that we have used in Thailand. Therefore, it is encouraging to perform this study.

The results of this study revealed a small field size dependence for the field size less than 15x15 cm^2 for all energies, but for the field size larger than 15x15 cm^2, the difference in WTF was significant. The variation of WTF for the field size dependence may be attributable to change in (i)

the scatter radiation in the water phantom due to the nonuniform primary photon fluence, (ii) the amount of backscatter radiation from the wedge filter into monitor chamber, and (iii) head scatter radiation. This is the amount of scatter photons that reach the point of measurement after undergoing interactions in the flattening filter, the primary collimator, and the secondary field defining collimator.[6]

The variation of WTF with depth is probably due to beam hardening effects where the low energy photons are attenuated much more than the high energy ones.[7] This can explain the greater change in cobalt-60 (3.5%) and 6 MV (4.4%) compared to the 10 MV (2.0%) and 15 MV (2.8%).

CONCLUSIONS

In this paper we have attempted to show that there is a definite dependence of wedge transmission factors on field size and depth. Therefore, a wedge factor measured for a reference field size and depth may not be valid for all field sizes and depths. The magnitude of error in assuming one wedge factor is less than 3% for the field sizes less than 15x 15 cm^2 and the depth is less than 10 cm. But for the field size greater than 15x15 cm^2 up to 25x25 cm^2 and the depth deeper than 10 cm, the error is seem to be significant.

It is suggested that, before a new cobalt-60 unit and linear accelerators are accepted for treatment it is very important to perform thorough studies of all mentioned parameters when using wedge filters.

REFERENCES

1. Knoos T, Wittgren L. Which depth dose data should be used for dose planning when wedge filters are used to modify the photon beam?. Phys Med Biol 1991;36:-255-267.
2. American Associated of Physics in Medicine, RTC Task Group 21. A Protocol for the Determination of Absorbed Dose from High-Energy Photon and Electron Beams. Med Phys 1983;10:741-771.
3. International Commission on Radiation Units and Measurements (ICRU): Report No 24. Determination of Absorbed Dose in a Patient Irradiated by Beams of X or Gamma Rays in Radiotherapy Procedures. Washington . D C., Natonal Bureru of Standards 1976;12-14 .
4. Jatinder R, Palta. Inder daftari, Suntharalingam N. Field size dependence of wedge factor. Med Phys 1988;15:624-626.
5. McCullough E C, Janet Gortney, Robert Blackwell C. A Depth Dependence Determination of the Wedge Transmission Factor for 4-10 MV Photon Beams. Med. Phys 1988;15:621-623.
6. Kase K R, Svenson G K. Head scatter data for several linear accelerators (4-18 MV). Med Phys 1986;13:530.
7. Sharma S C, Johnson M W. Recommendations for measurement of tray and wedge factors for high energy photons. Med Phys 1994;21:573-575.

RECOMMENDATION FOR DEPTH MEASUREMENT OF WEDGE TRANSMISSION FACTORS FOR HIGH ENERGY PHOTON BEAMS

C. KAKANAPORN[1], N. MANATRAKUL[2], P. SOPHONPIS[3], P. PROMYART[3]

ABSTRACT

In clinical practice, it is often assumed that wedge transmission factor (WTF) is independent of depth. Measurements have been experimented which demonstrated a clinically significant variation in WTF, as much as 6.8% for A 60° wedge between 5 and 15 cm. depth. The measurements were performed for various field sizes at depth of maximum dose (d_{max}) , 5, 10 and 15 cm. depths. It made with ionization chamber in solid phantom with 80 cm. SSD for Co-60, and 100 cm. SSD for three linear accelerator x-ray beams with energies of 6, 10 and 15 MV. From our experiments, these systematic measurements on WTF show that in general there is a definite dependence at various depths varies with beam energy and wedge angle. And the recommended depth of measurement should be 5 cm depth for Co-60 gamma ray, 6 and 10 MV x-rays, and 5 cm or 10 cm depth for 15 MV x-rays.

INTRODUCTION

Wedge filters are routinely placed into the path of high energy photon beams to modify the isodose distributions which are invaluable in the dose treatment planing to achieve homogeneous dose distribution and the presence of wedge filter decreses the beam intensity and this must be taken into account in the treatment dose calculation. The change in the beam is characterized by relative isodose distribution and a WTF. ICRU[1] defines the wedge transmission factor (WTF) or wedge factor (WF) as the ratio of dose in phantom at a point on the central axis with and without wedge. In clinical practice, it is assumed that WTF is independent of depth and field size. In many institutions, a single value of WTF is determined at a specified reference depth such as depth of maximum dose (d_{max}) and reference field size such as $10x10^2$ cm field. It is then used in the calculation of monitor unit settings or timer setting for all wedge fields. Palta et al[2] found that the error for 4 or 6 MV x-rays when using a single WTF with 60° wedge could reach 3.5% for a $16x16^2$ cm field and 7% for a $20x20^2$ cm field. Our previous study,[3] the result demonstrated variation in the WTF of up to 5%, 5.5%, 6% and 4.5% for Co-60 gamma rays, 6, 10, and 15 MV x-rays respectively, for field size of 22x22 cm^2 moreover, for 25x25 cm^2 field introduced error of up to 7.6% for 6 and 15 MV x-rays.

To determine whether WTF should be measured as function of depth, McCullough et al[4] reported that for 4 to 10 MV x-ray beams and for depths less than or equal to 10 cm, the WTF at

[1] Division of Radiation Oncology, Department of Radiology, Faculty of Medicine, Siriraj Hospital, Mahidol University
[2] Division of Radiation Oncology, National Cancer Institute, Bangkok
[3] Department of Radiological Technology, Faculty of Medical Technology, Mahidol University

depth was less than 2% different from that determined at d_{max}, for a nominal wedge angle in excess of 45° with depth greater than 10 cm, the WTF at depth differed from the WTF determined at d_{max} by up to 5%. However it is unclear where the depth of measurement should be used for calculation or dose planning when wedge filters are used to modify the photon beams

The purpose of this work was to investigate and examine systematically the depth dependence of in phantom WTF for Co-60 gamma rays, 6, 10 and 15 MV x-rays and 15°- 60° wedges (norminal wedge angle) and to use these results to suggest the depth of WTF measurements.

MATERIALS AND METHODS

WTF measurements were performed to Co-60 (Theratron 780 C), 6 MV x-rays (Siemens-MD Mevatron), 10 MV x-rays (Mitsubishi-ML-15 M) and 15 MV x-ray (Siemens-KD Mevatron) using standard wedge filters provided by the manufacturer with nominal wedge angle of 15°, 30°, 45° and 60°. For all wedge filters, transmission measurements were obtained with a Farmer ionization chamber in solid water phantom coupled to Farmer electrometer (model 2570/1). all measurements were performed at d_{max} (0.5 cm for Co-60, 1 cm for 6 MV x-rays, 2.3 cm for 10 MV x-rays and 3 cm for 15 MV x-rays), 5, 10 and 15 cm depths for various field sizes (from 5x5 cm^2 to 15x15 cm^2), using a source surface distance of 80 cm for Co-60 and a target surface distance of 100 cm for linear accelerators. To confirm that the wedge was centered,the measurements with wedge filters were repeated for 180° collimator rotation. For each beam energy, measurements for open fileds were performed at the same depth and field size. The WTF at any given depth and field size was determined as the ratio of reading with and without wedge.

RESULTS AND DISCUSSION

The dependence of WTF on depth of measurement is shown in table 1 for Co-60, 6, 10 and 15 MV x-rays respectively. The WTFs were normalized to the mean of each given field size and for each given energy and wedge angle. The results of this study showed dependence on depth. If the WTF from one depth of measurement were to be used for each wedge it seems that the measurement for each given field size at a depth of 5 cm would represent a good choice for Co-60, 6 and 10 MV x-rays, and the recommendation of measurement depth for 15 MV x-rays should be 5 or 10 cm depth. For our experiment, we also studied the variation of the WTF with depth. Using a depth-normalized relative wedge factor (RWF_d) for various depths, d and it was defined as

$$RWF_d = WTF(d,A)/WTF\ (d = 5\ cm, A)$$

Where RWF_d provided a direct estimate of depth dependence of the WTF for each field size relative to that determine at 5 cm depth.

Table 2 presents a summary of the RWF_d for 15°- 60° wedge angles for various field sizes for Co-60, 6, 10 and 15 MV x-rays respectively. From the results, they are shown to be affected by hardening for x-rays and softening for Co-60 gamma rays.

For Co-60 gamma ray beams filtered by a wedge, the wedge effect on the beam spectrum, which is nearly monoenergetic, has been assumed to be minimum.[1] However Co-60 wedge transmission measurements were found to be increase with depth, as much as 3.3% for 60° wedge at 15 cm depth, It has been speculated that the depth dependence of a WTF in Co-60 beams may be due to secondary photons from the wedge filter itself, by compton scattering[5]

Table 1. WTF for Co-60, 6, 10 and 15 MV x-rays. Factors normalizedd to the mean value of WTF for each wedge filter.

Beam	Depth	15° wedge			30° wedge			45° wedge			60°wedge		
Energy	(cm)	5x5 (cm^2)	10x10 (cm^2)	15x15 (cm^2)	5x5 (cm^2)	10x10 (cm^2)	15x15 (cm^2)	5x5 (cm^2)	10x10 (cm^2)	15x15 (cm^2)	5x5 (cm^2)	10x10 (cm^2)	15x15 (cm^2)
Co-60	0.5	0.994	0.992	0.997	0.988	0.986	0.992	0.993	0.996	0.998	0.969	0.963	-
(Theratron)	5.0	1.001	0.999	0.997	0.997	0.992	0.996	1.002	0.996	0.992	1.003	0.991	-
	10.0	0.999	0.998	1.005	1.003	1.006	1.008	0.999	0.998	1.003	1.017	1.022	-
	15.0	1.001	1.012	1.002	1.012	1.016	1.004	1.006	1.009	1.007	1.010	1.023	
	-												
6 MV	1.0	0.992	0.992	0.988	0.977	0.979	0.982	0.966	0.974	0.971	0.965	0.974	0.980
(Siemens)	5.0	1.002	0.999	0.998	0.990	1.002	0.996	0.977	0.992	0.989	0.991	0.995	0.972
	10.0	0.989	0.998	1.002	1.009	0.993	1.003	1.016	0.999	1.003	1.014	0.995	1.011
	15.0	1.018	1.012	1.013	1.025	1.025	1.019	1.021	1.035	1.038	1.030	1.037	1.038
	-												
10 MV	2.3	0.988	0.992	0.995	0.995	0.992	0.996	0.999	0.995	0.995	1.006	1.002	1.000
(Mitsubishi)	5.0	1.000	1.002	1.003	1.002	1.003	1.003	0.995	0.998	1.000	1.005	1.006	1.005
	10.0	0.998	0.999	0.997	0.996	0.994	0.993	0.995	0.995	0.996	0.985	0.985	0.985
	15.0	1.014	1.008	1.005	1.007	1.010	1.008	1.011	1.012	1.009	1.003	1.006	1.009
	-												
15 MV	3.0	0.995	0.991	0.992	0.995	0.995	0.993	0.990	1.000	0.991	0.983	0.979	0.979
(Siemens)	5.0	0.996	0.998	1.004	1.005	1.003	1.005	0.996	0.994	1.002	1.001	1.007	1.007
	10.0	1.002	0.997	0.994	0.999	1.002	0.998	1.010	0.995	0.999	1.009	1.003	1.007
	15.0	1.007	1.015	1.010	1.001	0.999	1.004	1.004	1.011	1.007	1.007	1.012	1.007

Table 2. RWF_d 15°-60° (nominal wedgs angle for 5x5 to 15x15 cm. fields for Co-60 unit, 6, 10, and 15 MV x-rays. Factors normalized to 5 cm. depth.

Beam	Depth	15° wedge			30° wedge			45° wedge			60°wedge		
Energy	(cm)	5x5 (cmxcm)	10x10 (cmxcm)	15x15 (cmxcm)	5x5 (cmxcm)	10x10 (cmxcm)	15x15 (cmxcm)	5x5 (cmxcm)	10x10 (cmxcm)	15x15 (cmxcm)	5x5 (cmxcm)	10x10 (cmxcm)	15x15 (cmxcm)
Co-60	0.5	0.993	0.993	0.999	0.991	0.994	0.997	0.990	1.000	1.006	0.966	0.972	-
(Theratron)	5.0	1.000	1.000	1.000	1.000	1.000	1.000	1.000	1.000	1.000	1.000	1.000	-
	10.0	0.998	0.999	1.007	1.007	1.013	1.012	0.996	1.001	1.011	1.014	1.032	-
	15.0	1.005	1.013	1.005	1.016	1.024	1.009	1.004	1.013	1.015	1.008	1.033	-
	-												
6 MV	1.0	0.990	0.993	0.990	0.987	0.977	0.987	0.970	0.982	0.982	0.974	0.979	1.009
(Siemens)	5.0	1.000	1.000	1.000	1.000	1.000	1.000	1.000	1.000	1.000	1.000	1.000	1.000
	10.0	0.987	1.000	1.004	1.020	0.991	1.007	1.019	1.007	1.014	1.024	1.000	1.040
	15.0	1.016	1.013	1.015	1.035	1.023	1.023	1.025	1.044	1.050	1.039	1.042	1.068
	-												
10 MV	2.3	0.988	0.990	0.992	0.993	0.988	0.993	1.004	0.997	0.995	1.001	0.996	0.995
(Mitsubishi)	5.0	1.000	1.000	1.000	1.000	1.000	1.000	1.000	1.000	1.000	1.000	1.000	1.000
	10.0	0.999	0.997	0.995	0.993	0.990	0.990	1.000	0.999	0.996	0.980	0.979	0.981
	15.0	1.014	1.006	1.003	1.005	1.006	1.005	1.016	1.015	1.010	0.998	0.999	1.003
	-												
15 MV	3.0	0.999	0.993	0.988	0.996	0.992	0.988	0.994	1.007	0.989	0.982	0.972	0.973
(Siemens)	5.0	1.000	1.000	1.000	1.000	1.000	1.000	1.000	1.000	1.000	1.000	1.000	1.000
	10.0	1.006	0.999	0.989	0.995	0.999	0.993	1.014	1.001	0.997	1.008	0.996	1.000
	15.0	1.011	1.017	1.006	0.996	0.996	0.999	1.008	1.018	1.008	1.005	1.005	1.000

For x-ray bems, the variation of the WTF with depth has been attributed to the effect of the beam hardening which results from preferential absorption of low energy photon component in the beam.[5,6,7] The low energy photons are attenuated much more than high energy photons. This can explain the greater changes were found up to 6.8% for 6 MV x-rays at depth of 15 cm and for 60° wedge. The beam hardening effect expected to be smaller for 10 and 15 MV x-ray beams.

CONCLUSION

In this experiment, we have studied the characteristics of depth dependence of the WTF for various energy beams. Based on the analysis of RWF_d, there is a definite dependence of WTF upon the depth of measurement. The degree of dependence varies with beam energy and wedge angle. For 6 MV x-rays, the deviation increase with depth up to 6.8% at 15 cm for 60° wedge, indicating some hardening of the beam by the wedge filter. The most important finding in this study is that the suggestion for depth of WTF measurement for Co-60, 6 and 10 MV x-rays should be 5 cm, and 15 MV x-rays should be measured at 5 or 10 cm depth.

As pointed out in our study[3] and other investigators,[2,4,6,7] it is clearly necessary to take the dependence of the WTF on field size and larger depth into account in clinical dose calculation.

REFERENCE

1. ICRU (International Commission on Radiation Units and Measurements), Determination of Absorbed dose in patient irradiated by beam of x or gamma rays in radiotherapy procedures, ICRU : Bethesda, 1976.
2. Palta JR, Daftar I, Suntharalingam N. Field size dependence of wedge factors. Med Phys, 1988;15:624-626.
3. Manatrakul N, Kakanaporn C, Pitsuttisup Y. The field size and depth dependence of wedge transmission factor for high energy photon beams. In the world congress on Medical Physics and Biomedical engineering, Nice, 1997.
4. McCullough EC, Gortney J, Blackwell CR. A depth dependence determination of the wedge transmission factor for 4-10 MV photon beams. Med Phys, 1988;15:621-623.
5. Patomaki LK. Percentage depth dose values in wedge fields of Co-60 beams. In Xlll International congress in Radiology, Madrid, 1979.
6. Wu A, Zwicker RD, Krasin F, Steonick ES, Dosimetry characteristics of large wedges for 4 and 6 MV x-rays. Med Phys, 1984;-11:186-188.
7. Knoos T, Wittgren L. Which depth dose data should be used for dose planning when wedge filters are used to modify the photon beam?. Phys. Med. Bio, 1991;36:-255-267.

SURVIVAL OF BREAST CANCER PATIENTS WITH BONE METASTASIS

Saipin TANGKARATT, M.D.

ABSTRACT

This study attempted to evaluated the survival of breast cancer patients, who were treated with palliative radiation to the affected matastatic bone regions.

A total of 137 breast cancer patients with evidence of bone metastasis was evaluated. All were treated with external beam radiation to the affected bones, using either Co-60 teletherapy or Linac 6 MV., with tumor doses of 3,000-3,500 cGy, 250-300 cGy per day, five fractions per week. All patients were follow-up closely until dead.

Eighty-seven patients (63.5%) developed only bone metastasis, other fifty patients (36.5%) had associated visceral organs (lungs, brain, liver etc.) metastasis at the same period of bone metastasis. The median survival of patients with associated visceral organs metastasis was 3 months, compared with 7.2 months for the patients with only bone metastasis.

Patients with multiple organs metastasis had short survival, most of them died from brain, or lungs or liver metastasis rather than bone metastasis. Patients with only bone metastasis have better survival and quality of life after palliative radiation.

INTRODUCTION

Breast cancer was the second most common cancer in Thai women,[1] precedented by uterine cervical cancer. Some patients came in with advanced stage, especially patients who lived in the rural areas. These patients were often treated unproperly at the beginning, including indefinite clinical and surgical staging, delayed surgery or delayed systemic treatment. These problems lead to poor treatment out-come, including loco-regional recurrence, and systemic metastasis. Among the systemic metastasis, bone was the most common followed by pulmonary and brain metastasis.

The objective of the retrospective study of breast cancer patients with bone metastasis was to evaluate the survival of the patients who had isolated bone metastasis compared to patients who had combined bone and other organs metastases.

MATERIALS AND METHODS

Patient selection

The records of 137 breast cancer patients with bone metastases, between January 1990 to December 1996 at National Cancer Institute were

National Cancer Institute

reviewed. This analysis was limited to the data about surgical stage and regimens of adjuvant systemic treatment.

Treatment

All of 137 patients were treated with external beam radiation, to the affected bone regions, using either Co-60 Teletherapy or Linac 6 MV accelerator. Most of them were given with a dose of 3,000 cGy in 10 fractions, a few were given with a dose of 4,000 cGy in 20 fraction, with minimized portal of treatment. For patients with generalized bone metastases (4 anatomical sites). Half body radiation were given with a dose of 500-550 cGy in one fraction.

Follow-up

The records about pain relief, neurological symptoms, radiation toxicity and survival were reviewed.

RESULTS

Table 1 Age Distribution

AGE	NUMBER	PERCENTAGE
20-29	1	0.7
30-39	33	24.1
40-49	37	27.0
50-59	37	27.0
60-69	25	18.2
> 70	4	2.9
TOTAL	**137**	**100**

The Youngest = 28 years old
The Oldest = 84 years old

Table 1, showed the age distribution of the patients in this study. The youngest patients was 28 years old, the oldest one was 84 years old. Peak incidence was between 40-59 years old (about 54%).

Table 2 Classification of metastasis

Metastasis	Number	Percentage
Bone	87	63.5
Multiple organs	50	36.5
Total	**137**	**100**

Table 2, Classification of metastasis, 87 of 137 patients (63.5 %) had only bone metastasis as compare to 50 patients (36.5 %) with multiple organs metastasis.

Table 3 Classifcation of bone metastasis

Bone metastasis	Number of patients	Percentage
- one anatomical site	62	45.3
- more than 1 anatomical site	68	49.6
- generalized (> 4 sites)	7	5.1
Total	**137**	**100**

Table 3, Anatomical sites of bone metastasis, the majority of cases had more than one anatomical sites of bone metastasis.

Table 4 Anatomical distribution

SITE	NUMBER	PERCENTAGE
Skull	3	1.4
C-Spines	19	8.6
T-Spines	73	33.0
L-Spines	49	22.2
Pelvic Bone	14	6.3
Hip, femur	36	16.3
Shoulder	13	5.9
Ribs	7	3.2
Generalized	7	3.2
TOTAL	221	100

Table 4, showed the anatomical distribution of bone metastasis. The most common site was thoracic spines (account about 33%), followed by lumbar spines (about 22.2%), hip and femur (about 16.3%). Only 7 patients came with generalised diffused bone metastasis at the first onset (more than > 4 anatomical regions), 62 patients (about 45.3%) had only one anatomical region of metastasis.

Only 25 patients (about 18.3%) had one recurrent episode of bone pain, other 112 cases (about 81.7%) had more than one recurrent episode of bone pain, and most of them occurred within 2 months after the first treatment.

Table 5 Visceral organs of distance metastasis

ORGAN	NUMBER	PERCENTAGE
Brain	17	30.9
Liver	7	12.7
Lungs	26	47.3
Soft tissue	2	3.6
Other (Generalized)	3	5.5
Total	**55**	**100**

Table 5, showed distribution of visceral organs metastasis. Lungs are the most common organ among visceral metastases (account about 47.3%), followed by brain (account about 31%). 5 patients presented with 2 organs metastases at the first episode, 3 patients had brain and lung metastases, other 2 patients had lung and liver metastases.

Table 6 Subjective response of pain relief

PAIN RELIEF CATEGORY	NUMBER	PERCENTAGE
CR	87	63.5
PR	38	27.7
SR	10	7.3
NC	2	1.5
PD	0	0.0
Total	**137**	**100**

Pain relief Classification :
CR - complete pain relief
PR - partial pain relief more than 50%
SR - some relief less than 50%
NC - no change
PD - progressive disease, or worsening of pain

Table 6, showed subjective response of pain relief after radiation treatment. The majority of patients (87 cases or 63.5%) had complete response of pain relief. 38 patients (27.7%) had partial pain relief. 10 patients (7.3%) had some pain relief. Only 2 patients showed no change of pain. 12 out of 137 patients had symptoms of cord compression, 10 out of 12 had complete recovery of neurological deficit, and 2 out of 12 patients remained paralysis after radiation.

Table 7 Median survival of the patients

	month
patients with bone metastasis	7.2
patients with bone and other visceral metastasis	3

Table 7, showed median survival of the patients. Patients with only bone metastasis had longer survival as compared to patients with bone and visceral metastases. 49 of 50 patients with visceral metastases died within 5 month after onset of metastasis, only 1 patients died at the sixth month after metastases.

Patients with only bone metastasis survived longer, the median survival was 7.2 months.

Table 8 Acute Radiation Toxicity

	grade o	grade 1	grade 2	grade 3	grade 4
Hemoglobin	(none)	25	10	2	0
White blood count	-	15	16	-	-
Platelet count	-	3	10	-	-
Nausea, vomiting	-	20	14	-	-
Diarrha	-	3	3	-	-
Hematuria	-	2	1	-	-
Fever	-	2	7	-	-
Pneumonitis	-	-	-	-	-

Table 8, showed acute radiation toxicity. The majority of cases tolerated well to radiation, only grade 1 toxicity was obverved. No severe or fatal toxicity was demonstrated. Most of the patients with bone marrow and gastro-intestinal toxicity during radiation also had chemotherapy for their visceral metastases.

DISCUSSION

In this study, bone involvement was the most frequent metastasis[2] in breast cancer. Among these, thoracic spines was the most common site, but there were only 12 patients who developed signs of cord compression and 10 of the 12 patients had complete recovery after radiation. The rest did not recover because of late presentation with complete cord compression more than 72 hours.

Most of the patients with visceral organs involvement had extensive systemic chemotherapy who showed some degree of bone marrow suppression, poor tolerance to radiation treatment and shorter survival. None of these patients survived more than 6 months even with extensive chemotherapy. Most of them died within 2-3 months after the onset of multiple organs metastasis, the causes of death, mostly came from pulmonary metastases.

Patients with only bone metastasis yielded longer survival and better performance status.[3] These were 16 of 87 patients survival more than 2 years, 52 of 87 patients survival more than 1 year. Even in patients with generalized bone metastasis, who had half body radiation, 3 of them survival more than 6 months with maintenance of pain relief.[4-5] 27 of 137 patients who had recurrent pain at the radiation sites had received repeated treatment with the same radiation dose, with satisfactory pain relief.[6] Our results showed effective pain relief by radiation as reported in the literatures.

CONCLUSION

Bone metastasis was the most common metastasis in breast cancer. Palliative radiation yielded effective pain relief and recovery of neurological deficit. Most of the patients died from lung, brain, liver metastasis rather than bone metastasis. Proper diagnosis, combined modality of treatment, including surgery, radiation and systemic chemotherapy will improve the survival in breast cancer.

REFERENCES

1. Annual Report National Cancer Institute, Department of Medical Services, Ministry of Public Health , 1994
2. Sherry MM, Greco FA, Johnson DH, et al : Metastatic breast cancer confined to the skeletal system. Am J Med 81:381, 1986
3. Tong C , Gillick L, Hendrickson FR : The palliation of symptomatic osseous metastases: Final results of the study by the Radiation Therapy Oncology Group. Cancer 50:893, 1982
4. Price P, Hoskin PJ, Easton D, et al : Low dose single fraction radiotherapy in the treatment of metastatic bone pain: A pilot study. Radiother Oncol 12:297, 1988
5. Salazar OM, Rubin P, Hendrickson FR, et al : Single-dose half-body irradiation for palliation of multiple bone metastases from solid tumors. Cancer 58:29, 1986
6. Rubin P, Heilmann H-P : Large field trials. Int J Radiat Oncol Bio Phys 14:S65,-1988

Message from

Professor Dr. Kawee Tungsubutra

Editor-in-Chief, The Asean Journal of Radiology.

This is the No. II of Vol. IV of the Asean Journal of Radiology published by the co-operation of the Radiologists both from the Asean and from other countries outside Asean. Without the kind support from Bracco International amidst the economic crisis in all the Asean countries, it might be impossible to continue publishing the Journal. We have only another 1½ years to keep the standard and the regularity of the publishing of the Journals so that it can be accepted to appear in the Index Medicus. I just received a by-passed operation for my heart in July and hope to regain health soon. I must apology for the delay of the distribution of the journals to our member countries. I hope all will receive the Journals through the post soon, not later than August.

Kawee Tungsubutra.

Kawee Tungsubutra

May-August 1998.

AAR Journal of Radiology
for Authors

Instructions

1. The AAR Journal of Radiology publishes the papers on Radiological Sciences, such as research work, review articles, case reports, innovations in Medical Sciences related to all branches of Radiology, and letters to the editor. The aforementioned materials can be written in English only.

2. The authors have to submit 2 copies of the manuscript and a diskette: **to Prof. Dr. Kawee Tungsubutra,** 318 Kaweevej Hospital, Tarksin Road, Dhonburi, Bangkok 10600, Thailand. **or to the Associate Editors** at the Radiological Society of Malaysia, Indonesia, Philippine, Singapore and Brunei. The names and adresses of the Associate Editors in each country were published in the front page of this Journal.

3. The original copy to be submitted must be typed in a double space on one side of the page of 8.1/2"x 11.1/2" paper.

4. The format of the article must include :

a. Title page and address of the author (s)
b. Abstract
c. Introduction (Background)
d. Material and Method
e. Results and discussion (Tables and Illustrations)
f. Acknowledgement (if any)
g. References (Follow the Vancouver style developed by ICMJE)

5. We will provide 25 copies of reprints for the author (s) who submit (s) an article for publication in the AAR Journal.

6. The illustrations and tables must be clearly prepared with legends in English as they are the art works to be reproduced.

7. The authors are responsible for the contents of the article as to its facts and findings.

8. Ethics.

Paper reporting studies which might be interpreted as human experimentation (e.g. controlled trials) should conform to the standards of the Declaration of Helsinki (see British Medical Journal 1964:2:177) and should indicate that, approval that such studies may proceed, has been granted by the local or hospital Ethics Committee.

When reporting experiments on animals indicate whether the institution's or the National Research Council's guide for, or any national law on, the care and use of laboratory animals was followed.